UNITED NATIONS EDUCATIONAL, SCIENTIFIC AND CULTURAL ORGANIZATION
INTERNATIONAL ATOMIC ENERGY AGENCY
INTERNATIONAL CENTRE FOR THEORETICAL PHYSICS

SMR: 960/4

WORKSHOP ON NONLINEAR CONTROL AND CONTROL OF CHAOS

(17 - 28 June 1996)

"Nonlinear Dynamics and Control in Mechanical Systems"

presented by:

Hans Troger
Technische Universität Wien
Institut für Mechanik
Wiedner Hauptstrasse 8-10/325
A-1040 Wien
Austria

2 J. M. Kelly, G. Leitmann, and A. Soldatos, Robust control of base-isolated structures under earthquake excitation, *J. Optimization Theory Appl.* 53:159–181 (1987).
3 Y. H. Chen and J. Piontek, Robust modal control of distributed parameter systems with uncertainty, in *Proc. American Control Conference*, San Diego, CA, 1990, pp. 2014–2019.
4 J. Rodellar, G. Leitmann, and E. P. Ryan, Output feedback control of uncertain coupled systems, *Internat. J. Control* 58(2):445–457 (1993).
5 M. Corless and G. Leitmann, Adaptive control of systems containing uncertain functions and unknown functions with uncertain bounds, *J. Optim. Theory Appl.* 41:155–168 (1983).
6 E. P. Ryan, A universal adaptive stabilizer for a class of nonlinear systems, *Systems Control Lett.* 16:219–218 (1991).
7 R. I. Skinner, W. H. Robinson, and G. H. McVerry, *An Introduction to Seismic Isolation*, Wiley, Chichester, 1993.
8 J. Inaudi, F. López Almansa, J. M. Kelly, and J. Rodellar, Predictive control of base isolated structures, *Earthquake Eng. Struct. Dynam.* 21:471–482 (1992).
9 J. Inaudi and J. M. Kelly, A simple active isolation scheme, in *8th VPI and SU Symposium on Dynamics and Control of Large Structures*, Blacksburg, VA, 1991, pp. 219–231.
10 J. N. Yang, Z. Li, A. Danielians, and S. C. Liu, Aseismic hybrid control of nonlinear and hysteretic structures, I and II, *J. Eng. Mech.* 118(7):1423–1456 (1992).
11 S. Nagarajaiah, M. Riley, A. Reinhorn, and M. Shinozuka, Hybrid control of sliding isolated bridges, in *Proc. 1992 Presure Vessels and Piping Conf.*, ASME/PVP-237, 2:83–89 (1992).
12 M. Q. Feng, M. Shinozuka, and S. Fujii, Friction-controllable sliding isolated system, *J. Eng. Mech.* 119(9):1845–1864 (1993).

NORTH-HOLLAND

Center Manifold Approach to the Control of a Tethered Satellite System

W. Steiner, A. Steindl, and H. Troger

Technical University Vienna
A-1040 Vienna, Austria

Transmitted by F. E. Udwadia

ABSTRACT

It is well known that in a linearized analysis the in-plane oscillation of a tethered satellite system about the radial earth pointing position decouples from the out-of-plane oscillation. By tension control, therefore, only the in-plane but not the out-of-plane oscillation can be affected. Hence, using tension control linearization of the equations of motion cannot be used and a nonlinear problem must be treated. For a simple mechanical model of a tethered satellite system we show by means of center manifold theory that for the nonlinear system the out-of-plane oscillations can be stabilized by tension control.

1. INTRODUCTION

In [1] Bainum and Kumar study the control problem of a simple tethered satellite system consisting of a space shuttle moving on a prescribed circular orbit and a subsatellite modeled by a pointmass and connected to the shuttle by a massless always straight tether as in Figure 1.

The nominal operating position of the subsatellite is the stable radial earth pointing equilibrium position. An important technical question now is how to regain this radial position as fast as possible if perturbations of the radial position lead to oscillations about this state.

There are several ways to control the position of the subsatellite, for example, by means of the use of rockets mounted at the subsatellite. However, the simplest control strategy would be to try to control the motion of the subsatellite by tension control of the tether [2]. Tension control can be easily realized by controlling the torque at the reeling drum.

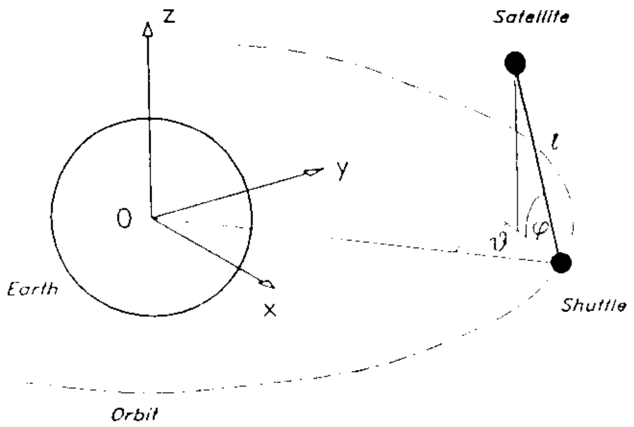

FIG. 1 System geometry showing the shuttle on a prescribed circular orbit and the in-plane angle ϑ and out-of-plane angle φ of the straight tether of length l connecting the subsatellite to the shuttle.

However, performing a linearized analysis of the control problem it turns out that only the oscillations in the orbital plane can be controlled, whereas the out-of-plane oscillations in the linearized problem cannot be controlled by tension control as shown in the analysis given below.

In [1] it is conjectured that in a nonlinear analysis the nonlinear coupling between the in-plane and out-of-plane motion could result in the possibility to control also the out-of-plane motion by tension control.

The aim of this paper is to give such a nonlinear analysis.

2. MECHANICAL MODEL AND EQUATIONS OF MOTION

We use exactly the same model as in [1]. We assume that the motion of the shuttle is prescribed on a circular orbit with angular velocity ω and further that it will not be affected by the motion of the subsatellite. The subsatellite is given by a point mass which is connected to the shuttle by a straight massless inextensible tether. Hence, the problem has three degrees of freedom, namely, the two angles ϑ and φ which are so-called Tait–Brayant angles describing the system's pitch motion in the orbital plane and roll motion out of the orbital plane, respectively, and the length l of the tether as in Figure 1.

As external forces we only include the gravitational effect of the spherical earth and neglect all other influences which, for example, could be air drag, the earth's magnetic field, or effects following from the nonsphericity

In the equations of motion of the subsatellite we obtain due to the action of the cable the generalized forces $Q_l, Q_\vartheta, Q_\varphi$. However, here only Q_l is of relevance because the other two vanish for the straight cable configuration because no moments can be transferred by the cable.

The equations of motion in the variables ϑ, φ, and l can be taken from [1]. In dimensionless form they are

$$\begin{aligned}
\xi'' - \xi[(\varphi'^2 + (\vartheta' - 1)^2 + 3\cos^2\vartheta)\cos^2\varphi - 1] &= \frac{Q_l}{M\omega^2 l_c} \\
\vartheta'' + \tfrac{3}{2}\sin 2\vartheta - 2(\vartheta' - 1)\varphi'\tan\varphi + 2\tfrac{\xi'}{\xi}(\vartheta' - 1) &= 0 \\
\varphi'' + \tfrac{1}{2}((\vartheta' - 1)^2 + 3\cos^2\varphi)\sin 2\varphi + 2\tfrac{\xi'}{\xi}\varphi' &= 0.
\end{aligned} \tag{1}$$

Here $\xi = l/l_c$, where l_c is the nominal length of the cable in the station keeping operating condition. M denotes the mass of the subsatellite. $(\ )'$ designates the derivative with respect to a dimensionless time $\tau = \omega t$.

We study now the problem with constant tether length. In case we would study the control problem for variable tether length, for example, for the operations of deployment or retrieval of the subsatellite then l_c would be time dependent and a much more complicated mathematical problem would be obtained.

From the equations of motion follows that the radial equilibrium position $\varphi = 0, \vartheta = 0, l = l_c$ (respectively, $\xi = 1$) is a solution resulting into the static tether tension $Q_l^{\text{stat}} = -3M\omega^2 l_c$. For the further analysis we introduce a new variable ε defined by $\xi = 1 + \varepsilon$.

3. LINEARIZED CONTROL PROBLEM

We perform now the linearization of (1) about the radial state. This results in

$$\begin{aligned}
\varepsilon'' - 3\varepsilon + 2\vartheta' &= 3 + \frac{Q_l}{M\omega^2 l_c} \\
\vartheta'' + 3\vartheta - 2\varepsilon' &= 0 \\
\varphi'' + 4\varphi &= 0.
\end{aligned} \tag{2}$$

We see that only the in-plane angle ϑ can be affected by variation of the cable tension Q_l whereas the out of plane motion φ completely decouples in the linearized case and, hence, by tension control will not be affected

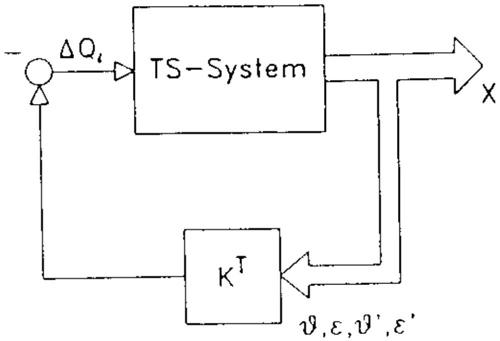

FIG. 2. Control system for the components $\vartheta, \vartheta', \varepsilon$, and ε' by means of a linear controller.

Introducing the vector

$$\mathbf{x}^T = (\varepsilon, \varepsilon', \vartheta, \vartheta', \varphi, \varphi') = (x_1, x_2, x_3, x_4, x_5, x_6) \tag{3}$$

we can write (2) as a system of equations of first order in the form

$$\mathbf{x}' = \mathbf{A}\mathbf{x} + \mathbf{b}u, \tag{4}$$

where

$$\mathbf{A} = \begin{bmatrix} 0 & 1 & 0 & 0 & 0 & 0 \\ 3 & 0 & 0 & -2 & 0 & 0 \\ 0 & 0 & 0 & 1 & 0 & 0 \\ 0 & 2 & -3 & 0 & 0 & 0 \\ 0 & 0 & 0 & 0 & 0 & 1 \\ 0 & 0 & 0 & 0 & -4 & 0 \end{bmatrix}. \tag{5}$$

The control quantity u will be the variation of the cable force Q_l from its static value Q_l^{stat} and is given by

$$u = \Delta Q_l = \frac{Q_l - Q_l^{\text{stat}}}{M\omega^2 l_c} = \frac{Q_l}{M\omega^2 l_c} + 3 \tag{6}$$

and is introduced into the system by the vector $\mathbf{b}^T = \{0, 1, 0, 0, 0, 0\}$.

Following the analysis given in [1] we realize a feedback control system as in Figure 2 by stipulating a simple linear controller in the form

Introducing (7) into (14) we obtain the linear closed loop control system in the form

$$\mathbf{x}' = (\mathbf{A} - \mathbf{b}\mathbf{k}^T)\mathbf{x} = \mathbf{D}\mathbf{x}. \tag{8}$$

Since we only are able to affect the first four components of $\mathbf{x}$ we set $\mathbf{k}^T = \{K_1, K_2, K_3, K_4, 0, 0\}$. The linear operator $\mathbf{D} = \mathbf{A} - \mathbf{b}\mathbf{k}^T$ then reads

$$\mathbf{D} = \begin{bmatrix} 0 & 1 & 0 & 0 & 0 & 0 \\ 3 - K_1 & -K_2 & -K_3 & -2 - K_4 & 0 & 0 \\ 0 & 0 & 0 & 1 & 0 & 0 \\ 0 & 2 & -3 & 0 & 0 & 0 \\ 0 & 0 & 0 & 0 & 0 & 1 \\ 0 & 0 & 0 & 0 & -4 & 0 \end{bmatrix}. \tag{9}$$

In preview of the treatment of the nonlinear system we decouple the linear system into two parts by introducing the following notation

$$\begin{aligned} \mathbf{x}_s' &= \mathbf{J}_s\mathbf{x}_s \\ \mathbf{x}_c' &= \mathbf{J}_c\mathbf{x}_c. \end{aligned} \tag{10}$$

Here $\mathbf{x}$ is partitioned into the vector $\mathbf{x}_s^T = (x_1, x_2, x_3, x_4) = (\varepsilon, \varepsilon', \vartheta, \vartheta')$ of the so-called *noncritical variables* and into a vector $\mathbf{x}_c^T = (x_5, x_6) = (\varphi, \varphi')$ of the *critical variables*. The corresponding matrices are

$$\mathbf{J}_s = \begin{pmatrix} 0 & 1 & 0 & 0 \\ 3 - K_1 & -K_2 & -K_3 & -2 - K_4 \\ 0 & 0 & 0 & 1 \\ 0 & 2 & -3 & 0 \end{pmatrix} \qquad \mathbf{J}_c = \begin{pmatrix} 0 & 1 \\ -4 & 0 \end{pmatrix}. \tag{11}$$

Following [1] the control parameters K_i are selected in such a way that the eigenvalues of $\mathbf{J}_s$ are located in the left half plane. According to Routh's criterion the necessary and sufficient conditions for the stability of the closed loop, that is, of the components of $\mathbf{x}_s$, are

$$\begin{aligned} K_1 &> 3; \\ K_2 &> 0; \\ K_4 &> \frac{K_3}{K_2} - \frac{K_1 + 1}{2}; \end{aligned}$$

The eigenvalues of $\mathbf{J}_c$ are purely imaginary and cannot be influenced by the controller. The corresponding variables are the components of $\mathbf{x}_c$ and their stability depends on the nonlinear system.

If we consider the flow of the linear vectorfield given by (10) in the six-dimensional phase space we note that there is a contraction of the flow (the variables $x_1, \ldots, x_4$) to the plane spanned by the two coordinates x_5 and x_6. This shows that the time evolution of the linearized system is such that after some time only a two-dimensional flow is obtained. Hence, quite naturally the system reduces its dimension from six to two. However, the two-dimensional system is not structurally stable [3] because its phase portraits are a family of circles which depend on the initial conditions and the slightest perturbation due to nonlinear terms will change the qualitative type of behavior.

In fact if we look at the problem from the point of view of bifurcation theory [3] a Hopf bifurcation is given which allows us to judge the stability of the out of plane oscillation from the nonlinear system equations. "Center manifold theory" [3, 4] will allow us to perform the reduction process, which quite naturally was obtained above for the linear problem, as well as for the nonlinear problem.

4. CENTER MANIFOLD REDUCTION TO A TWO-DIMENSIONAL SYSTEM

We introduce now $\xi = 1 + \varepsilon$ and the following expressions up to third order in the variables

$$\begin{aligned} \sin\varphi &= \varphi - \frac{\varphi^3}{3!} + O(\varphi^5) \qquad & \cos\varphi = 1 - \frac{\varphi^2}{2!} + O(\varphi^4) \\ \tan\varphi &= \varphi + \frac{\varphi^3}{3!} + O(\varphi^5) \qquad & \xi'/\xi = \varepsilon' - \varepsilon'\varepsilon + \varepsilon'\varepsilon^2 + O(\varepsilon^4) \end{aligned}$$

into (1). This results in the nonlinear system up to third-order nonlinear terms

$$\begin{aligned} \frac{Q_1}{M\omega^2 l_c} + 3 &= \varepsilon - 3\varepsilon + 2\vartheta' + \big(4\varphi^2 + 3\vartheta^2 - \varphi'^2 - \vartheta'^2 + 2\vartheta'\varepsilon \\ &\quad - 2\vartheta'\varphi^2 + 4\varepsilon\varphi^2 + 3\varepsilon\vartheta^2 - \varepsilon\varphi'^2 - \varepsilon\vartheta'^2\big) \\ 0 &= \vartheta'' + 3\vartheta - 2\varepsilon' + \big(2\varepsilon\varepsilon' + 2\varphi'\varphi + 2\varepsilon'\vartheta' - 2\vartheta^3 - 2\vartheta'\varphi'\varphi \\ &\quad - 2\varepsilon'\varepsilon^2 - 2\varepsilon\varepsilon'\vartheta'\big) \\ 0 &= \varphi'' + 4\varphi + \big(2\varepsilon'\varphi' - 2\vartheta'\varphi - \tfrac{8}{3}\varphi^3 - 3\vartheta^2\varphi + \vartheta'^2\varphi - 2\varepsilon\varepsilon'\varphi'\big). \end{aligned} \tag{12}$$

Transforming to the variables x_i according to (11) we obtain the nonlinear dynamic system

$$\mathbf{x}' = \mathbf{A}\mathbf{x} + \boldsymbol{N}(\mathbf{x}) + \boldsymbol{b}u, \tag{14}$$

where $\mathbf{A}$, $\boldsymbol{b}$, and u are given as above and the nonlinear term $\boldsymbol{N}(\mathbf{x})$ is given by

$$\boldsymbol{N}(\mathbf{x}) = \begin{pmatrix} 0 \\ -4x_5^2 - 3x_3^2 + x_6^2 + x_4^2 \quad 2x_1x_4 + 2x_4x_5^2 - 4x_1x_5^2 - 3x_1x_3^2 \\ + x_1x_6^2 + x_1x_4^2 \\ 0 \\ -2x_1x_2 - 2x_5x_6 - 2x_2x_4 + 2x_3^3 + 2x_4x_5x_6 + 2x_1^2x_2 + 2x_1x_2x_4 \\ 0 \\ -2x_2x_6 + 2x_4x_5 + \frac{8}{3}x_5^3 + 3x_3^2x_5 - x_4^2x_5 + 2x_1x_2x_6 \end{pmatrix}. \tag{15}$$

The equations corresponding to (8) and (10) are

$$\mathbf{x}' = (\mathbf{A} - \boldsymbol{b}\boldsymbol{k}^T)\mathbf{x} + \boldsymbol{N}(\mathbf{x}) = \mathbf{D}\mathbf{x} + \boldsymbol{N}(\mathbf{x}) \tag{16}$$

and

$$\begin{aligned} \mathbf{x}_s' &= \mathbf{J}_s\mathbf{x}_s + \boldsymbol{N}_s(\mathbf{x}_c, \mathbf{x}_s) \\ \mathbf{x}_c' &= \mathbf{J}_c\mathbf{x}_c + \boldsymbol{N}_c(\mathbf{x}_c, \mathbf{x}_s). \end{aligned} \tag{17}$$

As already mentioned in the previous section also for the nonlinear system (17) a reduction to a two-dimensional system in the two critical variables x_5, x_6 is possible. However, this cannot be done as for the linear system of equations by simply neglecting the so-called stable components because due to nonlinear couplings the stable components can influence the critical ones. However, by applying center manifold theory the stable components can be eliminated in a correct way supplying a reduced system which locally has the same stability properties as the original full-dimensional system, that is, we must express the stable components by the critical ones in the form

$$\mathbf{x}_s = \mathbf{h}(\mathbf{x}_c). \tag{18}$$

Inserting (18) into the critical part of (17) we obtain

$$\mathbf{x}_c' = \mathbf{J}_c\mathbf{x}_c + \boldsymbol{N}_c(\mathbf{x}_c, \mathbf{h}(\mathbf{x}_c)), \tag{19}$$

The main task to be performed is the calculation of $\mathbf{h}$. This is explained in detail in [3] or in [4]. Hence without much explanation we perform the calculations. The basic equation to calculate $\mathbf{h}$ is

$$\mathbf{h}'(\mathbf{x}_c)(\mathbf{J}_c\mathbf{x}_c + \boldsymbol{N}_c(\mathbf{x}_c, \mathbf{h}(\mathbf{x}_c)) = \mathbf{J}_s\mathbf{h}(\mathbf{x}_c) + \boldsymbol{N}_s(\mathbf{x}_c, \mathbf{h}(\mathbf{x}_c)) \tag{20}$$

with the conditions at zero: $\mathbf{h}(\mathbf{0}) = (\mathbf{0})$ and $\mathbf{h}'(\mathbf{0}) = (\mathbf{0})$. An exact solution of (20) is equivalent of solving the original problem and hence hardly possible. However, as it is shown in [3, 4] it is possible to satisfy (20) up to any desired order by a power series expansion. Since we are only treating a nonlinear problem up to third-order terms a power series expansion of $\mathbf{h}$ up to second-order terms in the critical variables will be sufficient [3]. Hence we set

$$\mathbf{h}(\mathbf{x}_c) = \sum_{i=2}^{\infty} \mathbf{H}^{(i)}(\mathbf{x}_c), \tag{21}$$

where the $\mathbf{H}^{(i)}(\mathbf{x}_c)$ designate terms of i-th order. Restricting to the second-order terms we have

$$\mathbf{h}(\mathbf{x}_c) = \mathbf{H}^{(2)}(\mathbf{x}_c) + O(|\mathbf{x}_c|^4). \tag{22}$$

The coefficients of $\mathbf{H}^{(2)}$ taking into account of (20) follow from

$$\mathbf{H}^{(2)'}\mathbf{J}_c\mathbf{x}_c = \mathbf{J}_s\mathbf{H}^{(2)} + \boldsymbol{N}_s^{(2)}(\mathbf{x}_c). \tag{23}$$

Here $\boldsymbol{N}_s^{(2)}(\mathbf{x}_c)$ designates all the nonlinear terms in the critical variables of second order of $\boldsymbol{N}_s$. For the treated problem we have

$$\begin{aligned} \mathbf{H}^{(2)} &= \left(H_1^2(x_5,x_6), H_2^2(x_5,x_6), H_3^2(x_5,x_6), H_4^2(x_5,x_6)\right)^T \\ H_i^2 &= \alpha_{i20}x_5^2 + \alpha_{i11}x_5x_6 + \alpha_{i02}x_6^2, \end{aligned} \tag{24}$$

yielding that we have to determine 12 coefficients.

Moreover, we have

$$\boldsymbol{N}_s^{(2)}(\mathbf{x}_c) = (0, -4x_5^2 + x_6^2, 0, -2x_5x_6)^T, \tag{25}$$

$$\mathbf{H}^{(2)'} = \begin{pmatrix} \dfrac{\partial H_1^2}{\partial x_5} & \dfrac{\partial H_1^2}{\partial x_6} \\ \vdots & \vdots \\ \dfrac{\partial H_4^2}{} & \dfrac{\partial H_4^2}{} \end{pmatrix} \quad \mathbf{H}^{(2)'}\mathbf{J}_c\mathbf{x}_c = \begin{pmatrix} -4\dfrac{\partial H_1^2}{\partial x_6}x_5 + \dfrac{\partial H_1^2}{\partial x_5}x_6 \\ \vdots \\ \dfrac{\partial H_4^2}{} \quad \dfrac{\partial H_4^2}{} \end{pmatrix} \tag{26}$$

and

$$\mathbf{J}_s\mathbf{H}^{(2)} = \begin{pmatrix} H_2^2 \\ (3-K_1)H_1^2 - K_2H_2^2 - K_3H_3^2 - (2+K_4)H_4^2 \\ H_4^2 \\ 2H_2^2 - 3H_3^2 \end{pmatrix}. \tag{27}$$

The four components in (23) yield four relations

$$\begin{aligned} -4\frac{\partial H_1^2}{\partial x_6}x_5 + \frac{\partial H_1^2}{\partial x_5}x_6 &= H_2^2 \\ -4\frac{\partial H_2^2}{\partial x_6}x_5 + \frac{\partial H_2^2}{\partial x_5}x_6 &= (3-K_1)H_1^2 - K_2H_2^2 - K_3H_3^2 \\ &\quad - (2+K_4)H_4^2 - 4x_5^2 + x_6^2 \\ -4\frac{\partial H_3^2}{\partial x_6}x_5 + \frac{\partial H_3^2}{\partial x_5}x_6 &= H_4^2 \\ -4\frac{\partial H_1^2}{\partial x_6}x_5 + \frac{\partial H_1^2}{\partial x_5}x_6 &= 2H_2^2 - 3H_3^2 - 2x_5x_6, \end{aligned} \tag{28}$$

from which after substitution from (24) and comparing coefficients the following linear algebraic system

$$\mathbf{M}\boldsymbol{\alpha} = \boldsymbol{L} \tag{29}$$

for the coefficients $\alpha_{ijk}(j+k=2)$ follows. For notational simplicity the coefficients have been collected in the vector

$$\boldsymbol{\alpha}^T = (\alpha_{120}, \alpha_{111}, \alpha_{102}, \alpha_{220}, \alpha_{211}, \alpha_{202}, \alpha_{320}, \alpha_{311}, \alpha_{302}, \alpha_{420}, \alpha_{411}, \alpha_{402}).$$

The matrix $\mathbf{M}$ is given by

$$\mathbf{M} = \begin{pmatrix}
0 & -4 & 0 & -1 & 0 & 0 & 0 & 0 & 0 & 0 & 0 & 0 \\
2 & 0 & -8 & 0 & -1 & 0 & 0 & 0 & 0 & 0 & 0 & 0 \\
0 & 1 & 0 & 0 & 0 & -1 & 0 & 0 & 0 & 0 & 0 & 0 \\
K_1-3 & 0 & 0 & K_2 & -4 & 0 & K_3 & 0 & 0 & 2+K_4 & 0 & 0 \\
0 & K_1-3 & 0 & 2 & K_2 & -8 & 0 & K_3 & 0 & 0 & 2+K_4 & 0 \\
0 & 0 & K_1-3 & 0 & 1 & K_2 & 0 & 0 & K_3 & 0 & 0 & 2+K_4 \\
0 & 0 & 0 & 0 & 0 & 0 & 0 & -4 & 0 & -1 & 0 & 0 \\
0 & 0 & 0 & 0 & 0 & 0 & 2 & 0 & -8 & 0 & -1 & 0 \\
0 & 0 & 0 & 0 & 0 & 0 & 0 & 1 & 0 & 0 & 0 & -1 \\
0 & 0 & 0 & -2 & 0 & 0 & 3 & 0 & 0 & 0 & -4 & 0 \\
0 & 0 & 0 & 0 & -2 & 0 & 0 & 3 & 0 & 2 & 0 & -8 \\
0 & 0 & 0 & 0 & 0 & -2 & 0 & 0 & 3 & 0 & 1 & 0
\end{pmatrix} \tag{31}$$

The right-hand side of (29) is

$$\boldsymbol{L}^T = (0,0,0,-4,0,1,0,0,0,0,-2,0). \tag{32}$$

Inserting $\mathbf{x}_s = \mathbf{H}^{(2)}(\mathbf{x}_c)$ into the critical part of (17) we obtain the bifurcation equation (19). Up to third-order terms in the bifurcation equations we have

$$\begin{aligned} x_5' &= x_6 \\ x_6' &= -4x_5 - 2H_2^2 x_6 + 2H_4^2 x_5 + \tfrac{8}{3}x_5^3 + O(|\mathbf{x}_c|^4). \end{aligned} \tag{33}$$

We note that there are no quadratic nonlinearities in the bifurcation equations which determine the nonlinear stability of the out of plane oscillations.

5. NONLINEAR STABILITY ANALYSIS

Introducing the linear transformation $x_5 = z_1$ and $x_6 = -2z_2$ in (33) we obtain equations in the linear normal form for a Hopf bifurcation

$$\begin{aligned} z_1' &= -2z_2 \\ z_2' &= 2z_1 + a_{30}z_1^3 + a_{21}z_1^2 z_2 + a_{12}z_1 z_2^2 + a_{03}z_2^3 \end{aligned} \tag{34}$$

with the coefficients

$$\begin{aligned} a_{30} &= -\tfrac{4}{3} - \alpha_{420}, \qquad a_{21} = 2(\alpha_{411} - \alpha_{220}), \\ a_{12} &= 4(\alpha_{211} - \alpha_{402}), \qquad a_{03} = -8\alpha_{202}. \end{aligned} \tag{35}$$

Equations (34) present still a complicated stability problem for $z_1 = z_2 = 0$,

simplification of (34) is possible without changing the qualitative stability properties of the equilibrium. This can be done by "normal form theory" as it is explained in detail in [3, 5]. However, here the simpler approach by means of the "averaging principle" will be applied as it is explained in [3, Chap. 6.1].

For the application of the averaging principle we transform (34) to polar coordinates $z_1 = \sqrt{\mu}r\cos\varphi$, $z_2 = \sqrt{\mu}r\sin\varphi$ where μ is a *small* scaling factor. (34) then reads

$$\begin{aligned} r' &= \mu S(r,\varphi) \\ \varphi' &= 2 + \mu T(r,\varphi). \end{aligned} \tag{36}$$

Here $S(r,\varphi)$ and $T(r,\varphi)$ are 2π-periodic functions in φ given by

$$\begin{aligned} S(r,\varphi) &= r^3\big(a_{30}\cos^3\varphi\sin\varphi + a_{21}\cos^2\varphi\sin^2\varphi \\ &\qquad + a_{12}\cos\varphi\sin^3\varphi + a_{03}\sin^4\varphi\big) \\ T(r,\varphi) &= r^2\big(a_{30}\cos^4\varphi + a_{21}\cos^3\varphi\sin\varphi \\ &\qquad + a_{12}\cos^2\varphi\sin^2\varphi + a_{03}\cos\varphi\sin^3\varphi\big) \end{aligned}$$

The averaging principle now states that the behavior of the flow of system (36) and the "averaged system"

$$\begin{aligned} \overline{r}' &= \mu\widehat{S}(\overline{r}) = \mu A\overline{r}^3 \\ \overline{\varphi}' &= 2 + \mu\widehat{T}(\widehat{r}) = 2 + \mu B\overline{r}^2 \end{aligned}$$

is qualitatively the same [6]. Here the right-hand sides are calculated as the averaged values of S and T given by

$$\begin{aligned} \widehat{S} &= \frac{1}{2\pi}\int_0^{2\pi} S(\overline{r},\overline{\varphi})d\overline{\varphi} = \tfrac{1}{8}(3a_{03} + a_{21})\overline{r}^3 = A\overline{r}^3 \\ \widehat{T} &= \frac{1}{2\pi}\int_0^{2\pi} T(\overline{r},\overline{\varphi})d\overline{\varphi} = \tfrac{1}{8}(3a_{30} + a_{12})\overline{r}^2 = B\overline{r}^2. \end{aligned}$$

Hence, the stability analysis of the out-of-plane motion has been reduced to the question of whether the coefficient $A = (3a_{03} + a_{21})/8$ is negative. Of course, we are especially interested to know how the control parameters K_1, K_2, K_3, K_4 influence A. With (35) we obtain

$$A = -3\alpha_{202} + \tfrac{1}{4}(\alpha_{411} - \alpha_{220}). \tag{37}$$

The coefficients $\alpha_{202}, \alpha_{411}$, and α_{220} follow from (29). The solution of (29)

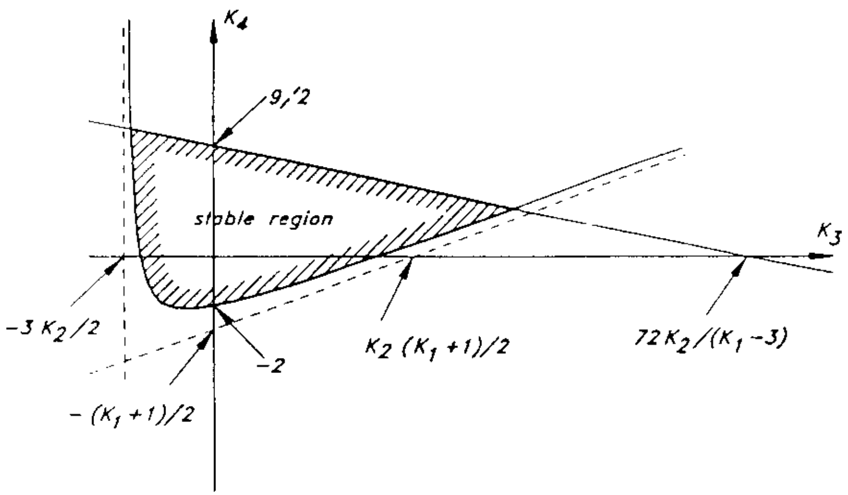

FIG. 3. Stability boundary in K_3, K_4 control parameter space for $K_1 > 3$ and $K_2 > 0$. The whole area above the hyperbola is the stable domain of the linear system following from the conditions (12). The restriction below the straight line follows from the nonlinear condition (38).

Hence we are able to obtain an explicit stability condition in the form

$$A = \frac{K_1(-104K_2 + (K_1 - 3)K_3 + 16K_2(2 + K_4))}{K_1((32K_4 + 13K_1 - 208)^2 + (52K_2 - 8K_3)^2 + 208^2)} < 0. \qquad (38)$$

Since the denominator (the determinant of $\mathbf{M}$ given by (31)) after canceling of K_1 is positive for all control parameters the inequality reduces to

$$-104K_2 + (K_1 - 3)K_3 + 16K_2(2 + K_4) < 0. \qquad (39)$$

Condition (39) in addition to conditions (12) following from the linearized stability analysis define now the stability region for the control parameters. We follow now the representation given in [1]. There, for fixed values $K_1 > 3$ and $K_2 > 0$ the stability conditions (12) are plotted in the K_3, K_4 parameter plane. The result is shown in Figure 3 where the stable region for the linear problem is above the hyperbola. However, the nonlinear stability condition in addition reduces the domain from an unlimited one to a finite one. This is a very important result from a practical point of view because it shows that too large values K_3, K_4 to effect ϑ and ϑ' in the linearized control problem will have a destabilizing effect on the out of plane motion.

This research project has been supported by the Austrian Science Foundation (FWF) under the project P07003.

REFERENCES

1. P. M. Bainum and V. K. Kumar, Optimal control of the shuttle-tethered-subsatellite system, *Acta Astronautica* 7:1333–1348 (1980).
2. C. C. Rupp, A Tether Tension Control Law for Tethered Subsatellites Deployed along the Local Vertical, Technical Report TMX-64963, NASA, 1975.
3. H. Troger and A. Steindl, *Nonlinear Stability and Bifurcation Theory. An Introduction for Engineers and Applied Scientists*, Springer-Verlag, Vienna, New York, 1991.
4. J. Carr, *Applications of Centre Manifold Theory*, Vol. 35, Applied Mathematical Sciences, Springer–Verlag, New York, Heidelberg, Berlin, 1981.
5. J. Guckenheimer and P. Holmes, *Nonlinear Oscillations, Dynamical Systems, and Bifurcations of Vector Fields*, Vol. 42, Applied Mathematical Sciences, Springer–Verlag, Berlin, Heidelberg, New York, 1983.
6. U. Kirchgraber and E. Stiefel, *Methoden der analytischen Störungsrechnung und ihre Anwendungen*, B. G. Teubner, Stuttgart, 1978.

(vii) The determinacy of bifurcation equations in several variables, for example, equations (4.15) and (4.18) is not always easy to decide if some of the coefficients of third order are zero (Section 6.3).

4.2 Loss of stability of periodic motions: an example from robotics

In this section, we explain an important step in the stability analysis of periodic motions, namely, the explicit calculation of the lowest order nonlinear terms of the corresponding Poincaré mapping.

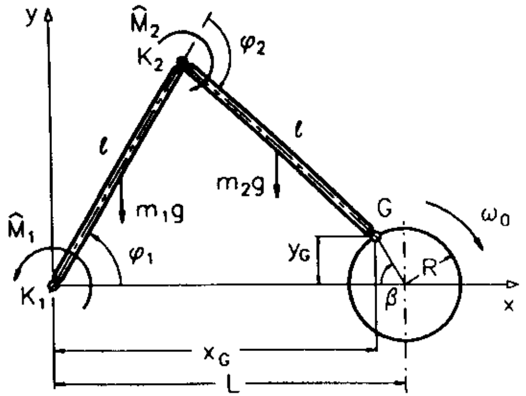

Figure 4.12. Mechanical model of a simple planar two bar robot under the action of two drive moments $\hat{M}_1, \hat{M}_2$ yielding a prescribed circular motion of the endpoint G

We perform these calculations when investigating the dynamics of the simple robot sketched in Fig. 4.12. For example, such robots are used in the automobile manufacturing industry for painting. During such operations, the automobile is passing along the robot endpoint G with constant speed, while the robot endpoint G performs a prescribed motion. At the robot endpoint a painting device (spray pistol) may be mounted. For such a painting process, stability problems can become important, especially when parameters are varied. First, if the speed of the assembly line is increased, the endpoint of the robot must move faster and, hence, a loss of stability of the basic, periodic motion can occur if the parameters of the controller are kept fixed. Second, a change of the spray pistol to one with different mass can also result in a loss of stability of the prescribed motion.

4.2.1 Mechanical model and equations of motion

The mechanical model is a double pendulum with two drive moments $\hat{M}_1$ and $\hat{M}_2$ acting at its hinges. The motion of the endpoint G is assumed to follow a circle with constant angular velocity ω_0. Making use of Lagrange's equations we obtain ([87])

$$\begin{pmatrix} \frac{\varrho}{3} + \frac{4}{3} + \cos\varphi_2 & -\left(\frac{1}{3} + \frac{1}{2}\cos\varphi_2\right) \\ -\left(\frac{1}{3} + \frac{1}{2}\cos\varphi_2\right) & \frac{1}{3} \end{pmatrix} \begin{pmatrix} \ddot{\varphi}_1 \\ \ddot{\varphi}_2 \end{pmatrix} +$$
$$+ \begin{pmatrix} k_1 & 0 \\ 0 & k_2 \end{pmatrix} \begin{pmatrix} \dot{\varphi}_1 \\ \dot{\varphi}_2 \end{pmatrix} + \begin{pmatrix} \frac{1}{2}\dot{\varphi}_2(\dot{\varphi}_2 - 2\dot{\varphi}_1)\sin\varphi_2 \\ \frac{1}{2}\dot{\varphi}_1^2 \sin\varphi_2 \end{pmatrix} + \tag{4.25}$$
$$+ k_G \begin{pmatrix} \left(\frac{\varrho}{2} + 1\right)\cos\varphi_1 + \frac{1}{2}\cos(\varphi_2 - \varphi_1) \\ -\frac{1}{2}\cos(\varphi_2 - \varphi_1) \end{pmatrix} = \begin{pmatrix} M_1 \\ M_2 \end{pmatrix},$$

where the following dimensionless quantities (Fig. 4.12)

$$\varrho = \frac{m_1}{m_2}, \quad t = \tau\omega_0, \quad M_i = \frac{\hat{M}_i}{m_2\ell^2\omega_0^2}, \quad k_i = \frac{K_i}{m_2\ell^2\omega_0}, \quad k_G = \frac{g}{\omega_0^2\ell}$$

are used.

The components φ_1, φ_2 of the vector $\varphi = (\varphi_1, \varphi_2)^T$ are the two degrees of freedom and $\mathbf{M} = (M_1, M_2)^T$ is the vector of the drive moments, acting at the hinges of the robot. k_i are the viscous friction coefficients in the joints and k_G is a gravitational constant.

To obtain the prescribed circular motion of the endpoint G, the first thing to do is the calculation of the moment $\mathbf{M}(t) = \mathbf{M}_0(t)$. This requires the solution of the so-called inverse problem of robotics and is done in [87] for this special problem. More generally it is treated in [34]. The goal of this analysis is to express the left-hand side of (4.25) by the coordinates

$$\begin{aligned} x_G &= L - r\cos\beta \\ y_G &= r\sin\beta \end{aligned} \tag{4.26}$$

and their derivatives under the condition

$$\dot{\beta} = \omega_0 = \text{const.} \tag{4.27}$$

One starts with $x_G(t)$ and $y_G(t)$ in the form

$$\begin{aligned} x_G &= \ell(\cos\varphi_1 + \cos(\varphi_2 - \varphi_1)) \\ y_G &= \ell(\sin\varphi_1 - \sin(\varphi_2 - \varphi_1)), \end{aligned} \tag{4.28}$$

which follow from Fig. 4.12. The dependence of all quantities ($\ddot{\varphi}_1, \ddot{\varphi}_2, \dot{\varphi}_1, \dot{\varphi}_2, \cos\varphi_1, \cos\varphi_2, \cos(\varphi_2-\varphi_1), \sin\varphi_2$) appearing on the left-hand side of (4.25) on ($x_G, y_G, \dot{x}_G, \dot{y}_G, \ddot{x}_G$ and $\ddot{y}_G$) can be calculated by lengthy, but straightforward calculations ([87], [34]). For example, one obtains for $\dot{\varphi}_2$ the following expression

$$\dot{\varphi}_2 = -2\frac{x_G\dot{x}_G + y_G\dot{y}_G}{(x_G^2+y_G^2)(4\ell^2 - x_G^2 - y_G^2)} . \tag{4.29}$$

If we introduce these quantities into the left-hand side of (4.25), the two components of $\mathbf{M}_0(t)$ are obtained in their dependence on the motion of the endpoint G. These give rise to a periodic motion $\varphi_0(t)$, which is the basic state to be investigated for its stability. In order to formulate the stability problem, a control loop (Fig. 4.13) must be superposed to

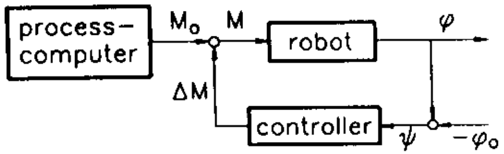

Figure 4.13. Control loop for the robot

the system. The task of the controller is to correct deviations from the prescribed motion. Mathematically this can be done by introducing new coordinates $\boldsymbol{\psi} = (\psi_1, \psi_2)^T$ in the form

$$\varphi_i = \varphi_{0i} + \psi_i \qquad i = 1, 2 . \tag{4.30}$$

These new coordinates can be interpreted as deviations or perturbations from the fundamental motion. To force the robot back to its required motion the drive moment $\mathbf{M}_0$ must be corrected. We express this in the following way

$$M_i = M_{0i} + \Delta M_i \qquad i = 1, 2. \tag{4.31}$$

Now we transform to a system of first order equations by setting

$$x_1 = \psi_1, \qquad x_2 = \dot{\psi}_1, \qquad x_3 = \psi_2, \qquad x_4 = \dot{\psi}_2. \tag{4.32}$$

The resulting equations of motion can be written in the form

$$\dot{\boldsymbol{x}} = \overline{\mathbf{A}}(t,\boldsymbol{\lambda})\boldsymbol{x} + \mathbf{C}(t,\boldsymbol{\lambda})\boldsymbol{u} + \mathbf{f}(t,\boldsymbol{x},\dot{\boldsymbol{x}},\boldsymbol{\lambda}) \tag{4.33}$$

where $\boldsymbol{x}, \mathbf{f} \in \mathbf{R}^4$, $\overline{\mathbf{A}}$ is a 4×4 matrix, $\boldsymbol{u} = (\Delta M_1, \Delta M_2)^T$ and C is a 4×2 matrix. The vector $\mathbf{f}$ contains terms up to third order which have been obtained from a series expansion of the nonlinear terms in (4.25).

To eliminate the vector $\boldsymbol{u}$ from (4.33), a control law must be introduced. A simple compensation of the deviation from the prescribed motion is stipulated. Hence, the following relations are introduced:

$$u_1 = \Delta M_1 = Rx_1, \qquad u_2 = \Delta M_2 = \frac{1}{3}Rx_3 . \tag{4.34}$$

To keep the number of parameters as small as possible, only one controller constant R is used which, of course, must have a negative value. To obtain a first order system, we substitute (4.34) into (4.33) and express the terms containing $\dot{\boldsymbol{x}}$ in $\mathbf{f}$ in (4.33) by means of its linear and quadratic terms, as it is explained in Appendix O.2. This yields

$$\dot{\boldsymbol{x}} = \mathbf{A}(t,\boldsymbol{\lambda})\boldsymbol{x} + \mathbf{f}_2(t,\boldsymbol{x},\boldsymbol{\lambda}) + \mathbf{f}_3(t,\boldsymbol{x},\boldsymbol{\lambda}) + O(|\boldsymbol{x}|^4) \tag{4.35}$$

where $\mathbf{A}(t,\boldsymbol{\lambda})$, $\mathbf{f}_2(t,\boldsymbol{x},\boldsymbol{\lambda})$ and $\mathbf{f}_3(t,\boldsymbol{x},\boldsymbol{\lambda})$ are periodic in t with the period T of the given fundamental motion of the robot and the vectors $\mathbf{f}_2$ and $\mathbf{f}_3$ contain nonlinear functions of the variables of second and third order, respectively. The parameter vector $\boldsymbol{\lambda}$ is two-dimensional and given by

$$\boldsymbol{\lambda} = \begin{pmatrix} \omega_0 \\ R \end{pmatrix} \tag{4.36}$$

with ω_0 defined by (4.27) and R by (4.34).

4.2.2 Calculation of the power series expansion of the Poincaré mapping

The stability analysis of the prescribed periodic motion $\varphi_0(t) = \varphi_0(t+T)$ reduces in the formulation of (4.35) to the investigation of the trivial solution

$$\boldsymbol{x}_0(t) = \mathbf{0}. \tag{4.37}$$

For a linearized stability analysis of $\boldsymbol{x}_0$ *Floquet theory* ([103]) could be used. However, we will soon see that the investigation of the Poincaré mapping includes the linear stability analysis supplied by Floquet's theory ([7] p. 282). In the case under investigation, the calculation of the Poincaré mapping, that is, the calculation of the points of intersection with a transversal surface is not very difficult. Because of the T-periodicity of (4.35) we only have to calculate the solution at time $T, 2T, \ldots$ and so on. The result of these calculations is sometimes called a *time-T* mapping. From Fig. 4.14 follows that the trajectory $\boldsymbol{x}(\boldsymbol{x}_1, t)$ leaving $\boldsymbol{x}_1$, in the neighborhood of the periodic solution $\boldsymbol{x}_0$, hits the surface again at $\boldsymbol{x}_2$. Hence, the following equation results

$$\boldsymbol{x}_2 = \mathbf{P}(\boldsymbol{x}_1) = \boldsymbol{x}(\boldsymbol{x}_1, T), \tag{4.38}$$

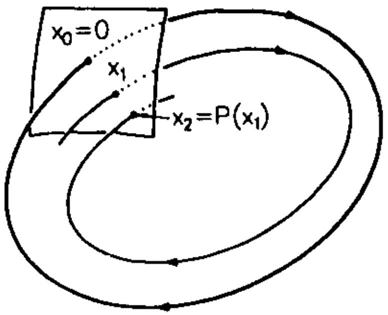

Figure 4.14. Poincaré mapping in the neighborhood of the periodic solution x_0

where in the notation of Section 2.1, $\mathbf{P}_T$ instead of $\mathbf{P}$ should have been used. However, since T is fixed, we omit the index.

To calculate the Poincaré mapping in the neighborhood of the periodic solution, which is given by the fixed point $\boldsymbol{x}_0$ in the surface of section, the following formal power series expansion

$$\mathbf{P}(\boldsymbol{x}_0+\boldsymbol{\xi}) = \mathbf{P}(\boldsymbol{x}_0) + \mathbf{P}'(\boldsymbol{x}_0)\boldsymbol{\xi} + \frac{1}{2}\mathbf{P}''(\boldsymbol{x}_0)(\boldsymbol{\xi},\boldsymbol{\xi}) + \frac{1}{6}\mathbf{P}'''(\boldsymbol{x}_0)(\boldsymbol{\xi},\boldsymbol{\xi},\boldsymbol{\xi}) + \dots \tag{4.39}$$

is introduced, where $\mathbf{P}(\boldsymbol{x}_0) = \boldsymbol{x}_0$, because $\boldsymbol{x}(\boldsymbol{x}_0, T) = \boldsymbol{x}_0$. $\mathbf{P}'(\boldsymbol{x}_0)$, $\mathbf{P}''(\boldsymbol{x}_0)$, $\mathbf{P}'''(\boldsymbol{x}_0), \dots$ are obtained from the solution of a series of initial value problems. This is easy to understand if (4.38) is written in the form

$$\mathbf{P}(\boldsymbol{x}_0+\boldsymbol{\xi}) = \boldsymbol{x}(\boldsymbol{x}_0+\boldsymbol{\xi}, T) = \boldsymbol{x}(\boldsymbol{x}_0, T) + \frac{\partial \boldsymbol{x}}{\partial \boldsymbol{x}_0}(\boldsymbol{x}_0, T)\boldsymbol{\xi} + \tag{4.40}$$

$$+\frac{1}{2}\frac{\partial^2 \boldsymbol{x}}{\partial \boldsymbol{x}_0^2}(\boldsymbol{x}_0, T)(\boldsymbol{\xi},\boldsymbol{\xi}) + \frac{1}{6}\frac{\partial^3 \boldsymbol{x}}{\partial \boldsymbol{x}_0^3}(\boldsymbol{x}_0, T)(\boldsymbol{\xi},\boldsymbol{\xi},\boldsymbol{\xi}) + \dots$$

where $\boldsymbol{x}_1 = \boldsymbol{x}_0 + \boldsymbol{\xi}$ is used. Comparing (4.39) and (4.40) yields

$$\mathbf{P}'(\boldsymbol{x}_0) = \frac{\partial \boldsymbol{x}}{\partial \boldsymbol{x}_0}(\boldsymbol{x}_0, T), \qquad \mathbf{P}''(\boldsymbol{x}_0) = \frac{\partial^2 \boldsymbol{x}}{\partial \boldsymbol{x}_0^2}(\boldsymbol{x}_0, T), \qquad \dots \tag{4.41}$$

To calculate $\partial \boldsymbol{x}/\partial \boldsymbol{x}_0$ the differential equation (4.35) is written in the form

$$\dot{\boldsymbol{x}} = \mathbf{F}(\boldsymbol{x}, t). \tag{4.42}$$

Taking the derivative of both sides of (4.42) with respect to $\boldsymbol{x}_0$, we obtain a differential equation for $\partial \boldsymbol{x}/\partial \boldsymbol{x}_0$ in the form

$$\left(\frac{\partial \boldsymbol{x}}{\partial \boldsymbol{x}_0}\right)^{\cdot} = \frac{\partial \mathbf{F}}{\partial \boldsymbol{x}}\frac{\partial \boldsymbol{x}}{\partial \boldsymbol{x}_0}. \tag{4.43}$$

To obtain the first term in (4.41), the system (4.43) of 4×4 linear homogeneous differential equations must be integrated from $t=0$ until $t=T$, with initial conditions $\partial \boldsymbol{x}/\partial \boldsymbol{x}_0\ (\mathbf{0}) = \mathbf{E}$, where $\mathbf{E}$ is the unit matrix. To calculate the next term in (4.41), the derivative of (4.43) with respect to $\boldsymbol{x}_0$ is taken, resulting in

$$\left(\frac{\partial^2 \boldsymbol{x}}{\partial \boldsymbol{x}_0^2}\right)^{\cdot} = \frac{\partial \mathbf{F}}{\partial \boldsymbol{x}}\frac{\partial^2 \boldsymbol{x}}{\partial \boldsymbol{x}_0^2} + \frac{\partial^2 \mathbf{F}}{\partial \boldsymbol{x}^2}\left(\frac{\partial \boldsymbol{x}}{\partial \boldsymbol{x}_0}\right)^2. \tag{4.44}$$

This system of $4\times 4\times 4$ linear inhomogeneous differential equations must be integrated from $t=0$ until $t=T$, with initial conditions $\partial^2 \boldsymbol{x}/\partial \boldsymbol{x}_0^2\ (\mathbf{0}) = \mathbf{0}$. Proceeding in this way, the coefficients of the third and higher order terms can be calculated. Of course, this process of numerical calculation of the higher order terms becomes computationally intense, if the dimension of (4.35) is large.

Introducing the notation $\boldsymbol{x}_2 = \boldsymbol{x}_0 + \boldsymbol{\xi}_{t+1}$ and $\boldsymbol{x}_1 = \boldsymbol{x}_0 + \boldsymbol{\xi}_t$ we obtain from (4.39) as result of these calculations the discrete dynamical system

$$\boldsymbol{\xi}_{t+1} = \mathbf{L}(\boldsymbol{\lambda})\boldsymbol{\xi}_t + \mathbf{Q}_2(\boldsymbol{\xi}_t,\boldsymbol{\xi}_t,\boldsymbol{\lambda}) + \mathbf{Q}_3(\boldsymbol{\xi}_t,\boldsymbol{\xi}_t,\boldsymbol{\xi}_t,\boldsymbol{\lambda}) + h.o.t. \tag{4.45}$$

in the form (3.34), where $\boldsymbol{\xi}_t \in \mathbf{R}^4$ and $\boldsymbol{\lambda} \in \mathbf{R}^2$. $\mathbf{Q}_2, \mathbf{Q}_3, \dots \in \mathbf{R}^4$ are vectors, the components of which are quadratic, cubic and higher order terms in the variables, respectively. For example, the first component of $\mathbf{Q}_2$ is of the form: $\sum_{i,j=1}^{4} \alpha_{1ij}(\boldsymbol{\lambda})\xi_{ti}\xi_{tj}$.

4.2.3 Stability boundary in parameter space

In order to investigate the stability of the fixed point $\boldsymbol{\xi}_t = \mathbf{0}$ which corresponds to the periodic solution $\varphi_0(t)$ given by (4.37), we study the linear part of (4.45). The corresponding matrix

$$\mathbf{L}(\boldsymbol{\lambda}) = \mathbf{P}'(\boldsymbol{x}_0) = \frac{\partial \boldsymbol{x}}{\partial \boldsymbol{x}_0}(\boldsymbol{x}_0, T) \tag{4.46}$$

is exactly the matrix also obtained using Floquet's theory. For a quasistatic variation of the distinguished parameter ω_0 (given by (4.27)) with the second parameter R (given by (4.34)) kept at a fixed value, we calculate the eigenvalues of (4.46). From the conditions given in Section 3.1.2, we know that the critical eigenvalues are those with modulus equal to one. Hence, we pick a parameter value of $\boldsymbol{\lambda}$ according to (4.36) such that all eigenvalues have modulus smaller than one. Now, ω_0 is increased quasistatically until the first time an eigenvalue μ with modulus equal to one is reached. Typically, in one parameter families only three different cases can occur ([7] p. 284 and Fig. 4.15):

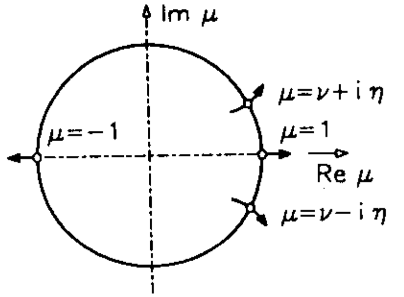

Figure 4.15. The typical cases of loss of stability in one parameter families of mappings are the three cases: $\mu = 1$; $\mu = -1$; $\mu = \nu \pm i\eta$, $|\mu| = 1$

$$
\begin{array}{lrcll}
(1) & \mu & = & 1 & \\
(2) & \mu & = & -1 & \\
(3) & \mu & = & \nu \pm i\eta & |\mu| = 1.
\end{array}
\tag{4.47}
$$

(1), (2) and (3) are called *saddle-node, flip* and *Hopf* bifurcation, respectively. These names will become clear from the analysis of the nonlinear cases in Section 6.6.3. In Fig. 4.16, the stability boundary in the

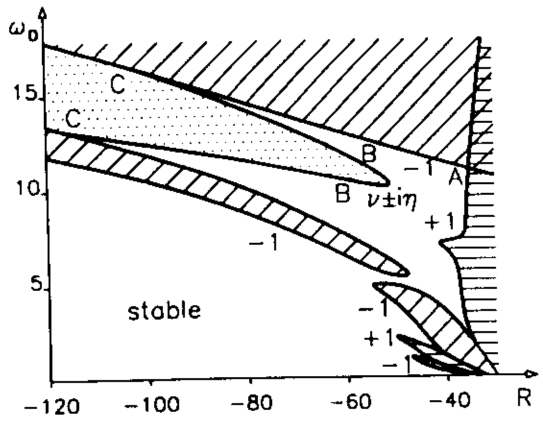

Figure 4.16. Stability boundary ω_{0c} in ω_0, R parameter space. Different types of loss of stability occur according to the critical eigenvalues $1, -1$ and $|\nu \pm i\eta| = 1$

(ω_0, R) parameter plane is shown. In the range of R shown in Fig. 4.16 ($-120 \leq R \leq -30$), the first instability obtained by increasing ω_0 is almost always due to a flip bifurcation ($\mu = -1$). However, saddle-node

bifurcations can also occur. If the system is operated at values of ω_0 bigger than those leading to the first instability region also Hopf bifurcations can occur. Above the first instability region parameter domains exist where the original periodic motion is again stable. This behavior can be explained from the fact that these bifurcations result from resonance phenomenona (parametric resonances).

4.2.4 Center manifold reduction

By the transformation of coordinates (3.40), the discrete dynamical system (4.45) takes the form (3.41) and after a proper rearrangement the form of (3.42).

We give now the explicit calculations of one and two dimensional bifurcation equations for the cases $\mu = 1$ and $\mu = \nu \pm i\eta$.

$\mu_1 = 1$: Saddle-node bifurcation

In this case, $n_c = 1$ and (3.42) takes the form

$$
\begin{aligned}
y_{t+1,1} &= y_{t,1} + g_1(y_{t,1}, y_{t,i}) = y_{t,1} + \sum_{j,k=1}^{4} a_{1jk} y_{t,j} y_{t,k} + \\
&\quad + \sum_{j,k,\ell=1}^{4} a_{1jk\ell} y_{t,j} y_{t,k} y_{t,\ell} + \ldots \qquad (4.48) \\
y_{t+1,i} &= \mu_i y_{t,i} + g_i(y_{t,1}, y_{t,i}), \qquad i = 2,3,4
\end{aligned}
$$

where for simplicity it has been assumed that the remaining eigenvalues μ_i ($i = 2,3,4$) are distinct and real. From (3.43) follows

$$y_{t,i} = h_i(y_{t,1}) \qquad i = 2,3,4.$$

For the calculation, we use the approximation $\mathbf{H}$ of $\mathbf{h}$ in the form

$$y_{t,i} = H_i(y_{t,1}) = \alpha_{i,2} y_{t,1}^2 + \alpha_{i,3} y_{t,1}^3 + \ldots, \tag{4.49}$$

which starts with at least quadratic terms considering the general property (3.18). To calculate the coefficients $\alpha_{i,j}$, we substitute (4.49) according to (3.45) into $(4.48)_2$ where use is made of $(4.48)_1$ to find

$$
\begin{aligned}
&\alpha_{i,2}[y_{t,1} + g_1(y_{t,1}, H_i(y_{t,1}))]^2 + \alpha_{i,3}[y_{t,1} + g_1(y_{t,1}, H_i(y_{t,1}))]^3 + \ldots \\
&\quad - \mu_i(\alpha_{i,2} y_{t,1}^2 + \alpha_{i,3} y_{t,1}^3 + \ldots) - g_i(y_{t,1}, H_i(y_{t,1})) = O(|y_{t,1}|^3). \qquad (4.50)
\end{aligned}
$$

We calculate the approximation $\mathbf{H}$ in (4.50) only up to quadratic terms. This approximation will give us bifurcation equations, correct up to and including third order terms as is explained in detail in Section 3.1.1. The quadratic terms follow from (4.50) to

$$\alpha_{i,2}y_{t,1}^2 - \mu_i\alpha_{i,2}y_{t,1}^2 - g_{i,2}y_{t,1}^2 = 0, \tag{4.51}$$

where $g_{i,2}$ are the coefficients of the quadratic terms in the series expansion of the nonlinear function g_i. From (4.51), we obtain the coefficients

$$\alpha_{i,2} = \frac{g_{i,2}}{1-\mu_i} \qquad i = 2,3,4. \tag{4.52}$$

Inserting (4.52) into $(4.48)_1$ gives the one-dimensional, third order bifurcation equation

$$y_{t+1,1} = y_{t,1} + a_{111}y_{t,1}^2 + (a_{1111} + a_{112}\alpha_{2,2} + a_{113}\alpha_{3,2} + a_{114}\alpha_{4,2})y_{t,1}^3 \dots \tag{4.53}$$

$\mu_{1,2} = \nu \pm i\eta$, $|\mu_{1,2}| = 1$: **Hopf bifurcation**

Now, $n_c = 2$. The most convenient way to handle this case is to use complex variables. Then system (3.41) takes the form

$$\begin{aligned} w_{t+1,1} &= \mu_1 w_{t,1} + g_1(w_{t,1}, \overline{w}_{t,1}, w_{t,j}, \overline{w}_{t,j}) \\ w_{t+1,j} &= \mu_j w_{t,j} + g_j(w_{t,1}, \overline{w}_{t,1}, w_{t,j}, \overline{w}_{t,j}) \end{aligned} \tag{4.54}$$

where in the robot example $j = 2$. In order to keep the treatment more general, $j = 2, \dots, N$ can be assumed. Here

$$w_{t,1} = y_{t,1} + iy_{t,2} \qquad \text{and} \qquad w_{t,1} = y_{t,1} - iy_{t,2}$$

are complex conjugate. Analogous to before, we set

$$w_{t,j} = H(w_{t,1}, \overline{w}_{t,1}) = \alpha_{11,j}w_{t,1}^2 + \alpha_{12,j}w_{t,1}\overline{w}_{t,1} + \alpha_{22,j}\overline{w}_{t,1}^2, \tag{4.55}$$

where from the outset, we look only for bifurcation equations $(4.54)_1$ of third order in $w_{t,1}, \overline{w}_{t,1}$. First, we write (4.55) for $(t+1)$

$$w_{t+1,j} = \alpha_{11,j}w_{t+1,1}^2 + \alpha_{12,j}|w_{t+1,1}|^2 + \alpha_{22,j}\overline{w}_{t+1,1}^2$$

and substitute for each $w_{t+1,1}$ from $(4.54)_1$ to find

$$w_{t+1,j} = \alpha_{11,j}\mu_1^2 w_{t,1}^2 + \alpha_{12,j}\mu_1\overline{\mu}_1 w_{t,1}\overline{w}_{t,1} + \alpha_{22,j}\overline{\mu}_1^2\overline{w}_{t,1}^2 + O(|w_1, \overline{w}_1|^3). \tag{4.56}$$

Second, we consider $(4.54)_2$ where we substitute (4.55) on the right-hand side to obtain

$$\begin{aligned} w_{t+1,j} &= \mu_j(\alpha_{11,j}w_{t,1}^2 + \alpha_{12,j}w_{t,1}\overline{w}_{t,1} + \alpha_{22,j}\overline{w}_{t,1}^2) + \\ &\quad + g_{11,j}w_{t,1}^2 + g_{12,j}w_{t,1}\overline{w}_{t,1} + g_{22,j}\overline{w}_{t,1}^2 + O(|w_1|^3). \end{aligned} \tag{4.57}$$

The $g_{k\ell,m}$ are the coefficients of the quadratic terms in the series expansion of g_m, $(m = 1, 2, \dots, N)$. Comparing the second order coefficients of (4.56) and (4.57), which corresponds to relation (3.45) with $q = 3$, we find

$$\begin{aligned} w_{t,1}^2 : &\qquad \alpha_{11,j}(\mu_1^2 - \mu_j) = g_{11,j} \\ w_{t,1}\overline{w}_{t,1} : &\qquad \alpha_{12,j}(\mu_1\overline{\mu}_1 - \mu_j) = g_{12,j} \\ \overline{w}_{t,1}^2 : &\qquad \alpha_{22,j}(\overline{\mu}_1^2 - \mu_j) = g_{22,j}\,. \end{aligned} \tag{4.58}$$

Inserting the coefficients $\alpha_{11,j}, \alpha_{12,j}, \alpha_{22,j}$ obtained from (4.58) into (4.55) and then (4.55) into $(4.54)_1$ results in third order bifurcation equations for the robot $(j = 2)$ in the form

$$\begin{aligned} w_{t+1,1} &= \mu_1 w_{t,1} + g_{11,1}w_{t,1}^2 + g_{12,1}w_{t,1}\overline{w}_{t,1} + g_{22,1}\overline{w}_{t,1}^2 + \\ &\quad + \sum_{k=0}^{3} a_{3-k,k,1}w_{t,1}^{3-k}\overline{w}_{t,1}^k \end{aligned}$$

or

$$\begin{aligned} w_{t+1} &= \mu_1 w_t + a_{20}w_t^2 + a_{11}w_t\overline{w}_t + a_{02}\overline{w}_t^2 + \\ &\quad + a_{30}w_t^3 + a_{21}w_t^2\overline{w} + a_{12}w_t\overline{w}_t^2 + a_{03}w_t^3 + O(|w_t, \overline{w}_t|^4) \end{aligned} \tag{4.59}$$

where we have omitted the index one.

The calculation of the coefficients of third order is straightforward. We do not write down their explicit form because in the further treatment of (4.59) it will turn out that in general not all coefficients are needed. In fact only one will be needed which follows from the application of the *normal form* theorem. This is explained in Section 6.1.

4.3 Loss of stability of finite- and infinite-dimensional statical systems

4.3.1 Buckling of a rod: discrete model

To explain the method of Ljapunov-Schmidt, we start with the double pendulum of Fig. 2.5a. This is one of the simplest examples of a model problem for buckling with more than one degree of freedom. It is a conservatively loaded system and if the load is applied quasistatically, the equilibrium equations can be derived from the potential function V (2.17). The bars are assumed to be massless. The torsional stiffnesses are $c_1 = c_2 = c$ and we divide V by c. Then from (2.17), we obtain the potential

$$V_1 = \frac{V}{c} = \frac{\psi_1^2}{2} + \frac{1}{2}(\psi_2 - \psi_1)^2 - F(2 - \cos\psi_1 - \cos\psi_2) \tag{4.60}$$

This results in two equations

$$\begin{aligned}\dot{\hat{r}} &= \varepsilon A\hat{r}^3 \\ \dot{\varphi} &= \omega + \varepsilon B\hat{r}^2 ,\end{aligned}$$

where the brackets in the following integrals for A and B are those from (6.47). Hence, we obtain

$$\begin{aligned}A &= \frac{1}{2\pi}\int_0^{2\pi}[a_{130}\cos^4\varphi + \ldots + a_{203}\sin^4\varphi]d\varphi \\ &= \frac{3}{8}(a_{130}+a_{203}) + \frac{1}{8}(a_{112}+a_{221}) \\ B &= \frac{1}{2\pi}\int_0^{2\pi}[a_{230}\cos^4\varphi + \ldots - a_{103}\sin^4\varphi]d\varphi \\ &= \frac{3}{8}(a_{230}-a_{103}) + \frac{1}{8}(a_{212}-a_{121}) .\end{aligned}$$

The expressions for A and B are identical to b_{21}^R and b_{21}^I in (6.41).

This example shows that not only a strong reduction of the complexity of the problem is possible by means of the averaging method, but also the close connection to normal form theory which is elaborated in [128].

A complete listing of the different normal forms for cases of codimension *one* and *two* together with the dependence of the coefficients in the normal form on the coefficients in the bifurcation equations which are obtained from the reduction process is given in Section 6.5.1. We give this listing in Section 6.5.1 because there we also include the unfolding parameters.

6.1.2 Time-discrete dynamical systems

We discuss the three cases of codimension *one* mentioned in Section 4.2.4.

We start with μ real. We can deal with the cases $\mu = +1$ (transcritical bifurcation) and $\mu = -1$ (flip bifurcation) simultaneously because after the center manifold reduction both are given by a one-dimensional bifurcation equation similar to (4.53). We write this equation following the notation of Section 6.1.1 in the form

$$y_{t+1} = \pm y_t + a_2y_t^2 + a_3y_t^3 + O(|y_t|^4) . \tag{6.55}$$

Similar to (6.2) the change of variables

$$y_t = z_t + h(z_t) \tag{6.56}$$

is introduced. First, we try to eliminate the second order term in (6.55). For this purpose, we assume

$$h(z_t) = \alpha_2 z_t^2 . \tag{6.57}$$

Considering (6.57) and inserting (6.56) into (6.55) we find

$$\begin{aligned}z_{t+1} + \alpha_2 z_{t+1}^2 &= \pm(z_t + \alpha_2 z_t^2) + \\ &\quad + a_2(z_t+\alpha_2 z_t^2)^2 + a_3 z_t^3 + O(|z_t|^4)\end{aligned}$$

or

$$\begin{aligned}z_{t+1} &= \pm(z_t + \alpha_2 z_t^2) - \\ &\quad - \alpha_2[\pm z_t \pm \alpha_2 z_t^2 + a_2 z_t^2 - \alpha_2 z_t^2]^2 + \\ &\quad + a_2(z_t+\alpha_2 z_t^2)^2 + a_3 z_t^3 + O(|z_t|^4)\end{aligned}$$

and finally

$$\begin{aligned}z_{t+1} &= \pm z_t + (\pm\alpha_2 - \alpha_2 + a_2)z_t^2 + \\ &\quad + [-2\alpha_2^2 \mp 2\alpha_2 a_2 \pm 2\alpha_2^2 + 2\alpha_2 a_2 + a_3]z_t^3 + \\ &\quad + O(|z_t|^4) .\end{aligned} \tag{6.58}$$

From (6.58) follows immediately that for $\mu = +1$, that is for the upper signs, the second order term cannot be removed. Hence, the normal form in this case is

$$z_{t+1} = z_t + A_2 z_t^2 + O(|z_t|^3) \tag{6.59}$$

where $A_2 = a_2$. However, if $\mu = -1$, that is for the lower signs in (6.58), the quadratic term can be removed for $\alpha_2 = a_2/2$ and the normal form reads

$$z_{t+1} = -z_t + A_3 z_t^3 + O(|z_t|^4) . \tag{6.60}$$

The coefficient A_3 is obtained from (6.58) by taking the lower signs and inserting the value $\alpha_2 = a_2/2$ to

$$A_3 = -4\alpha_2^2 + 4\alpha_2 a_2 + a_3 = a_2^2 + a_3 . \tag{6.61}$$

Second, we treat the Hopf bifurcation, that is, $\mu_{1,2} = \nu \pm i\eta$, $|\mu_{1,2}| = 1$. In this case after the center manifold reduction, the two-dimensional bifurcation system (4.59) is obtained which reads

$$w_{t+1} = \mu w_t + g(w_t, \overline{w}_t) \tag{6.62}$$

where

$$\begin{aligned}g(w_t,\overline{w}_t) &= a_{20}w_t^2 + a_{11}w_t\overline{w}_t + a_{02}\overline{w}_t^2 + \\ &\quad + a_{30}w_t^3 + a_{21}w_t^2\overline{w}_t + a_{12}w_t\overline{w}_t^2 + a_{03}\overline{w}_t^3 + \ldots\end{aligned} \tag{6.63}$$

We give the result for (6.62) in form of a *theorem* ([35] p. 242):

Theorem 6.1 (Hopf bifurcation of mappings) *If $g(w_t, \overline{w}_t)$ is given by* (6.63) *and μ is not a k-th root of unity for $k = 1, \ldots, 5$ then there exists a smooth change of coordinates*

$$w_t = v_t + h(v_t, \overline{v}_t) \tag{6.64}$$

that transforms (6.62) *into*

$$v_{t+1} = \mu v_t + A_{21} v_t^2 \overline{v}_t + O(|v_t|^5 + |\overline{v}_t|^5) \ . \tag{6.65}$$

Similar to the time-continuous case a very simple normal form (6.65) is obtained. There are no quadratic and fourth order terms, and only one cubic term.

In order to prove the theorem we begin by eliminating the second order terms in (6.63). We assume (6.64) to be given as

$$w_t = v_t + \alpha_{20} v_t^2 + \alpha_{11} v_t \overline{v}_t + \alpha_{02} \overline{v}_t^2 \ . \tag{6.66}$$

Inserting (6.66) into (6.62), we find

$$\begin{aligned} v_{t+1} &+ \alpha_{20} v_{t+1}^2 + \alpha_{11} v_{t+1} \overline{v}_{t+1} + \alpha_{02} \overline{v}_{t+1}^2 \\ &= \mu(v_t + \alpha_{20} v_t^2 + \alpha_{11} v_t \overline{v}_t + \alpha_{02} \overline{v}_t^2) + \\ &\quad + a_{20} v_t^2 + a_{11} v_t \overline{v}_t + a_{02} \overline{v}_t^2 + \\ &\quad + [a_{21} + 2a_{20}\alpha_{11} + a_{11}(\alpha_{20} + \overline{\alpha}_{11}) + 2a_{02}\overline{\alpha}_{02}] v_t^2 \overline{v}_t + \ldots \end{aligned} \tag{6.67}$$

Similarly as it was done for the time-continuous case the coefficient of the third order term $v_t^2 \overline{v}_t$ is also calculated. Inserting on the left-hand side of (6.67) for v_{t+1}^2 from the difference equation we obtain

$$\begin{aligned} v_{t+1} = \ & \mu v_t + \mu(\alpha_{20} v_t^2 + \alpha_{11} v_t \overline{v}_t + \alpha_{02} \overline{v}_t^2) + \\ & + a_{20} v_t^2 + a_{11} v_t \overline{v}_t + a_{02} \overline{v}_t^2 - \\ & - \alpha_{20} \mu^2 v_t^2 - \alpha_{11} \mu \overline{\mu} v_t \overline{v}_t - \alpha_{02} \overline{\mu}^2 \overline{v}_t^2 + O(|v_t|^3 + |\overline{v}_t|^3) \end{aligned}$$

and a similar expression for $\overline{v}_{t+1}$. Writing out only the quadratic terms this expression becomes

$$\begin{aligned} v_{t+1} = \ & \mu v_t + (-\mu^2 \alpha_{20} + \mu \alpha_{20} + a_{20}) v_t^2 + \\ & + (-\mu \overline{\mu} \alpha_{11} + \mu \alpha_{11} + a_{11}) v_t \overline{v}_t + \\ & + (-\overline{\mu}^2 \alpha_{02} + \mu \alpha_{02} + a_{02}) \overline{v}_t^2 \ . \end{aligned} \tag{6.68}$$

The second order terms in (6.68) can be annihilated by setting

$$\alpha_{20} = -\frac{a_{20}}{\mu - \mu^2} \ , \qquad \alpha_{11} = -\frac{a_{11}}{\mu - \mu \overline{\mu}} \ , \qquad \alpha_{02} = -\frac{a_{02}}{\mu - \overline{\mu}^2} \ . \tag{6.69}$$

However, $\mu - \overline{\mu}^2 = (\mu^3 - 1)/\mu^2$ vanishes if $\mu^3 - 1 = 0$. Hence, in this case of third order resonance the quadratic term $\overline{v}^2$ cannot be removed. The coefficient A_{21} of the third order term $v_t^2 \overline{v}_t$, after the second order terms had been eliminated, follows from (6.67) to

$$A_{21} = a_{21} + 2\alpha_{11} a_{20} + (\overline{\alpha}_{11} + \alpha_{20}) a_{11} + 2\overline{\alpha}_{02} a_{02} \ . \tag{6.70}$$

Thus, we can write the difference equation with third order terms as

$$w_{t+1} = \mu w_t + A_{30} w_t^3 + A_{21} w_t^2 \overline{w}_t + A_{12} w_t \overline{w}_t^2 + A_{03} \overline{w}_t^3 \ . \tag{6.71}$$

Here, the precise expressions for the coefficients A_{30}, A_{12}, A_{03} must not be given since they can be removed from (6.71). The calculation is straightforward. We insert

$$w_t = v_t + \alpha_{30} v_t^3 + \alpha_{21} v_t^2 \overline{v}_t + \alpha_{12} v_t \overline{v}_t^2 + \alpha_{03} \overline{v}_t^3$$

into (6.71) and find

$$\begin{aligned} v_{t+1} = \ & \mu v_t + (-\mu^3 \alpha_{30} + \mu \alpha_{30} + A_{30}) v_t^3 + \\ & + (-\mu^2 \overline{\mu} \alpha_{21} + \mu \alpha_{21} + A_{21}) v_t^2 \overline{v}_t + \\ & + (-\mu \overline{\mu}^2 \alpha_{12} + \mu \alpha_{12} + A_{12}) v_t \overline{v}_t^2 + \\ & + (-\overline{\mu}^3 \alpha_{03} + \mu \alpha_{03} + A_{03}) \overline{v}_t^3 + O(|v_t|^4 + |\overline{v}_t|^4) \ . \end{aligned} \tag{6.72}$$

To remove the third order terms, we have to set to zero the coefficients in (6.72). This results in

$$\alpha_{30} = -\frac{A_{30}}{\mu(1 - \mu^2)} \ , \qquad \alpha_{12} = -\frac{A_{12}}{\mu(1 - \overline{\mu}^2)} \ , \qquad \alpha_{03} = -\frac{A_{03}}{\mu - \overline{\mu}^3} \ .$$

However, we do not obtain a solution for α_{21} because the denominator $\mu(1 - \mu\overline{\mu})$ vanishes for any μ on the unit circle, which is exactly the situation under study. We also note that $\mu - \overline{\mu}^3 = (\mu^4 - 1)/\mu^3$. If $\mu^4 = 1$, the term $A_{03}\overline{w}^3$ cannot be removed as well. Continuing in this manner the remaining assertions of the theorem can also be proved.

Finally, we note that many of the transformation procedures of normal form and averaging theory can be performed automated using symbolic manipulation packages such as REDUCE, MACSYMA or SMP ([114]).

6.1.3 Statical systems

We have already mentioned in the Introduction that for statical systems described by a potential in one critical variable, transformation to normal form is trivial, because the lowest order nonvanishing nonlinear term is also the term appearing in the normal form, when the main (distinguished) parameters take their critical value. However, we shall see in

For a physical interpretation, we proceed as we did in the cases before. We start by drawing the axes system of the physical parameters U and c in the bifurcation diagram of Fig. 6.37. Next, we recall from Section 4.1.3 and Fig. 4.6 the physical meaning of the two parameters. U is the velocity of the fluid flow acting at m_1 which is responsible for a galloping instability. $c = c_2$ is the stiffness of the torsional spring located at the support of the pendulum. The system has two eigenmodes with amplitudes r_1 and r_2. They are depicted in Fig. 6.38. They show that

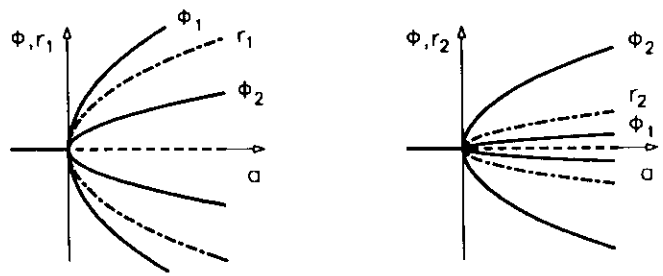

Figure 6.38. Eigenmodes ϕ_1 and ϕ_2 for (a) $c_2 < c_{2c}$ and (b) $c_2 > c_{2c}$ corresponding to domains (6) and (2) of Fig. 6.37

for a spring constant less than critical ($c_2 < c_{2c}$) the amplitude $\phi_1 > \phi_2$ and for a spring constant greater than critical ($c_2 > c_{2c}$) the amplitude $\phi_2 > \phi_1$. In these cases, both angles oscillate either with frequency ω_1 or ω_2, respectively. For loading paths as the one shown in Fig. 6.37 by the broken line, nothing special happens since the motion on the torus is unstable. Hence, only motions with one frequency are found for this example.

An application of this bifurcation case to a technical system is given in [66] where the loss of stability of the motion of a truck-trailer system is investigated.

In [50], it is shown that the complete classification of (6.114) contains twelve different cases.

6.6.3 Time-discrete dynamical systems

For time-discrete dynamical systems, exists a complete classification for codimension *one* ([7]). These are the three cases (6.121)–(6.123). We recall that (6.121)–(6.123) are the unfolded bifurcation equations which follow from application of center manifold reduction and normal form theory to the different types of loss of stabilty of the periodic motion of a robot. Hence, we shall discuss their physical significance by means of the robot example presented in Section 4.2.

1) $\mu = +1$: Saddle-node bifurcation (6.121)

The discussion of (6.121) is similar to that of (6.108) on p. 246. The details present no problems and will not be repeated here, because for the physical problem of the robot a different type of bifurcation called *transcritical bifurcation* applies. It is a bifurcation from the trivial solution as long as the perfect system is considered. Inclusion of imperfections leads to a higher degenerate (codimension *two*) case ([48]). The bifurcation equation for the perfect system is

$$u_{t+1} = (1 + a)u_t + A_2 u_t^2 + O(|u_t|^3) \ . \qquad (6.215)$$

The coefficient A_2 follows from the reduction process. The unfolding parameter a is given by

$$a = (\omega_0 - \omega_{0c}) \left. \frac{\partial \mu}{\partial \omega_0} \right|_{\omega_0 = \omega_{0c}} \ . \qquad (6.216)$$

Here ω_0 is the parameter whose quasistatic increase leads to the loss of stability of the basic periodic motion at ω_{0c}.

The fixed points of the mapping (6.215) follow from inserting $u_{t+1} = u_t$ into (6.215) to

$$u_{t0} = 0 \ , \qquad u_{t0} = -\frac{a}{A_2} \ . \qquad (6.217)$$

In Fig. 6.39, these solutions are shown for $A_2 < 0$. The stability of the solutions in Fig. 6.39 can be determined from a linearized stability ana-

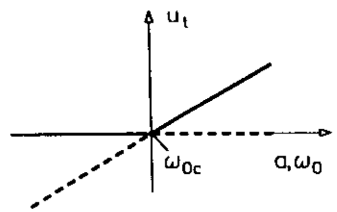

Figure 6.39. Transcritical bifurcation according to (6.215)

lysis. That is, one has to check whether the eigenvalues of the linearized map are smaller or larger than one. From (6.215) we obtain

$$f'(u_{t0}) = 1 + a + 2A_2 u_{t0} \ . \qquad (6.218)$$

The eigenvalues of the two solutions (6.217) follow from (6.218) to

$$f'(0) = 1 + a \ , \qquad f'\left(-\frac{a}{A_2}\right) = 1 - a \ .$$

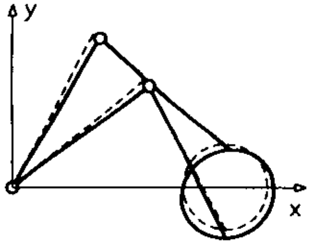

Figure 6.40. The full line gives the motion of the endpoint of the robot after a transcritical bifurcation in comparison to the motion before bifurcation given by the dotted line

Hence, the trivial solution $(6.217)_1$ is stable for $a < 0$ and unstable for $a > 0$. The bifurcated solution $(6.217)_2$ is stable for $a > 0$ and unstable for $a < 0$. To understand the behavior of the robot after loss of stability, the motion of the endpoint is depicted in Fig. 6.40. It can be seen that the bifurcated solution is still periodic moving along a closed curve which is similar to a circle but shifted away from the prescribed original circular path.

2) $\mu = -1$: Flip bifurcation (6.122)

The unfolding parameter a is as in (6.216). In Fig. 6.41, u_{t+1} is depicted as function of u_t for $A_3 > 0$. We observe that there are no non-trivial

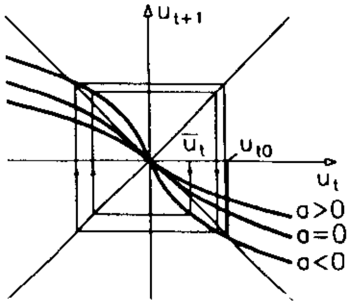

Figure 6.41. One-dimensional map (6.122) for three different values of a, possessing a two-periodic cycle u_{t0} for $a < 0$

fixed points bifurcating off $u_t = 0$ at $a = 0$ for $a \neq 0$ and a small (compare this figure with Fig. 2.4 which corresponds to the case $\mu = +1$). However, we notice that if for $a < 0$ an initial value $\bar{u}_t \neq 0$ is iterated, the orbit approaches a two-periodic cycle u_{t0}. Hence, it is natural to calculate the second iterate u_{t+2} to obtain

$$\begin{aligned} u_{t+2} = f(u_{t+1}) &= (-1+a)u_{t+1} + A_3 u_{t+1}^3 \\ &= (1-2a)u_t - 2A_3 u_t^3 + O(|u_t|^5) \,. \end{aligned} \tag{6.219}$$

Inserting $u_{t+2} = u_t$ into (6.219), the fixed points

$$u_{t0} = 0 \,, \qquad u_{t0} = \pm\sqrt{-\frac{a}{A_3}} \tag{6.220}$$

of the second iterate are obtained. That is, at $a = 0$ a bifurcation to a two-periodic motion occurs. In Fig. 6.42, the graph u_{t+2} is depicted

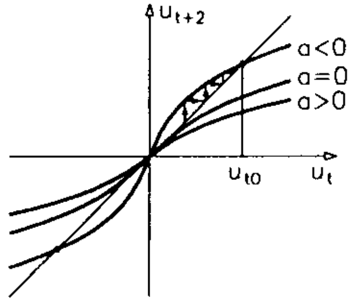

Figure 6.42. Second iterate u_{t+2} over u_t for the map (6.122)

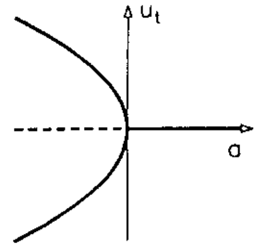

Figure 6.43. Flip bifurcation at $a = 0$ to an orbit of period two, for a variation of a from positive to negative values

as function of u_t. For $a < 0$, two nontrivial fixed points exist which correspond to period-two points of the original mapping. The bifurcation graph is shown in Fig. 6.43. Contrary to Fig. 6.39, we vary now a from positive to negative values. This is because as usually we start from a locally stable trivial solution, for which the modulus of the eigenvalue of the linear map must be smaller than one. The result of decreasing a is that the eigenvalue crosses the unit circle (Fig. 4.15) from inside to outside. In the theory of nonlinear oscillations the *period doubling* bifurcation is called *subharmonic bifurcation*. This is well understood from Fig. 6.44. The stability of the solutions in Fig. 6.43 can be similarly determined as it was done for the transcritical bifurcation. Finally, the motion of the endpoint of the robot is shown in Fig. 6.45. It is of the same type as depicted in Fig. 6.44.

3) $\mu_{1,2} = \nu \pm i\eta$, $|\mu_{1,2}| = 1$: Hopf bifurcation (6.123)

In this case the bifurcation equations take their simplest form in complex variables $w_t = u_t + iv_t$. First, we introduce polar coordinates both for

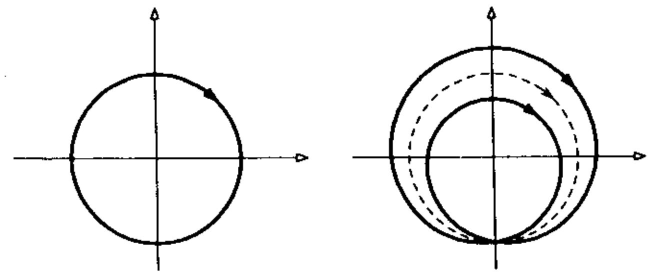

Figure 6.44. Transition from a periodic orbit to a two-periodic orbit due to a flip bifurcation

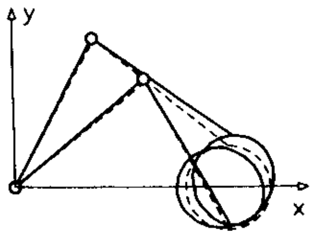

Figure 6.45. As in Fig. 6.40 but after a flip bifurcation

the variables and the coefficients

$$w_{t+1} = r_{t+1}e^{i\varphi_{t+1}},\ w_t = r_t e^{i\varphi_t},\ \mu = e^{i\alpha},\ c = ae^{i\gamma},\ C_3 = A_3 e^{i\beta}. \quad (6.221)$$

Inserting (6.221) into (6.123) yields

$$\begin{aligned} r_{t+1}e^{i\varphi_{t+1}} &= \left[\left(1 + ae^{i(\gamma-\alpha)}\right)e^{i\alpha} + A_3 e^{i\beta} r_t^2\right] r_t e^{i\varphi_t} \\ &= \left[1 + ae^{i(\gamma-\alpha)} + A_3 e^{i(\beta-\alpha)} r_t^2\right] r_t e^{i(\varphi_t+\alpha)} . \end{aligned} \quad (6.222)$$

Setting $\chi = \gamma - \alpha$ and $\psi = \beta - \alpha$ and taking the absolute value of each side of (6.222), we obtain

$$\begin{aligned} r_{t+1} &= \left|1 + a(\cos\chi + i\sin\chi) + A_3(\cos\psi + i\sin\psi)r_t^2\right| r_t \\ &= \sqrt{(1 + a\cos\chi + A_3\cos\psi r_t^2)^2 + (a\sin\chi + A_3\sin\psi r_t^2)^2}\, r_t \quad (6.223) \\ &= (1 + a\cos\chi + A_3\cos\psi r_t^2)r_t + O(|r_t|^4 + |ar_t^2| + |a|^2) . \end{aligned}$$

Here, the square root has been expanded into its power series. From (6.223) and setting $r_{t+1} = r_t$ to obtain the steady state solutions follows

$$(a\cos\chi + A_3\cos\psi r_t^2)r_t = 0$$

with the steady state amplitudes

$$r_{t0} = 0\ , \qquad r_{t0} = \sqrt{-\frac{a\cos\chi}{A_3\cos\psi}} \quad (6.224)$$

where

$$a = (\omega_0 - \omega_{0c})\frac{d}{d\omega_0}(\Re\mu)\bigg|_{\omega_0=\omega_{0c}} \quad \text{and} \quad \gamma = (\omega_0 - \omega_{0c})\frac{d}{d\omega_0}(\Im\mu)\bigg|_{\omega_0=\omega_{0c}} .$$

The nontrivial solution (6.224) represents the motion on a torus. As before the stability can be determined from a linearized analysis. If we have

$$f'(r_{t0}) = 1 + a\cos\chi + 3A_3\cos\psi r_{t0}^2 < 1 \quad (6.225)$$

then the solution is stable. Inserting (6.224) into (6.225) yields the stability behavior giving one or the other case shown in Fig. 6.46.

Finally, we describe the motion of the robot after the prescribed periodic motion loses stability by a Hopf bifurcation. For this case, the scenario of Fig. 4.14 applies. The original motion is given by a closed curve and corresponds to the fixed point $x_0 = 0$. After a supercritical Hopf bifurcation we obtain the motion on a torus which is represented by an asymptotically stable limit cycle in the Poincaré map. The cross-section of the torus is depicted in Fig. 6.47, where several iterated paths (transients) are marked. The motion of the endpoint of the robot is depicted in Fig. 6.48 and is shown to stay within two limiting circles. The motion on the torus can be either periodic or quasiperiodic depending whether the ratio of the frequency ω_0 of the basic periodic motion and the frequency η obtained from the Hopf bifurcation are rational or not. The orbit of the periodic motion is closed whereas the orbit of the quasiperiodic motion densly (uniformly) covers the whole torus ([5] p. 287).

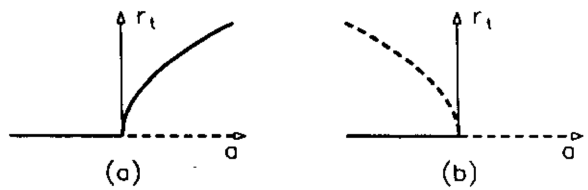

Figure 6.46. Hopf bifurcation of the mapping (6.123): (a) supercritical, (b) subcritical

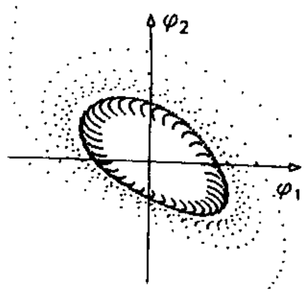

Figure 6.47. Poincaré section of the torus and nearby orbits after a Hopf bifurcation. The motion shown is quasiperiodic

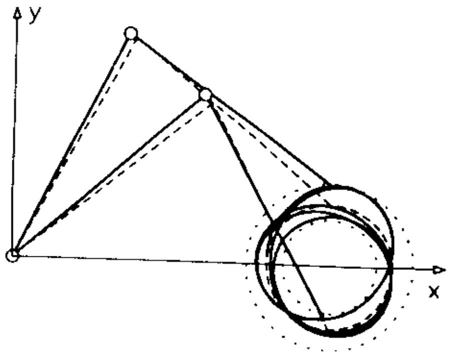

Figure 6.48. As in Fig. 6.40 but after a Hopf bifurcation. The motion is confined by two limiting circles

6.6.4 Symmetric dynamical systems

In this section, we discuss briefly the simple losses of stability of the trivial equilibrium position for the spherical double pendulum with the follower force loading described described in Section 5.1 and the fluid-carrying tube discussed in Section 5.3. Both systems are O(2)-symmetric, that is, they are equivariant both under a rotation and a reflection. Studying these systems will allow us to gain insight into the interesting phenomenon of symmetry breaking. Furthermore, we are able to treat both problems simultaneously because the structure of the bifurcation equations depends only on the matrix $\mathbf{J}_c$ given by (5.30)–(5.33). Partly they coincide for both cases. We will treat only the two simplest cases given by (5.30).

1) Two zero roots

In the corresponding bifurcation equations (5.40), the coefficient A_3 results from the center manifold reduction. The unfolding parameter a is

18

IAVSD - Symposium Prag 1989

MANEUVERABILITY OF A TRUCK-TRAILER COMBINATION AFTER LOSS OF LATERAL STABILITY

V. Kaçani, A. Stribersky and H. Troger

Institut für Mechanik, Technische Universität Wien,
A-1040 Vienna, Austria

SUMMARY

A nonlinear stability analysis of the steady state horizontal and downhill straight line motion of a controlled truck-trailer system is given. Special emphasis is given to the modelling of the controller simulating the steering actions of the driver. Two different types of controllers both including the effect of the reaction time of the driver are used. The basic question to be answered is whether the truck-trailer system after loss of stability of the steady state still is controlable by the driver or not. I.e. whether after loss of stability nearby stable states exist or not. A question which can only be answered by a nonlinear analysis. The answer is given for the variation of a number of parameters.

1. INTRODUCTION

Road safety is very much influenced by the behavior of heavy articulated trucks at high speed, especially in downhill motion. This, for example, has been demonstrated dramatically in July 1987 in the small city of Herborn in Hessen in West Germany, where a truck-trailer combination loaded with gasolin in downhill motion got out of control of the driver due to a failure of the brakes, crashed against a house and blew up in a devastating explosion killing more than five persons.

A major question in relation to such accidents which occur pretty frequently* is whether the driver of such an articulated vehicle is able to control his vehicle by steering corrections after a loss of stability of the straight line motion had occured.

Basically, this is a question of nonlinear stability theory, because it requires the knowledge of the behavior of the system after loss of stability. Hence it is necessary to study a nonlinear mechanical model of the truck-trailer system. Furthermore it is of significant influence that a proper model for the steering actions of the driver is used. In order to have a comparison concerning the influence of the driver's model on the obtained results we shall use two different models for a control system simulating the driver. Mathematically a positive answer to the question posed above whether the system can be controlled after loss of stability of the steady state is given if it can be shown that nearby attractors exist. Such attractors are generically either stable steady states or stable limit cycles or in more complicated situations, which in practical driving situations do not occur too often, coupled motions between two flutter modes, i.e. for example motion on a torus. We shall explain this situation further in section 3.

The methods of bifurcation theory as they are developed in [1-3] and applied to some problems concerning the motion of tractor-semitrailer vehicles in [4-6] will be used to treat the nonlinear stability problem.

* One accident of a similar way occured in Austria also in July 1987. Again a driver lost control over his truck-trailer system in downhill motion. It crashed against a car killing two women, one being the wife of the former Austrian minister of traffic.

2. MECHANICAL MODEL AND EQUATIONS OF MOTION

Though a truck or a trailer are flexible elastic structures, for a stability analysis a rigid body model seems to be quite appropriate. Hence our model has only the four degrees of freedom v, γ, ϕ_1 and ϕ_2 (Fig. 1). The motion of the truck-trailer system is assumed to take place on a flat road which is inclined by an angle χ. Aerodynamic forces will not be taken into account.

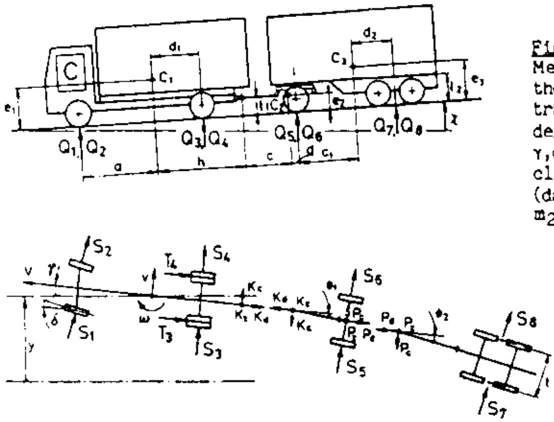

Fig. 1: Mechanical model of the controlled truck-trailer with the four degrees of freedom v, γ, ϕ_1 and ϕ_2 on an inclined (angle χ) road (data: m_1 = 13500 kg, $m_2 + m_3$ = 20500 kg).

With the notations given in Fig. 1 the following equations of motion are obtained for the truck ($T_3 = T_4 = T$, $\dot{\gamma} = \omega$):

$$m_1(-v\dot{\gamma}) = -(S_1+S_2)\sin\delta - 2T - K_d + m_1 g \sin\chi\cos\gamma \qquad (1)$$

$$m_1(\dot{v}+V\dot{\gamma}) = (S_1+S_2)\cos\delta + (S_3+S_4) + K_c - m_1 g\sin\chi\sin\gamma \qquad (2)$$

10

$$0 = -(Q_1+Q_2+Q_3+Q_4) - K_z + m_1 g\cos\chi \tag{3}$$

$$\begin{aligned}-I_{x_1z_1}\ddot{\gamma} &= -e_1(S_1+S_2)\cos\delta - e_1(S_3+S_4) + \frac{t}{2}(Q_1-Q_2) + \\ &+ \frac{t}{2}(Q_3-Q_4) + (\ell_1-e_1)K_c\end{aligned} \tag{4}$$

$$\begin{aligned}-I_{x_1z_1}\dot{\gamma}^2 &= -e_1(S_1+S_2)\sin\delta + a(Q_1+Q_2) - d_1(Q_3+Q_4) + \\ &- 2e_1T + (\ell_1-e_1)K_d - hK_z\end{aligned} \tag{5}$$

$$I_{z_1}\ddot{\gamma} = a(S_1+S_2)\cos\delta + \frac{t}{2}(S_2-S_1)\sin\delta - d_1(S_3+S_4) - hK_c \tag{6}$$

for the dolly:

$$\begin{aligned}m_2[-v\dot{\gamma} + h\dot{\gamma}^2 + c(\ddot{\gamma}+\ddot{\phi}_1)\sin\phi_1 + c(\dot{\gamma}+\dot{\phi}_1)^2\cos\phi_1] &= \\ = K_d - P_d - (S_5+S_6)\sin\phi_1 + m_2 g\sin\chi\cos\gamma\end{aligned} \tag{7}$$

$$\begin{aligned}m_2[\dot{v} + V\dot{\gamma} - h\ddot{\gamma} - c(\ddot{\gamma}+\ddot{\phi}_1)\cos\phi_1 + c(\dot{\gamma}+\dot{\phi}_1)^2\sin\phi_1] &= \\ = -K_c + P_c + (S_5+S_6)\cos\phi_1 - m_2 g\sin\chi\sin\gamma\end{aligned} \tag{8}$$

$$0 = K_z - P_z - (Q_5+Q_6) + m_2 g\cos\chi \tag{9}$$

$$\begin{aligned}-I_{x_2z_2}(\ddot{\gamma}+\ddot{\phi}_1) &= (e_2-\ell_1)(K_d\sin\phi_1+K_c\cos\phi_1) - \\ &- (e_2-\ell_2)(P_d\sin\phi_1+P_c\cos\phi_1) - e_2(S_5+S_6) + \frac{t}{2}(Q_5-Q_6)\end{aligned} \tag{10}$$

$$\begin{aligned}-I_{x_2z_2}(\dot{\gamma}+\dot{\phi}_1)^2 &= (e_2-\ell_1)(K_d\cos\phi_1-K_c\sin\phi_1) - \\ &- (e_2-\ell_2)(P_d\cos\phi_1-P_c\sin\phi_1) - cK_z - dP_z - d(Q_5+Q_6)\end{aligned} \tag{11}$$

$$I_{z_2}(\ddot{\gamma}+\ddot{\phi}_1) = -c(K_d\sin\phi_1+K_c\cos\phi_1) - d(P_d\sin\phi_1+P_c\cos\phi_1) - d(S_5+S_6) \tag{12}$$

and for the trailer:

$$\begin{aligned}m_3[-v\dot{\gamma} + h\dot{\gamma}^2 &+ (c+d)(\ddot{\gamma}+\ddot{\phi}_1)\sin\phi_1 + (c+d)(\dot{\gamma}+\dot{\phi}_1)^2\cos\phi_1 + \\ &+ c_1(\ddot{\gamma}+\ddot{\phi}_2)\sin\phi_2 + c_1(\dot{\gamma}+\dot{\phi}_2)^2\cos\phi_2] = \\ &= P_d - (S_7+S_8)\sin\phi_2 + m_3 g\sin\chi\cos\gamma\end{aligned} \tag{13}$$

$$\begin{aligned}m_3[\dot{v} + V\dot{\gamma} - h\ddot{\gamma} &- (c+d)(\ddot{\gamma}+\ddot{\phi}_1)\cos\phi_1 + (c+d)(\dot{\gamma}+\dot{\phi}_1)^2\sin\phi_1 - \\ &- c_1(\ddot{\gamma}+\ddot{\phi}_2)\cos\phi_2 + c_1(\dot{\gamma}+\dot{\phi}_2)^2\sin\phi_2] = \\ &= -P_c + (S_7+S_8)\cos\phi_2 - m_3 g\sin\chi\sin\gamma\end{aligned} \tag{14}$$

$$0 = P_z - (Q_7+Q_8) + m_3 g\cos\chi \tag{15}$$

$$-I_{x_3z_3}(\ddot{\gamma}+\ddot{\phi}_2) = (e_3-\ell_2)(P_d\sin\phi_2+P_c\cos\phi_2) - e_3(S_7+S_8) + \frac{t}{2}(Q_7-Q_8) \tag{16}$$

$$-I_{x_3z_3}(\dot{\gamma}+\dot{\phi}_2)^2 = (e_3-\ell_2)(P_d\cos\phi_2-P_c\sin\phi_2) - c_1P_z - d_2(Q_7+Q_8) \tag{17}$$

$$I_{z_3}(\ddot{\gamma}+\ddot{\phi}_2) = -c_1(P_d\sin\phi_2+P_c\cos\phi_2) - d_2(S_7+S_8) \tag{18}$$

Together with (see [6])

$$(Q_1-Q_2) = \kappa(Q_3-Q_4)\ , \tag{19}$$

which allows to calculate the wheelloads of the truck (κ characterizes the elastic deformability of the truck frame), we have 19 partly nonlinear ordinary differential equations for the 19 unknowns $v, \dot{\gamma}, \phi_1, \phi_2, Q_1, \ldots, Q_8, K_d, K_c, K_z, P_d, P_c, P_z$ and T. 2T is the resultant tangential tire force at the rear axle of the truck, which is necessary to maintain the prescribed steady state speed of the system, both on a horizontal road and on an inclined road in downhill motion. This latter case is very imporant in practical driving conditions because for longer lasting downhill motions the driver shifts into a lower gear and the engine makes the job of braking.

Depending on the used model for the driver an additional set of equations is obtained. As already mentioned we use two different driver models:

(a) Compensation of the yaw angle γ of the truck

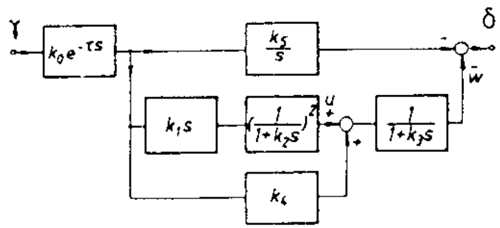

Fig. 2: Block diagram of the model of the active driver with reaction time τ for case (a). (data: k_0=0.1, k_1=0.11, k_2=0.14, k_3=0.1, k_4=1.0, k_5=1.7)

Making use of the model in [7] the block diagram of Fig. 2 is obtained, from which the relationship

$$\delta = - k_0 e^{-\tau s} \left(\frac{k_5}{s} + \left[k_1 s \left(\frac{1}{1+k_2 s}\right)^2 + k_4\right] \frac{1}{1+k_3 s}\right)\gamma \tag{20}$$

relating the yaw angle γ and the steering angle δ can be obtained. In (20) a delay term is present which enables us also to take care of the reaction time of the driver. (20) corresponds to the following system of functional equations

$$\dot{\delta} = - (k_0 k_5 \gamma(t-\tau) + \dot{w}) \tag{21}$$

$$k_2^2 \ddot{u} + 2k_2 \dot{u} + u = k_0 k_1 \dot{\gamma}(t-\tau) \tag{22}$$

$$k_3 \dot{w} + w = u + k_0 k_4 \gamma(t-\tau) \tag{23}$$

(b) Compensation of the lateral displacement y of the truck

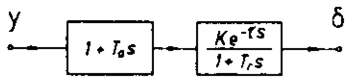

Fig. 3: Block diagram of the model of the active driver with reaction time τ for case (b). (data: T_a=50/V, T_r=0.2, K=-2.0)

Now use is made of the model used in [8]. The block diagram of the control model is shown in Fig. 3, from which the following relationship

$$\delta = K e^{-\tau s} \frac{(1+T_a s)}{(1+T_r s)} y \tag{24}$$

relating the lateral displacement y to the steering angle δ is given. From Fig. 1 the simple relationship between v and $\dot{y}$ can be seen. (24) corresponds to the functional differential equation

$$T_r \dot{\delta} + \delta = K(y(t-\tau) + T_a \dot{y}(t-\tau)) \ . \tag{25}$$

In [8] a parameter study is given to fit the constants appearing in (25) to practical driving situations. We shall pick such values of the parameters in both models which will allow us to compare the results.

In the further treatment of the equations of motion we express the tire side forces $S_1,\dots,S_8$ by the following expressions

$$\frac{S_i}{P_{ni}} = ((a_{1i}\pi_i + a_{2i}\pi_i^2)\tanh(b_i \alpha_i) + a_{3i}\pi_i \alpha_i) \sqrt{1-(\mu_{Ti}/\mu_{Tmax})^2} \tag{26}$$

where the $a_{1i},\dots,b_i$ are tire parameters, P_{ni} is a reference wheel-load, $\pi_i = Q_i/P_{ni}$ and

$$\alpha_{1,2} = \delta - \text{arctg} \frac{v+\dot{\gamma}a}{V\pm\dot{\gamma}t/2} \tag{27}$$

$$\alpha_{3,4} = - \text{arctg} \frac{v-\dot{\gamma}d_1}{V\pm\dot{\gamma}t/2} \tag{28}$$

$$\alpha_{5,6} = - \text{arctg} \frac{-V\sin\phi_1+(v-\dot{\gamma}h)\cos\phi_1-(\dot{\gamma}+\dot{\phi}_1)(c+d)}{V\cos\phi_1+(v-\dot{\gamma}h)\sin\phi_1\pm(\dot{\gamma}+\dot{\phi}_1)t/2} \tag{29}$$

$$\alpha_{7,8} = -\text{arctg} \frac{-V\sin\phi_2+(v-\dot{\gamma}h)\cos\phi_2-(c+d)(\dot{\gamma}+\dot{\phi}_1)\cos(\phi_2-\phi_1)-(\dot{\gamma}+\dot{\phi}_2)(c_1+d_2)}{V\cos\phi_2+(v-\dot{\gamma}h)\sin\phi_2-(c+d)(\dot{\gamma}+\dot{\phi}_1)\sin(\phi_2-\phi_1)\pm(\dot{\gamma}+\dot{\phi}_2)t/2} \tag{30}$$

are the tire slip angles. The square root in (26) accounts for the influence of the tangential tire force on the tire side force. μ_{Ti} and μ_{Tmax} are the actual and maximal tangential friction coefficients.

Introducing for $\dot{\phi}_1, \dot{\phi}_2, \dot{\gamma}$ and $\dot{u}$ respectively $\dot{y}$ new variables we form two vectors x and q, where for the controller model (a)

$$x^T = (v,\gamma,\dot{\gamma},\phi_1,\dot{\phi}_1,\phi_2,\dot{\phi}_2,\delta,u,\dot{u},w) \qquad \in R^{11} \tag{31}$$

and for the controller model (b)

$$x^T = (y,\dot{y},\gamma,\dot{\gamma},\phi_1,\dot{\phi}_1,\phi_2,\dot{\phi}_2,\delta) \qquad \in R^9 \tag{32}$$

whereas in both cases

$$q = [Q_1,Q_2,\dots,Q_8,K_d,K_c,K_z,P_d,P_c,P_z,T] \qquad \in R^{15} \tag{33}$$

will be obtained.

Adding the trivial equations $\dot{x}_2=x_3$, $\dot{x}_4=x_5$, $\dot{x}_6=x_7$, $\dot{x}_9=x_{10}$ to (31) and $\dot{x}_1=x_2$, $\dot{x}_3=x_4$, $\dot{x}_5=x_6$, $\dot{x}_7=x_8$ to (32) respectively we obtain the following set of first order differential equations

$$W(x)\dot{x} = f(x,x(t-\tau),q(x)) \tag{34}$$

$$V(x)\dot{x} = h(x,q(x)) \tag{35}$$

where $W(x)$ is a non-degenerate 11×11 matrix in case (a) and 9×9 matrix in case (b) and $V(x)$ is a 11×15 or 9×15 matrix respectively. From (34) and (35) the variables q given by (33) have to be eliminated. This can be done in the following way. First we obtain from

(34)

$$\dot{x} = W(x)^{-1} f(x, x(t-\tau), q(x)) \tag{36}$$

where the matrix $W(x)^{-1}$ up to the required order can be calculated numerically. By inserting (36) into (35) we can calculate $q(x, x(t-\tau))$ and after introducing it into (34) we obtain

$$\dot{x} = W^{-1} f(x(t), x(t-\tau), q(x(t), x(t-\tau)), \lambda) \tag{37}$$

which we write in the form

$$\dot{x} = G(x(t), x(t-\tau), \lambda) \ . \tag{38}$$

(38) is the desired form of the equations of motion. x is either given by (31) or (32) and $\lambda^T = (V, d_1, d_2, \chi)$ is the parameter vector, where V is the constant driving speed, d_1 and d_2 are parameters giving the loading condition of the truck and the trailer respectively by designating the position of the corresponding center of gravity and χ is the angle of inclination of the road. τ designates the time delay coming from the reaction time of the driver.
It is obvious that the straight line motion of the system

$$x_0 \equiv 0 \tag{39}$$

for arbitrary λ results in

$$G(0, 0, \lambda) = 0$$

and hence (39) is the solution which we want to study with respect to its stability.

3. STABILITY BOUNDARY AND NONLINEAR STABILITY ANALYSIS

Application of the methods of bifurcation theory ([1-3]) to the stability problem of (39) results in a strong reduction of the dimension of (38) which is either 11 or 9 depending on which of the two different models of the controller is used. This reduction is achieved by application of Centre Manifold Theory ([2]). We do not go into detail here as the analysis for the case where no time lag is present has been explained already in [6]. However, it must be emphasized that the treatment of (38) is more complicated than the one in [6], because (38) is a functional differential equation.

For the functional differential equation we use the code presented in [9], which is completely appropriate because only flutter instabilities (Hopf-bifurcations) can occur in controlled systems ([5]).

We assume, and this is quite reasonable from an engineering standpoint, that at low speed V the equilibrium position (39) is asymptotically stable. Now we increase the speed of the system quasistatically until the steady state looses its stability, i.e. until the first eigenvalue of the linear part crosses the imaginary axis. Expanding (38) into a power series with respect to the equilibrium position $x_0 = 0$ results in

$$\dot{x}(t) = A_1(\lambda) x(t) + A_2(\lambda) x(t-\tau) + g(x(t), x(t-\tau), \lambda) \tag{40}$$

where

$$A_1(\lambda) = \left[\frac{\partial G_i}{\partial x_j} \right]_{x=0} \tag{41}$$

$$A_2(\lambda) = \left[\frac{\partial G_i}{\partial x(t-\tau)_j} \right]_{x=0} \tag{42}$$

and $g(x(t), x(t-\tau), \lambda)$ does not contain linear terms.

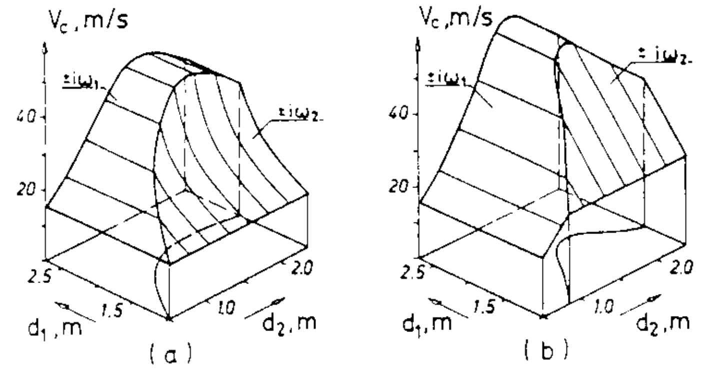

Fig. 4: Stability boundary in V, d_1, d_2 space for $\chi = 0$ and $\tau = 0$ for the two different controller models (a) and (b).

The stability boundary obtained from the linear part in (40) is shown in Fig. 4 for the two different types of the controller. As parameters we have selected d_1 and d_2 which designate the loading condition of the system. Two other quantities, i.e. the time lag τ and the inclination anlge χ are both set equal to zero for the results in Fig. 4, but we give the influence of these two parameters on the stability boundary below. From Fig. 4 follows that for both controllers a qualitatively similar stability boundary is obtained. We see that two surfaces intersect. For both surfaces we obtain a Hopf-bifurcation, i.e. we obtain an oscillating loss of stability which occurs generically either with frequency ω_1 or ω_2. The corresponding oscillation modes are shown in Fig. 5. The line of intersection of the two surfaces gives rise to a nongeneric loss of stability and leads to a coupling of two oscillatory motions.

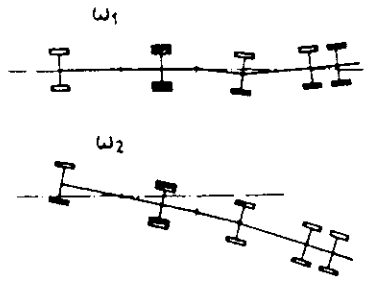

Fig. 5:
Modes of oscillation of the truck-trailer corresponding to the frequences ω_1 and ω_2 of Fig. 4.

Crossing the stability boundary we can ask now the question whether adjacent stable motions exist. If so the system would be steerable in a practical sense. If not, then the driver as it is given by one of the two controllers could not handle the system. To answer this question we have to treat a nonlinear problem.

The nonlinear analysis proceeds in several steps. First a reduction to a bifurcation system, the dimension of which is equal to the number of eigenvalues with zero realpart, is done by means of Center Manifold Theory ([2]). For the system with controller either a two-dimensional system corresponding to a pure imaginary pair of eigenvalues (Fig. 4) or a four-dimensional system corresponding to the coupling of two oscillatory states is obtained. The former occurs generically and corresponds to the surfaces in Fig. 4 whereas the latter only for special loading situations (intersection of the two surfaces) is found. It should be pointed out that by varying d_1 this more complicated coupled oscillation state is the one which corresponds to the maximum value of the critical speed V_c.

Having obtained the bifurcation equations we introduce polar coordinates. As limit cycles are obtained only the amplitudes r of these limit cycles are important. Therefore we obtain in the generic case ([3])

$$\dot{r} = \nu r + c_3 r^3 + (|r|^5) \ . \tag{43}$$

ν is the mathematical unfolding parameter. The connection between ν and the physical parameter $\lambda_1 = V - V_c$ is given by

$$\nu = \left.\frac{\partial \sigma_1}{\partial \lambda_1}\right|_{\lambda_1 = 0} \lambda_1 \ .$$

σ_1 is the realpart of the critical roots. For the coupled case and without time delay ($\tau = 0$) we obtain

$$\begin{aligned} \dot{r}_1 &= \nu_1 r_1 + c_{11} r_1^3 + c_{12} r_1 r_2^2 + (|r|^5) \\ \dot{r}_2 &= \nu_2 r_2 + c_{21} r_1^2 r_2 + c_{22} r_2^3 + (|r|^5) \end{aligned} \tag{44}$$

Here the c_{ij} are coefficients which are fixed for a given system and the ν_i are the mathematical unfolding parameters.

4. DISCUSSION OF SOME NUMERICAL RESULTS

Basically we want to study the influence of an inclined road expressed by the angle χ and secondly also the influence of the reaction time of the driver expressed by the time lag τ on the ability of the driver to control the truck-trailer combination. Further also the loading condition has an important influence.

(a) Influence of the inclination of the road

For a fixed value of d_2 we cut a slice out of the three-dimensinal diagram of Fig. 4a. The reaction time τ is assumed to be zero. In Fig. 6 the influence of the inclination angle χ on the stability boundary is given. Of course a strong reduction of the domain of stability is obtained. But it is interesting to see that only the mode of instability corresponding to ω_1 is affected. The corresponding nonlinear behavior of the system for the points 1,2,3,4 of the stability boundary is shown in Fig. 7. As an example the amplitudes $\|\phi_2\|$ of the limit cycle oscillations corresponding to 1 and 4 are drawn for a flat horizontal road with no reaction time of the driver. Point 1 shows a stable limit cycle which means that the system after loss of stability remains in an oscillatory state of small amplitude. But already for $\chi = 1^\circ$ corresponding to point 2 an unstable limit cycle is obtained which shows that the used controller will not be able to handle the system. The same also applies for the other points shown. Finally we also comment on the nongeneric case given by point 0 in Fig. 6 which gives a coupling between the two oscillatory modes of frequences ω_1 and ω_2, where ω_1 relates to a stable and ω_2 to an unstable limit cycle. In the center of Fig. 8 the bifurcation diagram which is a partition of the parameter space into domains of qualitatively similar behavior is given. The mathematical unfolding parameters ν_1 and ν_2 are related to the physical parameters ε_1 and ε_2 (Fig. 6) by

$$\nu_1 = \left.\frac{\partial \sigma_1}{\partial \varepsilon_1}\right|_{\sigma_1 = 0} \varepsilon_1 \ , \qquad \nu_2 = \left.\frac{\partial \sigma_2}{\partial \varepsilon_2}\right|_{\sigma_2 = 0} \varepsilon_2 \ ,$$

where σ_i are the realparts of the critical roots.

The behavior of the truck system can be understood from the phase plane diagrams shown in Fig. 8. On the axes the amplitudes of the two oscillatory motions described above are drawn. It can be seen that except the trivial state only in the fourth quadrant a nontrivial stable state exists, which corresponds to an oscillation with frequency ω_1 and the corresponding mode. The broken-dotted line in the bifurcation diagram of Fig. 8 gives the direction of increasing V by keeping d_1 fixed. Proceeding on this line to the right we obtain the bifurcation solutions in Fig. 9. Crossing the ν_2 axis the trivial state becomes unstable and the stable limit cycle bifurcates off. In the next section an unstable torus, i.e. a motion which depends on two frequencies simultaneously, exists which extinguishes at the border of this domain the limit cycle. Physically speaking this means that the system becomes uncontrolable, because the limit

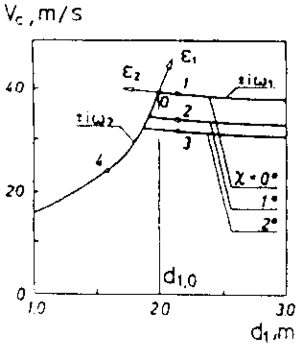

Fig. 6:
Influence of the inclination χ of the road on the stability boundary.

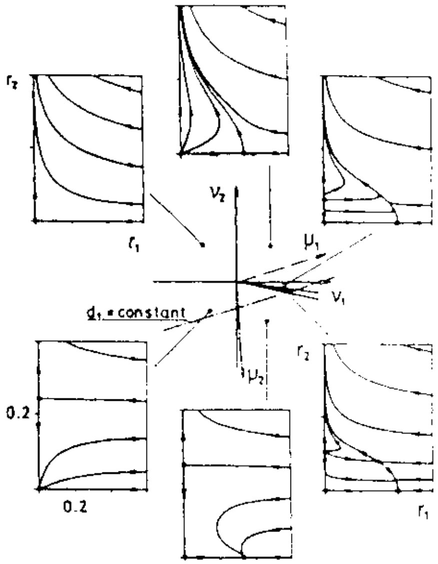

Fig. 8:
Bifurcation diagram and phase plane diagrams for the coupled motion of two oscillatory instabilities corresponding to point 0 in Fig. 6 ($\mu_1 \sim V - V_{c0}$, $\mu_2 \sim d_1 - d_{10}$).

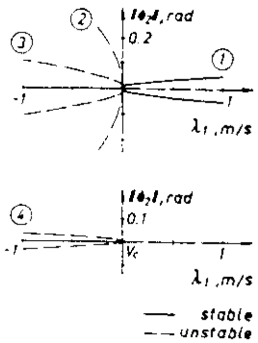

Fig. 7:
Amplitudes of stable and unstable limit cycles corresponding to the numbers in Fig. 6 ($\lambda_1 = V - V_c$).

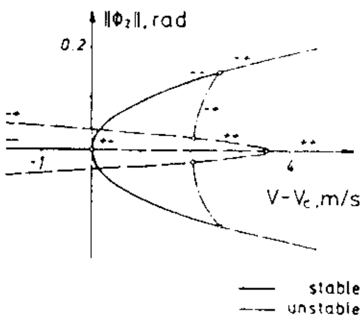

Fig. 9:
Bifurcation solutions corresponding to the broken-dotted line in Fig. 8, giving two limit cycles and one torus (-·-·-).

cycle loses its stability. In Fig. 9 the signs denote the stability behavior. A plus denotes a positive eigenvalue and hence means that the solution is unstable. Only two minus signs refer to a stable solution.

(b) Influence of the reaction time τ

For a horizontal road the strong influence of the time lag is given in Fig. 10. Again we see that only one mode is affected. Corresponding to the points 1-4 in Fig. 10 in Fig. 11 the limit cycles are given and it can be seen that for the points 1-3 unstable limit cycles are obtained which means that after loss of stability the system cannot be controlled.

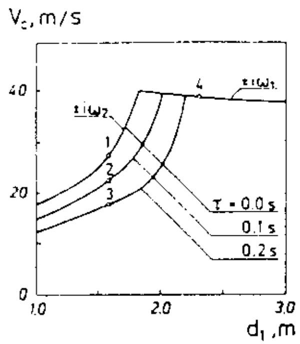

Fig. 10:
Influence of the reaction time τ on the stability boundary.

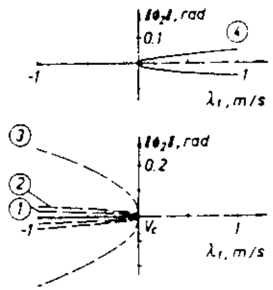

Fig. 11:
Amplitudes of stable (4) and unstable (1-3) limit cycles corresponding to the numbers in Fig. 10.

NOTATIONS

a_{ij}, b_i	tire parameters
d_1	position of c.g. of the truck
d_2	position of c.g. of the trailer
I_{xz}, I_z	components of inertia-tensor of the truck resp. dolly or trailer
$K_d, K_c, K_z, P_d, P_c, P_z$	joint forces
m_i	masses of truck, dolly and trailer
P_{ni}	norm load at wheel i
Q_i	load at wheel i
r_i	amplitudes of the limit cycles
S_i	side force at wheel i
t	time
T_i	tangential force at wheel i
u, w	variable of the controller
v	truck side-slip
V	driving speed
x	n-vector of physical variables
y	lateral displacement

α_i	slip angle at tire i
γ	yaw angle
δ	steering angle
ϵ_i	physical unfolding parameters
κ	expression depending on the elastic deformability of the truck
λ	vector of physical parameters
μ_T, μ_{Tmax}	tangential tire coefficients
ν_i	mathematical parameters in the bifurcation equation
σ_i	real parts of critical values
τ	time delay (reaction time)
ϕ_1	angle between truck axis and dolly axis
ϕ_2	angle between truck axis and trailer axis
χ	inclination of the road
ω	truck yaw angular velocity
ω_i	imaginary parts of critical eigenvalues

ACKNOWLEDGEMENT

This work has been supported by a grant of the Hochschuljubiläumsstiftung der Stadt Wien.

REFERENCES

1. Arnold V.I., Geometrical Methods in the Theory of Ordinary Differential Equations, Springer-Verlag, Heidelberg, New York 1983.
2. Carr J., Applications of Centre Manifold Theory, Applied Math. Sciences 35, Springer-Verlag, New York, Heidelberg 1981.
3. Guckenheimer J., P. Holmes, Nonlinear Oscillations, Dynamical Systems and Bifurcations of Vectorfields, Applied Math. Sciences 42, Springer-Verlag, New York, Heidelberg 1983.
4. Troger H., K. Zeman, A Nonlinear Analysis of the Generic Types of Loss of Stability of the Steady State Motion of a Tractor-Semitrailer, Vehicle System Dynamics 13 (1984) 161-172.
5. Scheidl R., A. Stribersky, H. Troger, K. Zeman, Nonlinear Stability Behavior of a Tractor-Semitrailer in Downhill Motion, Proc. 9th IAVSD-Symp. Linköping (S), (O. Nordström ed.), Swets and Zeitlinger B.V., Lisse, 1986, 509-522.
6. Kacani V., A. Stribersky, H. Troger, K. Zeman, Dynamics and Bifurcations in the Motion of Tractor-Semitrailer Vehicles, Conference Proceed. Canadian Math. Soc. vol. 8, (F.V. Atkinson, W.F. Langford, A.B. Mingarelli, eds.) 1987, 485-499.
7. Wallner F., Das Verhalten des Fahrzeuglenkers als regelungstechnisches Problem, Automobil Industrie 1 (1967) 54-62.
8. Legouis T., P.A. Bourassa, A. Laneville, C. Gosselin, On the Extension of the Gratzmüller Critical Velocity for Locked Steering Road Vehicle to the Case of Piloted Vehicle, Proc. 9th IAVSD-Symp., Linköping (S), (O. Nordström ed.), Swets and Zeitlinger B.V., Lisse 1986, 307-319.
9. Hassard B., A Code for Hopf Bifurcation Analysis of Autonomous Delay-Differential Systems, Conference Proc. Canad. Math. Soc. vol. 8 (F.V. Atkinson, W.F. Langford, A.B. Mingarelli, eds.) 1987, 447-463.

STABILIZATION OF ARTICULATED VEHICLES BY SEMI-ACTIVE CONTROL METHOD

Ichiro Kageyama[1]) and Yasushi Saito[2])

1) College of Industrial Technology, Nihon University, Japan
2) Saitama Institute of Technology, Japan

SUMMARY

This paper describes the stabilization of articulated vehicles at high speeds by a steering system set up on the trailer.

First, the equations of motion of the articulated vehicles with a steering system on the trailer were obtained. Furthermore, the steering angle of the trailer in the presence of disturbances was studied by solving these equations through the application of modern control theory. From such analysis, the magnitude of the optimal feedback coefficients of each state variable was obtained. It was found that the stability of articulated vehicles at high speeds was significantly improved by the active control method for the trailer steering system.

However, the active control system needs a power supply , and it is difficult to apply it to articulated vehicles at present, especially for passenger car-trailer combinations. Thus, a new trailer steering system with viscous coupling arms to be set between the tractor and trailer was proposed. Furthermore, the semi-active control method which controls the damping factor of viscous coupling arms on the trailer was studied by applying the optimal control theory. It was found that this method was quite effective for achieving stability of articulated vehicles at high speeds.

1. INTRODUCTION

In articulated vehicles, it is well known that low damping oscillation occurs at high speed, and once the critical velocity for stability is exceeded, their behavior becomes unstable. Thus, many studies have been done in this field [1,2].

As the first step of these studies, the principal consideration was given to the relation between their behavior and their design parameters. From these studies, IAVSD - Symposium, Lyon 1991

conditions is negligible, "^" - symbol of estimate or approximate value found experimentally or analytically.

Knowing $\hat{f}$ from the second equation 9 we similarly find estimate of wheel equivalent conicity parameter

$$\hat{\lambda} = \int_{t_0}^{T} \chi_3 \chi_4 \, dt \cdot [\int_{t_0}^{T} \chi_4^2 dt]^{-1},$$

where:

$$\chi_3 \quad I_w\ddot{\hat{\psi}}_1^* + 2b_1^2 h_x (\hat{\psi}_1^* - \hat{\psi}^*) + 2\hat{f} b_2^2 v^{-1}\dot{\hat{\psi}}_1^*,$$

$$\chi_4 = -\hat{f} b_2 r_0^{-1} (\hat{\Delta}_R^* + \hat{\Delta}_L^*).$$

So, to identify creep coefficients and wheel equivalent conicity parameter by means the above described method, one should know truck parameters m_w, I_w, k_y, k_x, β_y, β_x, a, b_1, b_2 and have experimental records of the processes $\ddot{y}$, $\ddot{y}_1$, $\ddot{\psi}$, $\ddot{\psi}_1$, Δ_R, Δ_L.

REFERENCES

1. Kalker, J.J.,Review of Wheel-Rail Rolling Contact Theories General Problem of Rolling Contact. Winter Annu. Meet. ASME, Chicago, III, Nov. 16-21, 1980 - New York, N.J., 1980, p. 77-92.
2. Sweet, L.M., Garrison-Phelan, P., Identification of Wheel/Rail Creep Coefficients from Steady and Dynamic Wheelset Experiments. General Problem of Rolling Contact. Winter Annu.Meet. ASME, Chicago, III, Nov. 16-21, 1980 - New York, N.J.,1980, p. 121-137.
3. Ushkalov, V.F., and Alexandrov, A.I., The Creep Force Model for Different Conditions of Wheel-Rail Rolling Contact. Rail Transportation. Winter Annu. Meet. ASME, San Francisko, Dec. 10-15, 1989 - New York, N.J., 1989, p. 189-196.
4. Alexandrov, A.I., Solution of Three-Dimensional Rolling Contact Problems in Elasticity. Nugrushennost' i nadeshnost' mechanicheskich sistem.Kiev,Naukova Dumka,1987,p.115-121.
5. Ushkalov, V.F., Reznikov, L.M., Ikkol, V.S., et al., Mathematical Modeling of Railway Vehicle Vibrations.Kiev,Naukova Dumka,1989.
6. Ushkalov, V.F., Random Vibrations of Railway Vehicles. Random Vibration-Status and Recent Developments. The S.H. Crandall Festschrift.Elsevier,Amsterdam-Oxford-New York-Tokyo,1986,p.475-496.
7. Ushkalov,V.F.,Redko,S.F.,Korotenko,G.M.,et al.,Identification of Vertical Profile and Cross Level Parameters.Kolebania Sloshnych Mechanicheskich Sistem. Kiev, Naukova Dumka, 1990, p. 39-44.
8. Broersen,P.M.T.,Evaluation of Railway Systems Dynamics by Model Adjustment. Doctoral Thesis, Delft Univ. of Techn., 1976.
9. Matsui,N., Analysis of Lateral Dynamics of a Railway Vehicle with Special Reference to Bogie Design. Vehicle System Dynamics.IUTAM Extensive Summaries,vol.6,No.2-3, Sept. 1977.
10. Ushkalov, V.F., Reznikov, L.M., and Redko, S.F., Statistical Dynamics of Railway Vehicles. Kiev, Naukova Dumka, 1982.

Swets & Zeitlinger 1992

NONLINEAR STABILITY ANALYSIS OF A BOGIE OF A LOW-PLATFORM WAGON

Gaofeng Xu, Alois Steindl and Hans Troger

Technische Universität Wien, Institut für Mechanik, Wiedner Hauptstraße 8-10, A-1040 Wien, Austria

Summary

The nonlinear stability behavior of a special railway bogie is investigated making use of the methods of bifurcation theory. By an artificial increase of the degeneracy of the stability problem of the steady state motion we are able to calculate a turning point in the amplitude curve of the hunting motion of the bogie by investigating still the steady state problem. The location of this turning point is important because it gives the stability limit V_n which practically is more important than the linear stability limit V_c. Further the influence of design measures like the application of special dampers on the location of the turning point is studied.

1 Introduction

Road transportation by heavy trucks cause health problems for the population and damage to the environment. Hence a steadily increasing demand arose in many European countries to shift the transportation of goods from the road to the rail. This is especially true for Austria where one of the most important transportation routes between Northern and Southern Europe passes through narrow Alpine valleys where the burden due to noise and pollution became unbeareable for the population and the environment in the last few years.

In order that such a shift from the road to the rail may be also accepted economically by the transportation business a main requirement is that the overall transportation time must not increase considerably. A combined road-rail transportation system which fulfils this requirement best is to load full size trucks and trailers on railway cars. This has the advantage that the truck can be driven on the car, and hence, loading and unloading can be done very fast and after arriving the final train station the truck-trailer vehicle can proceed its tour on the road immediately. However, this system requires the design of low-platform wagons. This is because of the height of a full size truck the existing tunnel profiles prescribe severe restrictions concerning the height of the railway cars. Usual railway cars cannot be used, and hence, a reduction of the height of the railway car is necessary. This can be achieved by special designs of the bogies where the radius of the wheels must be considerably reduced. In fact the radius of the wheels of these low-platform wagons is about only one third of the radius of an ordinary railway wheel. Due to the smaller wheel the pressure in the wheel rail contact area is strongly increased, and hence, the number of axles must be increased as well. This leads to a design of low-platform wagons with two bogies where each bogie consists of two frames and possesses four axles. Fig. 2 shows a mechanical model of such a bogie with 14 degrees of freedom.

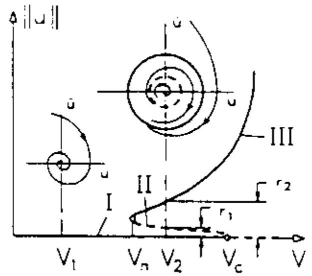

Figure 1: Experimentally obtained limit cycle amplitudes of the hunting motion of a railway bogie from [9]

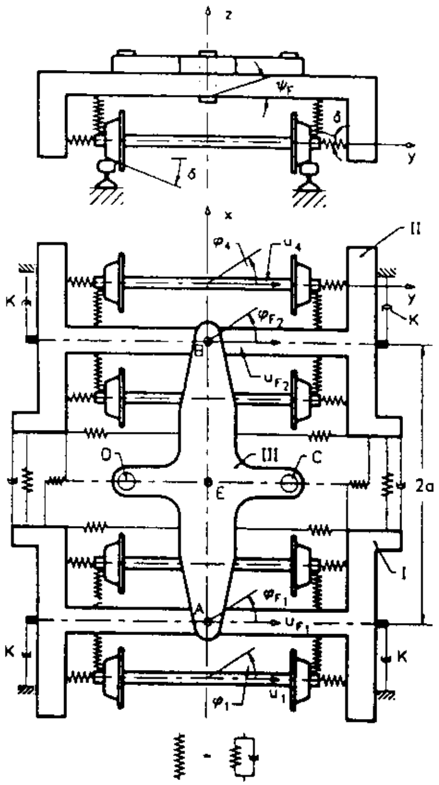

Figure 2: Mechanical model of a special railway bogie with two frames and four axles with 14 degrees of freedom

Ride experiences of the Austrian Railway Company with low-platform cars possessing bogies with small wheels as just mentioned showed that the stability behavior is considerably deteriorated in comparison to cars with regular wheels and already at moderate speeds hunting oscillations occur. In fact such self sustained oscillations were observed at velocities V far below the speed limit V_c predicted by the linear stability analysis.

The occurrence of hunting oscillations is generally well known from experimental investigations with railway systems ([9]) and is, qualitatively, depicted in Fig. 1 where the amplitudes of the existing limit cycles are drawn in the neighborhood of the linear stability limit V_c. We see that a quite complex behavior is obtained which can only be explained by a nonlinear stability analysis since at loss of stability of the straight motion of a railway vehicle, in general, a subcritical Hopf-bifurcation (a flutter instability in engineering terminology) occurs which leads to an oscillatory instability with an limit cycle oscillation of large amplitude (branch III in Fig. 1) at $V = V_c$. Because of the small amplitude of the unstable limit cycle (branch II) the domain of attraction of the stable straight motion (branch I for $V_n \leq V \leq V_c$) is insufficiently small, and therefore, the practically important stability limit is not given by V_c where the straight motion becomes linearly unstable but rather by V_n where the amplitude curve has a turning point. Hence the problem arises to calculate V_n. There are at least three possibilities which come in mind to perform this task.

The simplest but computationally most expensive method would be by pure numerical simulation. That is by integrating the equations of motion numerically for varying initial conditions and checking to which attractor the trajectories converge. This procedure allows to find V_n and also to determine the domain of attraction. However for a system with many degrees of freedom and several nonlinear components such as rail-wheel contact, friction, spring and damper characteristics and geometry, numerical simulation probably will not be the best way to handle such a problem. Especially the influnce of parameters will be difficult to study.

A second way to calculate V_n could be by means of a path following method ([10]). But this is a computationally complicated problem because a periodic solution of a high-dimensional nonlinear problem must be studied which most of the avaliable program packiges are not able to handle.

In fact the case under investigation has 14 degrees of freedom. In addition the wheel-rail contact, the proper modelling of which is most important for the applicability of the analysis to the real problem, even if it is modelled by a simplified Kalker theory ([6], [7]) will lead to nonlinear relations. Hence the equations of motion derived by means of Lagrange's method are a system of nonlinear ordinary differential equations which can be transformed into a system of first order. Hence the application of a path following method as it is, for example, described in [10], if applicable at all, requires large scale computers and is very time consuming.

However there is still a third very elegant but yet simple way to compute the location of the turning point in the amplitude curve in Fig. 1 without having to analyse a periodic solution of a high-dimensional nonlinear system. We note that in the graph depicted in Fig. 1 two local bifurcations occur if we vary the parameter V. The first at $V = V_c$ where the steady state motion loses its stability due to a Hopf bifurcation. The second bifurcation occurs at $V = V_n$ where the unstable limit cycle, that is, the unstable periodic solution changes into a stable one. Obviously the calculation of the turning point requires the solution of a stability problem where the considered state is a periodic solution. This is not an easy problem because already the determination of the (unstable) periodic solution is a nontrivial task.

However following an idea of M. Golubitsky ([4]) the,turning point V_n can be calculated still studying the steady state solution (the straight line motion with constant speed) as the basic motion if the problem is considered as a two parameter system instead of a one parameter (V) one. In this case the two local bifurcation problems at V_c and V_n can be incorporated in one "global" stability problem which, however, is of higher degeneracy. As second parameter besides the driving speed V the conicity δ of the wheels can be used. Studying the problem at those parameter values where not only the linear but also the third order terms vanish in the equation on the center manifold an unfolding of this codimension two case yields the curve with the turning point shown in the Fig. 1.

Hence, we proceed in the following way. First, we give a mechanical formulation of the problem and derive the equations of motion. Second, we linearize the equations of motion about the steady state and solve the corresponding linear eigenvalue problem. Then we apply center manifold theory ([4], [1], [5], [2], [11]) to reduce the full set of nonlinear equations of motion into a two-dimensional bifurcation system corresponding to the pure imaginary pair of eigenvalues which appear at loss of stability at the critical parameter value V_c. We note that this two-dimensional bifurcation system has exactly the same stability behavior as the original n-dimensional system if the deviations of the parameter values from the critical value are small. Introducing polar coordinates we can write this bifurcation system in the form

$$\dot{r} = A_5 r^5 + b r^3 + a r + O(r^7) \qquad (1.1)$$

where in (1.1) only the amplitude equation is given. Here terms up to fifth order have to be included in order to obtain both bifurcations at V_c and at V_n from one global equation. The coefficient A_5 follows from the reduction process and is determined by the parameters of the problem. The two parameters a and b are the two unfolding parameters and depend on the speed V and the conicity of the wheel δ, respectively. a and b vanish for $\delta = \delta_c$ and $V = V_c$. The relation between a, b and V, δ is given in Section 3.3. Fixing δ and varying V one obtains as solution the curve in Fig. 1.

We study the influence of special dampers (marked K) in Fig. 2 on the ride behavior and further we show how the four different axles move relatively to the frame.

Our results allow also to estimate the change in the stability behavior of a bogie during the lifetime of its wheelsets because due to the change of the conicity in the wheel-rail contact due to wear also the stability behavior changes.

2 Mechanical model and equations of motion

2.1 Degrees of freedom

The bogie of Fig. 2 consists of two frames (I,II) which are coupled by a balancier (III). Each of the frames has three degrees of freedom expressed by their transversal motions u_{F_i} in y-direction and the rotatory motions φ_{F_i}, ψ_{F_i} about the z- and x-axis, respectively. The angle φ is the yaw angle and ψ is the roll angle. In addition each axle has two degrees of freedom u_j, φ_j which results in 14 degrees of freedom for the whole bogie.

The motion of the balancier is determined by the motion of the two frames and follows to (Fig. 2)

$$u_B = \frac{u_{F1} + u_{F2}}{2}, \qquad \varphi_B = \frac{u_{F2} - u_{F1}}{2a}.$$

The balancier is fitted to the frames by two pins and friction plates A, B. The car body rests on the friction plates C, D and its position is fixed relative to the balancier by the pin E.

2.2 Suspension and friction forces

The friction force $\mathbf{R}$ at the contact plate is given by

$$\mathbf{R}(v_r) = -\mu P \frac{v_r}{|v_r|} \qquad (2.1)$$

where μ is the friction coefficient, P the vertical load and v_r the relative velocity. We approximate (2.1) by a fifth order polynomial in the form (Fig. 3)

$$\mathbf{R}(v_r) = c_1 v_r + c_3 v_r^2 v_r + c_5 v_r^4 v_r \qquad (2.2)$$

where the coefficients c_i depend on μ and P.

The caracteristics of the springs and dampers are assumed to be linear except those springs acting in vertical direction. They have nonlinear characteristics being progressive or hard springs.

2.3 Wheel-rail contact forces

One of the most important components in the mechanical modelling process is the proper description of the forces and moments resulting from the wheel rail contact. Here we follow [6], [7] where the accurate Kalker theory which, however, is not easy to implement in an analytical analysis, is approximated by a simplified theory which for a stability analysis of the overall motion seems to be still accurate enough.

For the application of this theory the following simplifying assumptions are made:

(1) The geometry of the wheel is a cone with angle δ and that of the rail in the neighborhood of the contact area a circular cylinder with its axis in the direction of the track.

(2) The contact area of the wheel rail contact is an ellipse. The axes a, b of the ellipse can be calculated from the geometry and material constants describing the wheel and rail material.

(3) There is no wheel lift and the wheels are always in contact with the rails. Hence the vertical and roll displacement (rotation about the x-axis) are related to the lateral (y) and yaw (ψ) displacement. Moreover the assumption is made that the dependence of the vertical and roll displacements on the yaw displacement is of second order, and therefore, they are considered to be functions of the lateral displacement, only. Hence we obtain $z = z(y)$ and $\varphi = \varphi(y)$.

Under these assumptions we are able to calculate creep coefficients f_{ij} given by

$$\begin{aligned} f_{11} &= c^2 G C_{11} & f_{23} &= c^3 G C_{23} = -f_{32} \\ f_{22} &= c^2 G C_{22} & f_{33} &= c^4 G C_{33} \end{aligned}$$

where c is the average radius of the contact ellipse and

$$G = \frac{2 G_W G_R}{G_W + G_R}$$

is a combined shear modulus consisting of the shear moduli G_W, G_R of the two materials.

The coefficients C_{ij} have been computed by Kalker ([8]) as a function of the semiaxis ratio a/b of the contact ellipse and the combined Poisson's number

$$\nu = \frac{G(G_W \nu_R + G_R \nu_W)}{2 G_W G_R} .$$

Detailed information about the computation of c and the socalled Kalker coefficients C_{ij} can be obtained from [8].

Now we may write down the following approximate nonlinear relationships

$$\begin{aligned} T_{xi} &= -\mu N_i \tanh\left(\frac{f_{11}}{\mu N_i}\xi_{xi}\right) \\ T_{yi} &= -\mu N_i \tanh\left(\frac{f_{22}}{\mu N_i}\xi_{yi} + \frac{f_{23}}{\mu N_i}\xi_{\varphi i}\right) \end{aligned} \tag{2.3}$$

where the ξ_{xi} and ξ_{yi} are the longitudinal and lateral creepages (the indices 1 and 2 designate the right and left wheel, respectively) and ξ_φ is the rotational creepage. The creepages are defined as ([3])

$$\begin{aligned} \xi_{x_1} &= -\frac{B}{V}\dot{\psi} - \frac{\delta}{r_0}y = -\xi_{x_2} \\ \xi_{y_1} &= \frac{1 - r_0\Gamma}{V}\dot{y} - \psi \\ \xi_{y_2} &= \frac{1 + r_0\Gamma}{V}\dot{y} - \psi \\ \xi_{\varphi_1} &= \frac{\dot{\psi}}{V} + \frac{\Gamma y}{r_0} = \xi_{\varphi_2} \end{aligned}$$

where $2B$ is the width, r_0 the nominal roll radius of the wheel and

$$\Gamma = \frac{\delta}{B - r_0\delta} .$$

In addition we must check that the forces calculated from (2.3) must fulfill the constraint

$$\left(\frac{T_{xi}}{\mu N}\right)^2 + \left(\frac{T_{yi}}{\mu N}\right)^2 \le 1$$

which means that the absolute value of the friction forces is limited by Coloumb's law. Further the validity of (2.3) is only given if $a/b \le 2$.

2.4 Equations of motion

In the derivation of the equations of motion we follow [7], [3] and [12] where they are given in detail. Concerning the limitation of space we cannot go into much detail, however, we want to point out one special feature of the equations of motion of such a railway vehicle by looking at one axle. Basically we obtain for the two degrees of freedom two second order nonlinear differential equations in the two variables u_ℓ and ψ_ℓ of the form

$$\mathbf{M}_\ell \ddot{\boldsymbol{q}}_\ell = \boldsymbol{f}_\ell(\boldsymbol{q}_\ell, \mathbf{T}_\ell(\mathbf{N}_\ell)) \tag{2.4}$$

where $\boldsymbol{q}_\ell = (u_\ell, \psi_\ell)^T$, $\mathbf{M}_\ell$ is the mass tensor and $\boldsymbol{f}_\ell$ a function of the variables and the contact forces. The contact forces themselves, according to (2.3) depend on the normal forces $N_{\ell i}$ which themselves are depending on the $T_{\ell i}$. That means that for one axle in addition to (2.4) also a system of constraint equations

$$\mathbf{N}_\ell = \boldsymbol{g}_\ell(\boldsymbol{q}_\ell, \mathbf{T}_\ell(\mathbf{N}_\ell)) \tag{2.5}$$

is obtained. Hence, to eliminate $\mathbf{N}_\ell$ in (2.4), that is, to express it by the variables $\boldsymbol{q}_\ell$, is not a completely trivial task since $\mathbf{T}_\ell$ appears in (2.5) which is an implicit equation for $\mathbf{N}_\ell$. We solve it by a series expansion in the variables $\boldsymbol{q}_\ell$ up to the required order we need to obtain fifth order terms in (1.1). That is, we obtain

$$N_{\ell i} = N_{\ell i 0} + \sum_j N_{\ell i j} q_{\ell j} + \sum_{j,k} N_{\ell i j k} q_{\ell j} q_{\ell k} + \dots$$

which we substitute into (2.4). This results in a set of equations of motion of the form

$$\mathbf{M}\ddot{\boldsymbol{q}} + \mathbf{Q}(\boldsymbol{q}, \dot{\boldsymbol{q}}) = 0 \tag{2.6}$$

where $\mathbf{Q}(\boldsymbol{q}, \dot{\boldsymbol{q}})$ contains terms up to fifth order in the variables $\boldsymbol{q}$ and $\dot{\boldsymbol{q}}$. For the whole bogie the equations of motion have also the form (2.6) but now the dimension of $\boldsymbol{q}$ is equal to 14. The introduction of new variables in the form $x_1 = u_{F1}$, $x_2 = \dot{u}_{F1}$, ... allows, in a straight forward calculation, since $\mathbf{M}$ is constant, to transform (2.6) into a system of first order in time of the form

$$\dot{\boldsymbol{x}} = \mathbf{F}(\boldsymbol{x}, \lambda) = \mathbf{F}_1(\lambda)\boldsymbol{x} + \mathbf{F}_3(\lambda)\boldsymbol{x}^3 + \mathbf{F}_5(\lambda)\boldsymbol{x}^5 \tag{2.7}$$

where $\mathbf{F}_1(\lambda)$, $\mathbf{F}_3(\lambda)$ and $\mathbf{F}_5(\lambda)$ are the matrices of the coefficients of the terms of first, third and fifth order. The parameter vector λ is given by

$$\lambda = \begin{pmatrix} V \\ \delta \end{pmatrix} .$$

The dimension of $\boldsymbol{x}$ is 28. By the notation $\boldsymbol{x}^3$ we mean a vector containing all possible monomials of third order in the 28 variables. To make this point clear we consider only two variables x_1, x_2. Then there exist four monomials of third order: x_1^3, $x_1^2x_2$, $x_1x_2^2$, x_2^3 and the matrix $\mathbf{F}_3$ would be a 2×4 matrix. The number four can be calculated from the following formula which supplies the number N of different objects where repeatedly occurring objects like $x_1x_2x_3 = x_1x_3x_2$ are already excluded

$$N = \begin{pmatrix} n+r-1 \\ r \end{pmatrix} = \frac{(n+r-1)!}{r!(n-1)!} . \tag{2.8}$$

In (2.8) is n the number of elements and r the order. For example for $n = 2$, $r = 3$ we obtain $N = 4$. If we turn to our problem we have for $n = 28$, $r = 3$: $N = 4060$ and for $n = 28$, $r = 5$: $N = 201376$. That is the matrix $\mathbf{F}_3$ is 28×4060 and the matrix $\mathbf{F}_5$ is 28×201376. However many of these terms are equal to zero and for the computations by means of a special algorithm only the nonzero terms are stored.

We note that no terms of quadratic and fourth order appear in the equations of motion. This fact expresses the reflectional symmetry of the problem with respect to the x,z-plane.

3 Bifurcation analysis

3.1 Critical speed and stability boundary in parameter space

The steady state motion of the bogie is given by $\boldsymbol{x}_0 = \mathbf{0}$, which is a solution of (2.7). The first step in the bifurcation analysis is the calculation of the linear stability limit, that is the critical speed V_c. Mathematically we have to calculate the eigenvalues of the linear operator $\mathbf{F}_1(\lambda)$ for quasistatically increased values of the speed V which is the distinguished component of λ. The second component of λ the angle δ is kept at a fixed value. For low speed all eigenvalues of $\mathbf{F}_1(\lambda)$ have a negative real part, and therefore, the steady state $\boldsymbol{x}_0$ is asymptotically stable. The critical speed will be reached when for the first time one or several eigenvalues cross the imaginary axis. In the simplest (generic) cases this happens either due to a simple zero eigenvalue or due to a pair of purely imaginary eigenvalues. For the bogie always a purely imaginary pair of eigenvalues occurs at the stability limit V_c. This is easy to understand physically because to a zero eigenvalue corresponds a divergent instability and to a purely imaginary pair of eigenvalues corresponds a flutter instability. Obviously for a rail vehicle divergent type of instabilities are not to be expected whereas flutter instabilities lead to hunting motions.

If in addition we vary the conicity angle δ we obtain the stability boundary in V, δ parameter space as depicted in Fig. 4.

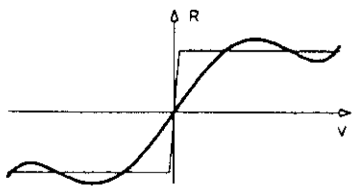

Figure 3: Approximation of the friction force (2.1) by the fifth order polynomial (2.2)

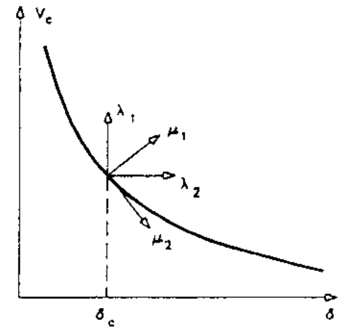

Figure 4: Linear speed limit V_c in its dependence on the conicity angle δ of the wheel

Having calculated V_c we want to know how the system behaves if V is increased through V_c. This requires the treatment of the nonlinear problem.

3.2 Center manifold reduction to a two-dimensional bifurcation system

Center manifold theory serves to reduce the 28-dimensional system of equations of motion (2.7) to a system of bifurcation equations the dimension of which is equal to the number of eigenvalues with real part zero at $\boldsymbol{\lambda} = \boldsymbol{\lambda}_c = (V_c, \delta)^T$. We do not explain this reduction in detail because it is well explained in [11] in chapters 3 and 4. We only mention the necessary calculations. First we perform a linear transformation of coordinates $\boldsymbol{x} \to \mathbf{B}\boldsymbol{y}$ which transforms the matrix $\mathbf{F}_1$ into Jordan form. The two variables y_1, y_2 which correspond to the two eigenvalues with zero real part are denoted as active variables and the $y_3, \ldots, y_{28}$ are called passive variables. Hence (2.7) can be written in the form

$$\begin{aligned} \dot{y}_1 &= -\omega y_2 + g_{13}(y_1, y_2, \boldsymbol{y}_s) + g_{15}(y_1, y_2, \boldsymbol{y}_s) \\ \dot{y}_2 &= \omega y_1 + g_{23}(y_1, y_2, \boldsymbol{y}_s) + g_{25}(y_1, y_2, \boldsymbol{y}_s) \\ \dot{\boldsymbol{y}}_s &= \mathbf{J}_s\boldsymbol{y}_s + \boldsymbol{g}_{s3}(y_1, y_2, \boldsymbol{y}_s) + \boldsymbol{g}_{s5}(y_1, y_2, \boldsymbol{y}_s) \end{aligned} \tag{3.1}$$

where $\boldsymbol{y}_s = (y_3, \ldots, y_{28})^T$, $\mathbf{J}_s$ is a 26×26 matrix whose eigenvalues have all a negative real part. $\boldsymbol{g}_3$ and $\boldsymbol{g}_5$ contain nonlinear terms of third and fifth order, respectively.

Intuitively one can expect that in a local neighborhood of the bifurcation point, that is, for $|V - V_c|$ small, the passive variables $\mathbf{y}_s$ will decay to zero because the corresponding eigenvalues have all a negative realpart, and hence, in (3.1) only the two equations in the active variables will be relevant. However this reasoning can lead to incorrect results if the passive variables are simple set to zero in (3.1). Instead they must be eliminated by means of center manifold theory. This is done by expressing the passive variables by the active variables in the form

$$\mathbf{y}_s = \mathbf{H}(y_1, y_2) \tag{3.2}$$

from $(3.1)_3$. From the general theory ([2], [11]) follows that

$$\mathbf{H}(y_1, y_2) = O(|y_1|^2 + |y_2|^2) \; . \tag{3.3}$$

If we only intended to derive third order bifurcation equations we could set $\mathbf{y}_s = 0$ in $(3.1)_{1,2}$. This follows from the fact that because of (3.3) at least fourth order terms would be obtained from the substitution of (3.2) into $(3.1)_{1,2}$. However, since we derive the equations of motion up to and including fifth order terms in any case the influence of the passive variables on the fifth order terms is given and we must calculate $\mathbf{H}(y_1, y_2)$ at least up to third order terms. The practical calculation is performed by series expansion and equating coefficients. Again also in (3.2) only odd order terms are present. After inserting (3.2) into $(3.1)_{1,2}$ we obtain

$$\begin{aligned} \dot{y}_1 &= -\omega y_2 + r_{13}(y_1, y_2) + r_{15}(y_1, y_2) + O(|\mathbf{y}|^7) \\ \dot{y}_2 &= \omega y_1 + r_{23}(y_1, y_2) + r_{25}(y_1, y_2) + O(|\mathbf{y}|^7) \; . \end{aligned} \tag{3.4}$$

3.3 Normal form and unfolding

The bifurcation equations (3.4) still can be considerably simplified. This can be done by applying normal form theory which allows to reduce the number of nonlinear terms in (3.4) without changing the qualitative behavior of the flow in the two-dimensional phase space spanned by y_1, y_2. The idea is to annihilate by a nonlinear change of variables $\mathbf{y} \rightarrow \mathbf{z}$ as many nonlinear terms as possible. If the linear part in (3.4) were not degenerate all nonlinear terms from (3.4) could be removed. However, due to the degeneracy of the linear part resonant terms occur that cannot be eliminated. Despite of this fact still a strong simplification can be achieved ([11]). If we further introduce polar coordinates $z_1 = r\cos\vartheta$, $z_2 = r\sin\vartheta$ we find

$$\begin{aligned} \dot{r} &= K_3 r^3 + K_5 r^5 + O(|r|^7) \\ \dot{\vartheta} &= \omega + K_2 r^2 + K_4 r^4 + O(|r|^6) \end{aligned} \tag{3.5}$$

where in general $K_3 \neq 0$. In this case the third order terms in (3.5) determine the local stability behavior of the bogie. However, if we want to calculate V_n from a steady state analysis we must use the second parameter δ to make K_3 to vanish. In Fig. 5 K_3 is plotted as a function of δ. To analyze this higher degenerate system terms of fifth order must be considered as they are already included in (3.5).

For $\delta = \delta_c$ we obtain $K_3 = 0$ and the amplitude equation $(3.4)_1$ becomes

$$\dot{r} = A_5 r^5 \tag{3.6}$$

The next step is a universal unfolding of (3.6), that is, an embedding of (3.6) in a parametrized family which includes all qualitative possible solutions of equations of the type of (3.6). The unfolding is given by (1.1). The mathematical unfolding parameters are

$$a = \left.\frac{\partial \alpha_1}{\partial \mu_1}\right|_{\mu_1=\mu_2=0} \mu_1 \; , \qquad b = \left.\frac{\partial K_3}{\partial \mu_2}\right|_{\mu_1=\mu_2=0} \mu_2$$

where α_1 is the real part of the critical eigenvalue. The coefficient $A_5 = K_5(\delta_c)$. The linear relationship between the mathematical unfolding parameters μ_1, μ_2 and the physical $\lambda_1 = V - V_c$ and $\lambda_2 = \delta - \delta_c$ can be seen from Fig. 4.

4 Numerical results

For the data taken for a bogie used by the Austrian Railway Company we obtained the results plotted in Fig. 6. Two things are remarkable from Fig. 6. First, a small

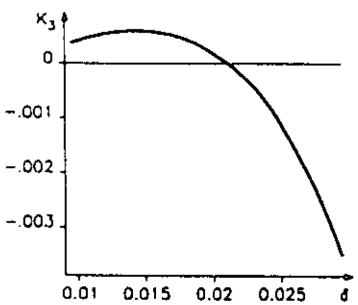

Figure 5: Coefficient K_3 in $(3.5)_1$ in its dependence on the conicity angle δ

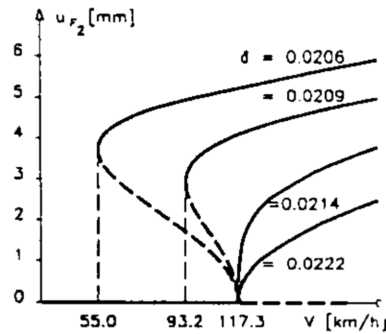

Figure 6: Stability limits V_n given by the turning points for some values of δ

variation of δ does not have a significant influence on the critical speed V_c but has a very significant influence on the location of the turning point. This figure also allows to estimate the change in the stability behavior of a bogie or a whole car due to the change of δ during the life time of a wheel set. Since already for quite low speeds hunting oscillations are predicted by Fig. 6 and have also been observed in practical operation, for example after passing a switch of these dampers certain design measures have been taken. One which proved to be very effective is the use of linear dampers between the frames of the bogie and the car body denoted by K in Fig. 2. There are four of these dampers for each bogie. Depending on their constants we obtain the graphs in Fig. 7 which show that above a certain amount of damping no turning points in the amplitude curve of the hunting motion occur, and hence, the linear stability limit V_c is the practically important critical speed.

From theoretical and experimental studies with bogies with two axles ([7]) it is well known that the front and rear axle oscillate with different amplitude. Hence it may be interesting to see how the different axles of a 4-axle bogie behave. The results are given in Fig. 8 for the bogie 2 of Fig. 7. For example we see that the rear axle has the maximum amplitude.

Finally we note that from the results of Fig. 6 and Fig. 7, which basically are for the two-dimensional bifurcation system (1.1) and $(3.5)_2$, we can return to the physical quantities x_i by performing all necessary steps in the derivation of the bifurcation system in backward direction ([11]). The result are the different motions depicted in Fig. 8. Hence we may conclude that after a hunting instability all components oscillate with the same frequency given by $(3.5)_2$ but different amplitudes.

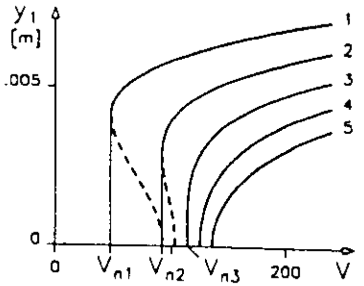

Figure 7: Influence of the dampers K of Fig. 2 on the amplitude of axle 1 for five different damping constants: $d_1 = 5 \cdot 10^4$, $d_2 = 10^5$, $d_3 = 1.5 \cdot 10^5$, $d_4 = 2 \cdot 10^5$, $d_5 = 2.5 \cdot 10^5$ $[N \sec/m]$

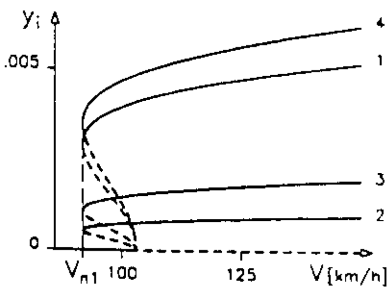

Figure 8: Amplitudes of the four different axles (front (1) – rear (4)) for d_2 of Fig. 7

Acknowledgement

This research project has been partly supported by the "Fonds zur Förderung der wissenschaftlichen Forschung in Österreich" under project P 7003.

References

[1] V. I. Arnold. *Geometrical Methods in the Theory of Ordinary Differential Equations*. Springer-Verlag, New York – Heidelberg – Berlin, 1983.

[2] J. Carr. *Applications of Centre Manifold Theory*, volume 35 of *Applied Math. Sciences*. Springer-Verlag, New York – Heidelberg – Berlin, 1981.

[3] V. K. Garg and R. V. Dukkipati. *Dynamics of Railway Vehicle Systems*. Academic Press, Toronto, 1984.

[4] M. Golubitsky, I. Stewart, and D. Schaeffer. *Singularities and Groups in Bifurcation Theory*, volume 51 and 69 of *Applied Math. Sciences*. Springer-Verlag, New York – Heidelberg – Berlin, 1985, 1988.

[5] J. Guckenheimer and P. Holmes. *Nonlinear Oscillations, Dynamical Systems, and Bifurcations of Vector Fields*, volume 42 of *Applied Math. Sciences*. Springer-Verlag, Berlin – Heidelberg – New York, 1983.

[6] A. Jaschinski. Anwendung der Kalkerschen Rollreibungstheorie zur dynamischen Simulation von Schienenfahrzeugen. Technical report, DFVLR-FB 87-07, 1987.

[7] A. Jaschinski. On the Application of Similiarity Laws to a Scaled Railway Bogie Model. Technical report, DLR-FB 90-06, 1990.

[8] J. J. Kalker. *On the Rolling Contact of Two Elastic Bodies in the Presence of Dry Friction*. PhD thesis, Delft University of Technology, 1967.

[9] D. Moelle and R. Gasch. Nonlinear Bogie Hunting. In A. H. Wickens, editor, *Proc. 7th IAVSD-Symposium in Cambridge (UK) 1981*, pages 455–467, Lisse, 1982. Swets and Zeitlinger B. V.

[10] R. Seydel. *BIFPACK: A program package for calculating bifurcations*. State University of New York, Buffalo, 1985.

[11] H. Troger and A. Steindl. *Nonlinear Stability and Bifurcation Theory: An Introduction for Engineers and Applied Scientists*. Springer-Verlag, Wien – New York, 1991.

[12] G. Xu. *Nichtlineare Dynamik von Eisenbahnfahrzeugen*. PhD thesis, TU-Wien, 1990.

Request for information about current subscription rates and prices for back volumes of
Nonlinear Dynamics, ISSN 0924-090X

Please fill in and return to

Kluwer Academic Publishers, Customer Service, P.O. Box 322, 3300 AH Dordrecht, the Netherlands

Kluwer Academic Publishers, Customer Service, P.O. Box 358, Accord Station, Hingham MA 02018-0358, USA

Please send information about current program and prices
Please send a free sample copy

NAME
INSTITUTE
DEPARTMENT
ADDRESS
Telephone
Telefax
Email

STAMP

Nonlinear Dynamics
Kluwer Academic Publishers,
P.O. Box 17
3300 AA Dordrecht
The Netherlands

TO : The Library
FROM:

V I A I N T E R D E P A R T M E N T A L M A I L

Nonlinear Dynamics **8**: 161–178, 1995.

One and Two-Parameter Bifurcations to Divergence and Flutter in the Three-Dimensional Motions of a Fluid Conveying Viscoelastic Tube with D_4-Symmetry

Dedicated to Professor P. R. Sethna on the Occasion of His 70th Birthday

ISSN 0924-090X

OFFPRINT FROM

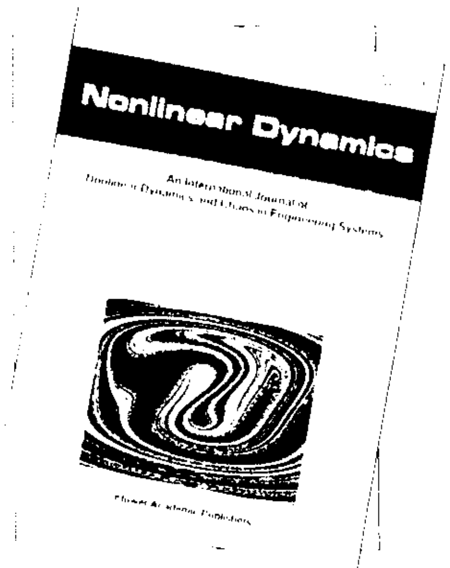

Providing a forum for the rapid publication of original research in the developing field of nonlinear dynamics

Remember the Library! they need your suggestions to service your needs

Kluwer academic publishers

lonlinear Dynamics

n International Journal of Nonlinear Dynamics and Chaos in Engineering Systems

Nonlinear Dynamics provides a forum for the rapid publication of original research in the developing field of nonlinear dynamics. The scope of the journal encompasses all nonlinear dynamic phenomena associated with mechanical, structural, civil, aeronautical, ocean, electrical and control systems. Original contributions based on analytical, computational, and experimental methods are solicited, dealing with such topics as perturbations, computational methods, symbolic manipulation, dynamic stability, local and global methods, bifurcations, chaos, deterministic and random vibrations, multibody dynamics, robotics, fluid solid interactions, system modeling and identification, friction models, signal analysis, and measurement techniques.

Nonlinear Dynamics is indexed/abstracted in *Applied Mechanics Reviews, Shock and Vibration Digest, SciSearch, Research Alert, Engineering Index; Compendex Plus; Ei Page One*

Kluwer Academic Publishers, P.O. Box 17, 3300 AA Dordrecht, The Netherlands

For information about current subscription rates and prices for back volumes for *Nonlinear Dynamics, ISSN 0924-090X* please contact one of the customer service departments of Kluwer Academic Publishers or return the form overleaf to:

Kluwer Academic Publishers, Customer Service, P.O. Box 322, 3300 AH Dordrecht, the Netherlands, Telephone (+31) 78 524 400, Fax (+31) 78 183 273, Email: services@wkap.nl

or

Kluwer Academic Publishers, Customer Service, P.O. Box 358, Accord Station, Hingham MA 02018-0358, USA, Telephone (1) 617 871 6600, Fax (1) 617 871 6528, Email: kluwer@world.std.com

Call for papers

Authors wishing to submit papers related to any of the themes or topics covered by *Nonlinear Dynamics* are cordially invited to prepare their manuscript following the 'Instructions for Authors'. Please request these instructions using the card below.

Author response card
Nonlinear Dynamics

I intend to submit an article on the following topic:

Please send me detailed 'Instructions for Authors'

NAME
INSTITUTE
DEPARTMENT
ADDRESS

Telephone
Telefax
Email

Library Recommendation Form

Route via Interdepartmental Mail

To the Serials Librarian at

From Dept./Faculty of

Dear Librarian,

I would like to recommend our library to carry a subscription to
Nonlinear Dynamics, ISSN 0924-090X
published by Kluwer Academic Publishers

Signed: Date

Nonlinear Dynamics **8**: 161–178, 1995.

One and Two-Parameter Bifurcations to Divergence and Flutter in the Three-Dimensional Motions of a Fluid Conveying Viscoelastic Tube with D_4-Symmetry

Dedicated to Professor P. R. Sethna on the Occasion of His 70th Birthday

A. STEINDL and H. TROGER
Technische Universität Wien, A-1040 Vienna, Austria

(Received: 4 June 1993; accepted: 19 July 1994)

Abstract. The loss of stability of the trivial downhanging equilibrium position of a slender circular tube conveying incompressible fluid flow is studied. The tube is clamped at its upper end and free at its lower end. Inbetween the three-dimensional transversal motion is constrained by an elastic support which is considered to be D_4-symmetric, that is, has the symmetry of the square (Figure 1). Kirchhoff's rod theory and the Kelvin–Voigt viscoelastic law are used to derive the tube equations under the assumption of large displacement but small strain.
The stability analysis is performed making use of the methods of equivariant bifurcation theory, that is, making use of the symmetry properties of the original system in deriving the amplitude equations of the critical modes. All cases of loss of stability which are possible for generic one-parameter bifurcations and the coincident case of a zero root and a purely imaginary pair of roots are investigated.

Key words: Fluid conveying tube, Kirchhoff rod theory, coincident eigenvalues, D_4-symmetry, equivariant bifurcation theory, heteroclinic cycles.

1. Introduction

In the fundamental papers [1] and [2] it is shown that for loss of stability of the vertically downhanging position of a rotationally symmetric tube a number of interesting motions occur. Extensions of the investigation presented in [2] in various respects are given in [3, 8, 10–16]. In this paper we consider a tube with an intermediate elastic support consisting of four springs at midspan that is at $\xi = 0.5$ (Figure 1). Since the tube itself is considered to be rotationally symmetric the whole system has the symmetry of the square or the D_4-symmetry.

By variation of the stiffness c_s of the springs we are able to create qualitatively different types of loss of stability [18]. Generically we have either a divergent (c_s large) or a flutter (c_s small) type of instability. However, for a special value of the stiffness of the elastic support we also obtain a codimension two bifurcation resulting in a coupled divergence and flutter instability. The eigenvalue structure of this coupled case is given by a zero eigenvalue and a purely imaginary pair. These three cases will be treated in this paper. We note that depending on the location of the elastic support expressed by ξ in Figure 1 for the coupled instability, besides the case, just mentioned, also a nilpotent double zero root eigenvalue structure is possible [18].

For the description of the motion of the tube we use Kirchhoff's rod theory [4, 9] which results in a large displacement but small strain model allowing in a straight-forward way to include internal damping into the model.

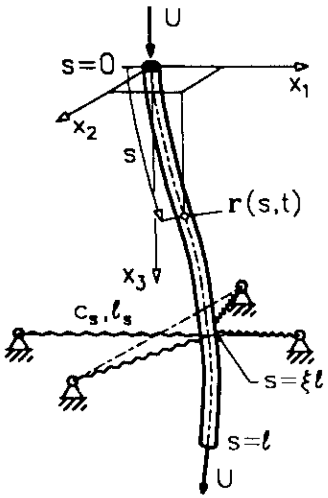

Fig. 1. Mechanical model of the fluid carrying tube with intermediate $\mathbf{D}_4$-symmetric elastic support.

To derive the amplitude equations of the critical modes (bifurcation equations) after loss of stability of the trivial downhanging state of the tube we make extensively use of the methods of equivariant bifurcation theory [6].

2. Equations of Motion and Reduction to Bifurcation Equations

2.1. Mechanical Model and Its Symmetry

A detailed description of the mechanical model and the derivation of the equations of motion is given in [13] and with less detail in [16]. We only indicate here some important points. Two quantities describe the deformation of the tube which is assumed to be an inextensible thin viscoelastic rod of uniform circular annular cross-section. First the radius vector $\mathbf{r}(s,t)$ defining the location of a point of the axis of the tube and second the rotation matrix $\mathbf{B}(s,t) \in \mathbf{SO}(3)$ defining the orientation of the cross-section of the tube given by the vectors $\mathbf{t}_1, \mathbf{t}_2, \mathbf{t}_3$ with respect to a space fixed triad $\mathbf{e}_1, \mathbf{e}_2, \mathbf{e}_3$ (Figure 2). In the following $(\ )' = \partial/\partial s$ and $(\dot{\ }) = \partial/\partial t$.

From the rotation matrix $\mathbf{B}$ we can calculate a skew symmetric matrix $\hat{\Omega}$ in the form

$$\hat{\Omega}(s,t) = \mathbf{B}^{-1}\mathbf{B}' = \begin{pmatrix} 0 & -\Omega_3 & \Omega_2 \\ \Omega_3 & 0 & -\Omega_1 \\ -\Omega_2 & \Omega_1 & 0 \end{pmatrix}, \tag{1}$$

where the quantities Ω_1 and Ω_2 measure bending of the rod about the axes $\mathbf{t}_1$ and $\mathbf{t}_2$ and Ω_3 measures the twist about $\mathbf{t}_3$. By $\hat{\Omega}$ a vector $\boldsymbol{\Omega} = (\Omega_1, \Omega_2, \Omega_3)^T$ is defined. The use of Eulerian angles to represent the rotation matrix results in singular situations at the trivial configuration. Hence, we follow [2] and use the coordinates x_1, x_2 and an angle describing the twist as variables. From the linear and angular momentum principles and the constitutive law we obtain the following set of nonlinear partial differential equations of motion in dimensionless

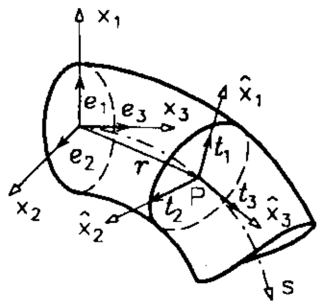

Fig. 2. The deformation of the tube is described by the position of the centerline $\mathbf{r}(s,t)$ and the orientation of the tripod $(\mathbf{t}_1, \mathbf{t}_2, \mathbf{t}_3)$.

variables

$$\begin{aligned} \mathbf{r}' &= \mathbf{B}\mathbf{e}_3 \\ \mathbf{B}' &= \mathbf{B}\hat{\Omega} \\ \mathbf{T}' &= \mathbf{T} \times \boldsymbol{\Omega} - \mathbf{F} \times \mathbf{e}_3 \\ \mathbf{F}' &= \mathbf{F} \times \boldsymbol{\Omega} + \mathbf{B}^T(-\gamma\mathbf{e}_3 + \alpha_e\dot{\mathbf{r}} + \ddot{\mathbf{r}} + 2\sqrt{\beta}\,\varrho\dot{\mathbf{r}}' + \varrho^2\mathbf{r}'') \end{aligned} \tag{2}$$

where $\mathbf{F}$ is the resultant force in the cross-section. Due to the inextensibility constraint and the neglection of shear deformation there exists no constitutive relationship involving $\mathbf{F}$ and only one between the moment vector $\mathbf{T} = (T_1, T_2, T_3)^T$ and the deformation vector $\boldsymbol{\Omega}$ in the form

$$\begin{aligned} T_1 &= -(\Omega_1 + \alpha_1\dot{\Omega}_1), \\ T_2 &= -(\Omega_2 + \alpha_1\dot{\Omega}_2), \\ T_3 &= -\gamma_3(\Omega_3 + \alpha_3\dot{\Omega}_3), \end{aligned} \tag{3}$$

where $\gamma_3 = GJ_T/EJ$ is the quotient between the torsional and bending stiffnesses and the α_i are material damping coefficients. β gives a ratio between the masses of the tube and the fluid. ϱ is proportional to the velocity U of the fluid flow and α_e is an external damping coefficient. Further we have now the boundary conditions at $s = 0$ and $s = 1$

$$\mathbf{r}(0) = \mathbf{0}, \quad \mathbf{B}(0) = \mathbf{E}, \quad \mathbf{F}(1) = \mathbf{0}, \quad \mathbf{T}(1) = \mathbf{0}, \tag{4}$$

and the jump condition for $\mathbf{F}$ at the location ξ of the elastic support

$$\mathbf{F}(\xi_+) - \mathbf{F}(\xi_-) = -\mathbf{B}^T(\xi)\mathbf{f}_s, \tag{5}$$

where $\mathbf{f}_s$ is the restoring force of the spring. For the $\mathbf{D}_4$-symmetric problem $\mathbf{f}_s$ is given up to third order terms by

$$\mathbf{f}_s = -c\begin{pmatrix} x_1 + \alpha_s\dot{x}_1 + \varepsilon_s^2(\frac{x_1}{2}(x_1^2 - 4x_2^2) + \alpha_2[(x_1^2 - x_2^2)\dot{x}_1 - 2x_1x_2\dot{x}_2]) \\ x_2 + \alpha_s\dot{x}_2 + \varepsilon_s^2(\frac{x_2}{2}(x_2^2 - 4x_1^2) - \alpha_2[(x_1^2 - x_2^2)\dot{x}_2 + 2x_1x_2\dot{x}_1]) \\ 0 \end{pmatrix} \tag{6}$$

where $c = \ell^3 c_s/(2EJ)$ is the dimensionless spring stiffness, α_s a damping constant and $\varepsilon_s = \ell/\ell_s$ where ℓ_s is the length of a spring. $\mathbf{f}_s$ becomes rotationally symmetric for $\ell_s \to \infty$.

Due to the circular cross-section of the tube and the arrangement of four springs, we have a $\mathbf{D}_4$-symmetric system, that is a system possessing the symmetry of the square.

If we designate the corresponding transformation $\mathbf{D} \in \mathbf{D}_4$, then it is either a rotation

$$\mathbf{D}_R = \mathbf{B}_3(\zeta) = \begin{pmatrix} \cos\zeta & -\sin\zeta & 0 \\ \sin\zeta & \cos\zeta & 0 \\ 0 & 0 & 1 \end{pmatrix} \tag{7}$$

about an angle $\zeta = 2k\pi/4$ or a reflection $\mathbf{D}_S$ expressed by

$$\mathbf{D}_S = \mathbf{B}_3(\zeta)\cdot\mathbf{I}_{xz}$$

where $\mathbf{I}_{xz} = \mathrm{diag}(1, -1, 1)$. All the expressions in (2), (4) and (5) are equivariant (see [18]) under the following operations

$$\begin{aligned} &\mathbf{r} \to \mathbf{Dr}, &&\mathbf{B} \to \mathbf{DBD}^T \\ &\mathbf{T} \to (\det \mathbf{D})\mathbf{DT}, &&\mathbf{F} \to \mathbf{DF} \end{aligned} \tag{8}$$

which can be checked by inserting (8) into (2), (4) and (5).

Since two of the conditions in (8) are not completely obvious we give short explanations.

The transformation $\mathbf{B} \to \mathbf{DBD}^T$ contains two rotations. The first is a rotation of the tube by an angle of $\pi/2$ about the x_3-axis. However, since the tube is clamped at $s = 0$ the rotated position violates the boundary conditions. Hence, the tube must be rotated by the same angle around the tangent to its deformed centerline in the opposite direction.

The relation $\tilde{\mathbf{T}} = (\det \mathbf{D})\mathbf{DT}$ can be derived in the following way. From $\mathbf{B}' = \mathbf{B}\hat{\Omega}$ according to (1) and $\tilde{\mathbf{B}} = \mathbf{DBD}^T$ follows

$$\tilde{\mathbf{B}}' = \mathbf{D}\mathbf{B}'\mathbf{D}^T = \mathbf{D}\mathbf{B}\hat{\Omega}\mathbf{D}^T = \tilde{\mathbf{B}}\hat{\tilde{\Omega}} = \mathbf{D}\mathbf{B}\mathbf{D}^T\hat{\tilde{\Omega}}. \tag{9}$$

Equating the third and fifth term results in

$$\hat{\tilde{\Omega}} = \mathbf{D}\hat{\Omega}\mathbf{D}^T. \tag{10}$$

Calculating this expression for $\mathbf{D}_S$ and $\mathbf{D}_R$ we obtain $\tilde{\Omega} = -\mathbf{D}_S\Omega$ and $\tilde{\Omega} = \mathbf{D}_R\Omega$, respectively. These two expressions can be summed up into: $\tilde{\Omega} = \det(\mathbf{D})\mathbf{D}\Omega$.

2.2. Stability Boundary and Center Manifold Reduction

In order to calculate the stability boundary [18] in the (ϱ, c) parameter space, we perform the linearization of the equations of motion about the trivial downhanging equilibrium position

$$\mathbf{r} = s\mathbf{e}_3, \quad \mathbf{B} = \mathbf{E}, \quad \mathbf{T} \equiv 0, \quad \mathbf{F} = (1-s)\gamma\mathbf{e}_3 \tag{11}$$

which is a solution to (2) for all values of ϱ and c. The state (11) is invariant under all transformations $\mathbf{D} \in \mathbf{D}_4$.

Due to the symmetry properties of the system we obtain two identical linearized bending equations (see [18]) which, in the dependent variables x_1, x_2 and χ where χ is the twisting angle [4], can be written in the form

$$\ddot{x}_i + \delta\dot{x}_i + x_i^{IV} + \alpha_i\dot{x}_i^{IV} + 2\sqrt{\beta}\,\varrho\dot{x}_i' + \varrho^2 x_i'' - \gamma[(1-s)x_i']' = 0 \tag{12}$$

for $i = 1, 2$. Further one equation

$$\gamma_3(\chi'' + \alpha_3\dot{\chi}'') = 0 \tag{13}$$

for χ is obtained which is decoupled from (12). Also the boundary and jump conditions decouple to

$$\begin{aligned} &x_i(0) = 0, \quad x_i'(0) = 0, \quad \chi(0) = 0, \\ &x_i''(1) + \alpha_1\dot{x}_i''(1) = 0, \quad x_i'''(1) + \alpha_1\dot{x}_i'''(1) = 0, \quad \gamma_3(\chi'(1) + \alpha_3\dot{\chi}'(1)) = 0, \\ &x_i'''(\xi_+) + \alpha_1\dot{x}_i'''(\xi_+) - (x_i'''(\xi_-) + \alpha_1\dot{x}_i'''(\xi_-)) = -c(x_i(\xi) + \alpha_s\dot{x}_i(\xi)). \end{aligned} \tag{14}$$

The trivial state (11) is asymptotically stable for zero flow rate $\varrho = 0$. This is obvious from an engineering point of view. Now we increase the flow rate ϱ quasistatically until the trivial downhanging state of the tube becomes unstable. The parameter value for which this is the case will be denoted by ϱ_c. In order to determine ϱ_c, we have to solve an inverse eigenvalue problem [18]. This can be done by the usual separation of variables technique, resulting in nonlinear boundary value problems for systems of ordinary differential equations. Since the solution of (13) is exponentially stable and the equations (12) for x_1 and x_2 are identical, only one equation of (12) must be solved. Of course, each eigenvalue obtained for this equation must be doubled. Hence the multiplicity of the critical eigenvalues is twice the value of the planar system. As it is described in [18] in a one parameter family (ϱ) both zero eigenvalues and purely imaginary pairs of eigenvalues occur generically depending on the stiffness c of the elastic support. For special values of c coincident eigenvalue cases occur, the structure of which depends on the location of the elastic support expressed by ξ as it is explained in [18]. For the case $\xi = 0.5$ considered here one purely imaginary pair and one zero root, both with multiplicity two, are found. This can be seen from the stability boundary shown in Figure 3. Here the curve denoted by the 0 is the boundary for the divergent instability and the curves denoted by $\pm i\omega$ are the boundaries for the flutter instability for two different values of internal damping α_1. The divergent curve is not affected by different damping values. The stable domain is below the bold curve. It is interesting to note that for small values of c, when a flutter instability is found, the internally damped tube has a smaller critical flow rate than the undamped tube. Thus small internal damping may have a destabilizing effect for the flow conveying tubes in case of a flutter instability for a weakly supported tube.

In the derivation of the bifurcation equations for the problem under study we will obtain three different sets of bifurcation equations which are either a set of two, four or six nonlinear first order ordinary differential equations depending on the value of c. These sets of bifurcation equations which are the amplitude equations of the critical modes are derived by center manifold theory [5, 18].

The key condition for the possibility of the reduction of the infinite system governed by partial differential equations to a low dimensional bifurcation system governed by ordinary differential equations is that besides the critical eigenvalues, which are located on the imaginary axis, all other eigenvalues must be strictly negative. Hence, not only the critical eigenvalues, but also the whole spectrum must be calculated [12]. We only shortly indicate the result of this calculation. The limiting behavior of the spectrum of the modes of higher spatial order is as follows: There exist two families of eigenvalues one of which converges rapidly to $-\infty$, whereas the second one accumulates at $\lambda = -1/\alpha_1$, due to the appearance of material damping in the highest order derivatives. The location of the remaining eigenvalues must be

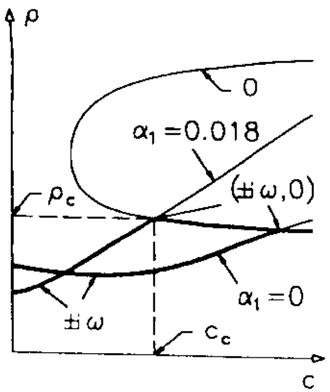

Fig. 3. Stability boundary in ρ, c parameter space for $\xi = 0.5$ and two values of internal damping $\alpha_1 = 0$ and $\alpha_1 = 0.018$. The stable domain is below the bold curve and the unstable domain above it.

calculated numerically. It can be shown that besides the critical eigenvalues all eigenvalues have strictly negative real parts which guarantees the contraction property of the flow towards the Center Manifold. Hence the requirements for the application of Center Manifold theory are satisfied.

For the calculation of the nonlinear terms in the bifurcation equations we have to note that though the bending and twisting motions decouple in the linearized case [(12) and (13)], there is a nonlinear coupling between bending and twisting in the nonlinear case, which must not be neglected.

Making use of (3) the differential equation for the twisting moment T_3 follows from $(2)_3$ to

$$T_3' = T_1\Omega_2 - T_2\Omega_1 = -\alpha_1(\dot{\Omega}_1\Omega_2 - \dot{\Omega}_2\Omega_1) \tag{15}$$

with the condition $T_3(1) = 0$. It has to be integrated for every distinct pair of functions. Now the material law can be regarded as an ordinary differential equation for Ω_3

$$\gamma_3(\Omega_3 + \alpha_3\dot{\Omega}_3) = -T_3 \tag{16}$$

which is solved as usual by a power series expansion.

2.3. Symmetry of the Bifurcation Equations

The bifurcation equations inherit the symmetry properties of the original system. It is convenient to write the bifurcation equations in complex variables z_1, z_2, z_3 introduced in [12] or [18]. Then the action of the rotation is expressed by (7):

$$z_1 \to e^{i\zeta}z_1, \quad z_2 \to e^{-i\zeta}z_2, \quad z_3 \to e^{i\zeta}z_3. \tag{17}$$

The mirror reflection is expressed by:

$$z_1 \leftrightarrow z_2, \quad z_3 \leftrightarrow \bar{z}_3. \tag{18}$$

The normal form reduction introduces the additional phase shift symmetry $\mathbf{S}^1$ into the equations of motion:

$$\vartheta \in \mathbf{S}^1 : (z_1, z_2, z_3) \to (e^{i\vartheta}z_1, e^{i\vartheta}z_2, z_3). \tag{19}$$

The actual calculation of the bifurcation equations is a nontrivial task due to the nonlinear coupling between bending and twisting.

3. Bifurcation Equations and Diagrams

3.1. One Zero Root with Multiplicity Two

If c is large a divergent instability occurs and the bifurcation equation is one scalar equation if we use the complex variable z_3 [18]. Up to third order terms it takes the form

$$\dot{z} = \sum_{j+k=3} a_{jk} z_3^j \bar{z}_3^k = g_3(z_3, \bar{z}_3). \tag{20}$$

The equivariance condition requires

$$g_3(\mathbf{D}_R\mathbf{z}) = \mathbf{D}_R g_3(\mathbf{z}) \tag{21}$$

where $D_R = D_{\pi/2}$ according to (7). Hence we obtain from (21)

$$e^{i\pi(j-k)/2} z_3^j \bar{z}_3^k = e^{i\pi/2} z_3^j \bar{z}_3^k \tag{22a}$$

yielding

$$i\frac{\pi}{2}(j-k) = i\frac{\pi}{2} + 2k\pi i \tag{22b}$$

or

$$j - k \equiv 1 \quad (\text{mod } 4). \tag{22c}$$

The solutions of (22) at third order $(j + k = 3)$ are

$$(1) \quad j = 2, k = 1, \quad (2) \quad j = 0, k = 3. \tag{23}$$

Hence we obtain the one-parameter (μ) unfolded bifurcation equation, where the parameter μ is proportional to the flow rate $\rho - \rho_c$

$$\dot{z}_3 = \mu z_3 + A_9 z_3^2 \bar{z}_3 + A_{12}\bar{z}_3^3. \tag{24}$$

The reflectional symmetry implies that all coefficients, that is μ, $A_9 = c_9 + id_9$ and $A_{12} = c_{12} + id_{12}$, must be real.

There are three different steady state solutions:

(a) Trivial state $z_3 = 0$. It is stable for $\mu < 0$ and unstable for $\mu > 0$.

(b) Buckled state in the direction of a spring. For $z_3 = b$, where b is real, we have

$$\mu b + c_9 b^3 + c_{12} b^3 = 0. \tag{25}$$

The stability of the buckled state is determined by the eigenvalues: $-4c_{12}b^2$ and $2(c_9 + c_{12})b^2$ which must be both negative for a stable state.

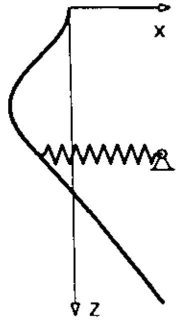

Fig. 4. Planar statically buckled tube corresponding to a stable postbifurcation state.

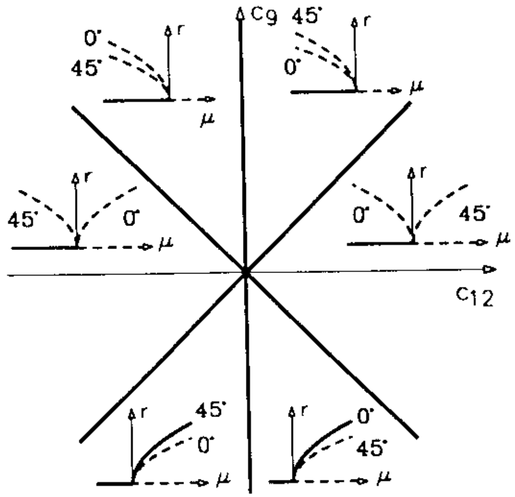

Fig. 5. Bifurcation diagram for the divergence bifurcation showing buckled solutions in directions of the springs (0°) and diagonal directions (45°). Full lines designate stable solutions and dashed lines unstable ones.

(c) Buckled state in diagonal (45°) direction. For $z_3 = e^{i\pi/4}b$ we obtain

$$\mu e^{i\pi/4}b + c_9 b^3 e^{i\pi/2} e^{-i\pi/4} + c_{12} e^{-i3\pi/4} b^3 = 0 \tag{26}$$

or

$$\mu b + (c_9 - c_{12})b^3 = 0. \tag{27}$$

The stability is determined by the eigenvalues: $4c_{12}b^2$ and $2(c_9 - c_{12})b^2$.

The form of the planar buckled tube is shown in Figure 4. The representation of the various solutions in a bifurcation diagram is given in Figure 5. The basic difference to the system with rotationally symmetric support treated in [18], where the position of the plane in which

the tube buckles remains undetermined, is that here the positions of the plane (in the direction of the spring or diagonal) in which the tube buckles are determined by the parameters of the problem, which enter in c_9 and c_{12}.

3.2. One Purely Imaginary Pair with Multiplicity Two

If c is small a flutter instability occurs and in complex coordinates the bifurcation equations are a two-dimensional system of the form

$$\dot{z}_i = (\mu + i\omega)z_i + g_i(z_1, \bar{z}_1, z_2, \bar{z}_2), \quad i = 1, 2 \tag{28}$$

where the third order terms are of the following form

$$g_i = \sum_{j+k+\ell+m=3} a_{ijk\ell m} z_1^j \bar{z}_1^k z_2^\ell \bar{z}_2^m \tag{29}$$

Application of the equivariance condition, taking the relations

$$\begin{aligned} g_j(\mathbf{D}_R\mathbf{z}) &= i^{j-k-\ell+m} g_j(\mathbf{z}) \\ g_j(\mathbf{D}_S\mathbf{z}) &= g_j(z_2, \bar{z}_2, z_1, \bar{z}_1) \\ g_j(\mathbf{R}_\vartheta\mathbf{z}) &= e^{i(j-k+\ell-m)\vartheta} g_j(\mathbf{z}), \end{aligned} \tag{30}$$

into account results in the following set of equations for g_1 (for g_2 we obtain -1 on the right hand side of the first equation to follow)

$$\begin{aligned} j - k - \ell + m &\equiv 1 \pmod 4 \\ j - k + \ell - m &= 1 \\ j + k + \ell + m &= 3. \end{aligned} \tag{31}$$

Their solution yields three terms in each equation

$$\begin{aligned} \dot{z}_1 &= (\mu + i\omega)z_1 + (A_1 z_1\bar{z}_1 + A_2 z_2\bar{z}_2)z_1 + A_3\bar{z}_1 z_2^2 \\ \dot{z}_2 &= (\mu + i\omega)z_2 + (A_1 z_2\bar{z}_2 + A_2 z_1\bar{z}_1)z_2 + A_3\bar{z}_2 z_1^2 \end{aligned} \tag{32}$$

with $A_j = c_j + id_j$. We look for periodic solutions of (32) which, following [6], we represent by

$$z_1 = \tilde{z}_1 e^{i\nu t}, \quad z_2 = \tilde{z}_2 e^{i\nu t}. \tag{33}$$

Inserting (33) into (32) we obtain

$$\begin{aligned} \dot{\tilde{z}}_1 &= (\mu + i\omega - i\nu)\tilde{z}_1 + (A_1\tilde{z}_1\bar{\tilde{z}}_1 + A_2\tilde{z}_2\bar{\tilde{z}}_2)\tilde{z}_1 + A_3\bar{\tilde{z}}_1\tilde{z}_2^2 \\ \dot{\tilde{z}}_2 &= (\mu + i\omega - i\nu)\tilde{z}_2 + (A_1\tilde{z}_2\bar{\tilde{z}}_2 + A_2\tilde{z}_2\bar{\tilde{z}}_1)\tilde{z}_2 + A_3\tilde{z}_1^2\bar{\tilde{z}}_2. \end{aligned} \tag{34}$$

There exist four different symmetric steady state solutions of (34):

(a) Trivial state: $\tilde{z}_1 = \tilde{z}_2 = 0$. It is stable for $\mu < 0$ and unstable for $\mu > 0$.

(b) Planar oscillation in the direction of the spring (SW_0): $\tilde{z}_1 = \tilde{z}_2 = a$ where a is real. From

$$(\mu + i\omega - i\nu)a + (A_1 + A_2 + A_3)a^3 = 0 \tag{35}$$

follows the nontrivial solution

$$a=\sqrt{-\mu/(c_1+c_2+c_3)},\qquad \nu=\omega+(d_1+d_2+d_3)a^2. \tag{36}$$

The stability of this solution is determined by the sign of $(c_1+c_2+c_3)$ the following two quantities, the calculation of which is explained in Appendix A:

$$\text{trace: } 2(c_1-c_2-3c_3)a^2,\quad \text{det: } 8a^4(|A_3|^2-\mathrm{Re}\{(A_1-A_2)\bar{A}_3\}). \tag{37}$$

For a stable state the trace must be negative and the determinant positive.

(c) Planar oscillation in diagonal (45°) direction (SW_{45}): $z_1=a$, $z_2=ia$. From

$$(\mu+i\omega-i\nu)a+(A_1+A_2-A_3)a^3=0 \tag{38}$$

follows

$$a=\sqrt{-\mu/(c_1+c_2-c_3)},\qquad \nu=\omega+(d_1+d_2-d_3)a^2,$$

$$\text{trace: } 2(c_1-c_2+3c_3)a^2,\quad \text{det: } 8a^4(|A_3|^2+\mathrm{Re}\{(A_1-A_2)\bar{A}_3\}). \tag{39}$$

(d) Rotating wave solution (TW) [18]: $z_1=a$, $z_2=0$. From

$$(\mu+i\omega-i\nu)a+A_1a^3=0 \tag{40}$$

follows

$$a=\sqrt{-\mu/c_1},\qquad \nu=\omega+d_1a^2,$$

$$\text{trace: } 2(c_2-c_1)a^2,\quad \text{det: } 4a^4(|A_2-A_1|^2-|A_3|^2). \tag{41}$$

In Figure 6 the bifurcation diagram showing the different domains of existence of the symmetric solutions is given. The corresponding solutions are shown in Figure 7. It is shown that 12 different domains exist. In domains 6 and 8 two stable solutions can exist [6]. In these cases the initial conditions decide which solution is attained.

In [17] it is shown that besides the above mentioned symmetric solutions also nonsymmetric solutions might exist, depending on the special nonlinearities appearing in the bifurcation equations. They, for example, could be periodic solutions which trace out approximate ellipses or be planar oscillations of the tube in a plane which is neither in the direction of a spring nor in diagonal direction. Additionally quasiperiodic oscillations are possible which are superpositions of two basic oscillating motions. We only indicate here that the elliptical solution exists for the tube problem, however, this solution is unstable [14] whereas the quasiperiodic motion could also be stable.

3.3. One Zero Root and One Purely Imaginary Pair with Multiplicity Two

For $c=c_c$ at the loss of stability coupling of divergence and flutter occurs. In complex coordinates the bifurcation equations are a three-dimensional system of the form

$$\dot z_i=(\mu+i\omega)z_i+g_i(z_1,\bar z_1,z_2,\bar z_2,z_3,\bar z_3),\quad i=1,2$$
$$\dot z_3=\lambda z_3+g_3(z_1,\bar z_1,z_2,\bar z_2,z_3,\bar z_3) \tag{42}$$

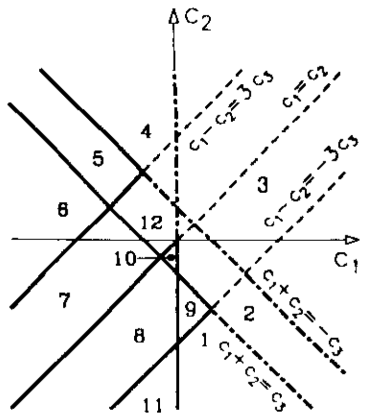

Fig. 6. The bifurcation diagram for the $\mathbf{D}_4$-Hopf bifurcation is partitioned into 12 qualitatively different domains in the (c_1,c_2)-plane for $c_3<0$. Fully drawn lines form the boundary of domains where stable solutions can exist.

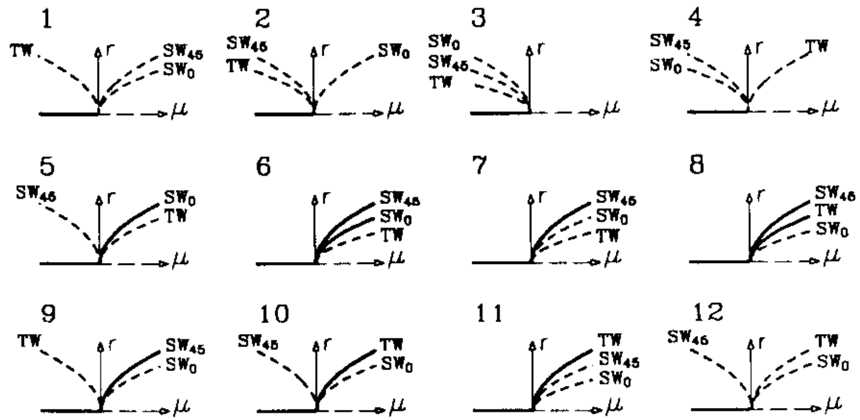

Fig. 7. Amplitudes of the periodic solutions corresponding to the domains in Figure 6. There are planar oscillations of the tube in direction of the springs (SW_0) and in diagonal direction (SW_{45}) and rotating tube motions (TW).

where the third order terms are of the following form

$$g_i=\sum_{j+k+\ell+m+r+s=3} a_{ijk\ell mrs}z_1^j\bar z_1^k z_2^\ell \bar z_2^m z_3^r\bar z_3^s. \tag{43}$$

Application of the equivariance conditions given by (17), (18) and (19) results in the following set of third order two parameter (λ,μ) unfolded equivariant bifurcation equations [12]

$$\dot z_1=(\mu-i\nu_1)z_1+(A_1z_1\bar z_1+A_2z_2\bar z_2+A_3z_3\bar z_3)z_1$$
$$\qquad +A_4z_2z_3^2+A_5\bar z_1z_3^2+A_6z_2\bar z_3^2,$$
$$\dot z_2=(\lambda+i\omega-i\nu_1)z_2+(A_2z_1\bar z_1+A_1z_2\bar z_2+A_3z_3\bar z_3)z_2$$

Table 1. Solutions of (44) and their isotropy subgroups. The solution (11) corresponds to degenerate stationary bifurcations and (12) describes either a spatial oscillation along an elliptic orbit or a standing wave in a plane, which is not a mirror-reflection plane.

No.	Orbit repr.	Σ	$\Sigma_x = \mathrm{Fix}(\Sigma)$	dim Σ_x
(0)	$(0,0,0)$	$\mathbf{D}_4 \times \mathbf{S}^1$	$(0,0,0)$	0 Trivial solution
(1)	$(0,0,b)$	$\mathbf{Z}_2(\kappa) \times \mathbf{S}^1$	$(0,0,x)$	1 Buckling mode 1
(2)	$(0,0,\sqrt{-i}\,b)$	$\mathbf{Z}_2(\kappa\zeta) \times \mathbf{S}^1$	$(0,0,\sqrt{-i}\,x)$	1 Buckling mode 2
(3)	$(a,a,0)$	$\mathbf{Z}_2(\kappa) \oplus \mathbf{Z}_2^c$	$(w,w,0)$	2 Standing wave 1
(4)	$(a,ia,0)$	$\mathbf{Z}_2(\kappa\zeta) \oplus \mathbf{Z}_2^c$	$(w,iw,0)$	2 Standing wave 2
(5)	$(a,0,0)$	$\tilde{\mathbf{Z}}_4 = \{(-\zeta,\zeta)\}$	$(w,0,0)$	2 Rotating wave
(6)	(a,a,b)	$\mathbf{Z}_2(\kappa)$	(w,w,x)	3 (1) ‖ (4)
(7)	(a,a,ib)	$\mathbf{Z}_2(\kappa\pi,\pi)$	(w,w,iy)	3 (1) ⊥ (4)
(8)	$(a,ia,\sqrt{-i}\,b)$	$\mathbf{Z}_2(\kappa\zeta)$	$(w,iw,\sqrt{-i}\,x)$	3 (2) ‖ (5)
(9)	$(a,ia,\sqrt{i}\,b)$	$\mathbf{Z}_2(\kappa\zeta\pi,\pi)$	$(w,iw,\sqrt{i}\,x)$	3 (2) ⊥ (5)
(10)	$(a,0,b)$	$\mathbf{1}$	$(w_1,\mathcal{O}(w_1,w_3),w_3)$	6 modulated wave
(11)	$(0,0,w)$	$\mathbf{S}^1$	$(0,0,w)$	2 asymmetric buckling
(12)	$(a,b,0)$	$\mathbf{Z}_2^c$	$(w_1,w_2,0)$	4 asymmetric oscillation
(13)	(a,a,w)	$\mathbf{1}$		4
(14)	(a,ia,w)	$\mathbf{1}$		4
(15)	(a,w_2,w_3)	$\mathbf{1}$		6

$$
\begin{aligned}
&+ A_4 z_1 \bar{z}_3^2 + A_5 z_1^2 \bar{z}_2 + A_6 \bar{z}_1 z_3^2, \\
\dot{z}_3 = {}& (\mu - i\nu_3) z_3 + (A_7 z_1 \bar{z}_1 + A_8 z_2 \bar{z}_2 + A_9 z_3 \bar{z}_3) z_3 \\
&+ A_{10} z_1 \bar{z}_2 \bar{z}_3 + A_{11} \bar{z}_1 z_2 \bar{z}_3 + A_{12} \bar{z}_3^3,
\end{aligned}
\tag{44}
$$

where according to (33) $z_i \to z_i e^{i\nu_1 t}$ ($i = 1, 2$) and $z_3 \to z_3 e^{i\nu_3 t}$ and $A_j = c_j + i d_j$ for $i = 1, \ldots, 12$, $A_8 = \bar{A}_7$ and $d_9, \ldots, d_{12} = 0$.

Zeros of (44) correspond to stationary states of the pipe ($\nu_j = 0$), periodic solutions ($\nu_1 \neq 0$, $\nu_3 = 0$) or quasiperiodic motions. Table 1 lists the different solutions, their isotropy subgroups Σ and the isotropy subspace $\mathrm{Fix}(\Sigma)$. The isotropy subgroup Σ is important to classify the symmetry properties of a solution $\mathbf{z}$. It is defined by

$$
\Sigma = \{g \in G : \mathbf{D}_g \mathbf{z} = \mathbf{z}\}, \tag{45}
$$

where G is the symmetry group and $\mathbf{D}_g$ its matrix representation. The isotropy subspace $\mathrm{Fix}(\Sigma)$ of the subgroup Σ is defined by

$$
\mathrm{Fix}(\Sigma) = \{\mathbf{z} : \mathbf{D}_\sigma \mathbf{z} = \mathbf{z} \quad \forall \sigma \in \Sigma\}. \tag{46}
$$

We discuss these concepts below.

The solutions are composed of the statically buckled state shown in Figure 4, the planar oscillation shown in Figure 8, the rotating motion shown in a top view of Figure 9, and of more complicated spatial configurations.

Now we discuss the solutions given in Table 1:

(0) Straight downhanging tube before loss of stability
(1) Planar buckled state in direction of a spring (e.g. in the x_1, x_3 plane)

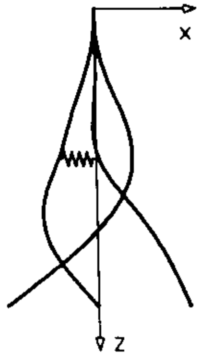

Fig. 8. Shape of the standing (SW) wave solutions for the symmetric Hopf bifurcation of the fluid conveying tube.

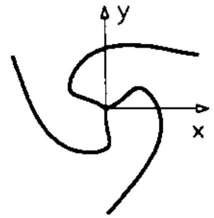

Fig. 9. Rotating or travelling (TW) wave solution for the symmetric Hopf bifurcation of the fluid conveying tube.

(2) Planar buckled state in diagonal direction of two springs (here in the $3\pi/4$ plane, the solution in the $\pi/4$ is $(0, 0, \sqrt{ib})$ and its symmetry is $\mathbf{Z}_2(\zeta\kappa) \times \mathbf{S}^1$)
(3) Planar oscillation in direction of spring
(4) Planar oscillation in diagonal direction
(5) Rotating solution
(6) Buckled state with superposed planar oscillation. Both in the direction of the same spring
(7) Buckled state and planar oscillation in directions of springs but orthogonal to each other
(8) Buckling and planar oscillation in diagonal direction
(9) Buckling and oscillation in diagonal directions but orthogonal to each other
(10) Modulated rotating solution
(11) Spatial (nonplanar) buckled degenerate solution
(12) Elliptical spatial rotating solution or planar oscillation in a plane which is not a symmetry direction, that is, which is not a mirror-reflection plane
(13) to (15) Tertiary solution branches (quasiperiodic motions)

Since in Table 1 the solutions are classified according to their symmetry the successive loss of symmetry of the solutions can best be seen from the isotropy lattice shown in Figure 10. We read the isotropy lattice in the opposite direction of the arrows. The trivial downhanging solution (0) has the full spatial and time shift ($\mathbf{S}^1$) symmetry. By the time shift symmetry we understand a translation in time that brings the solution into coincidence with itself. If the solution is time independent (for example, statically buckled) then an arbitrary translation in time is possible.

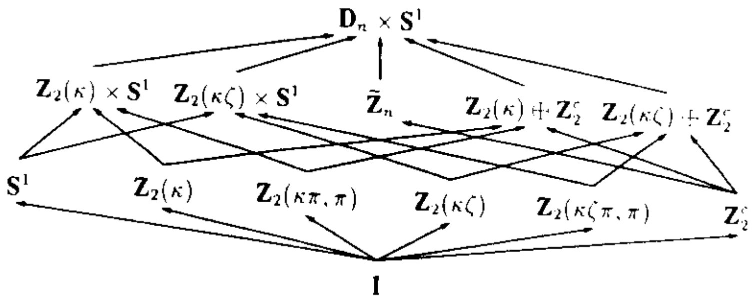

Fig. 10. Isotropy lattice for $n = 4k$ ($k = 1, 2, \ldots$).

After bifurcation from the trivial state we have five solutions with different symmetries which, however, are less symmetric than (0). The state (1) is invariant for a reflection about the (x_1, x_3) plane called $\mathbf{Z}_2(\kappa)$ where $\mathbf{Z}_2(\kappa) = \{E, \kappa\}$ is the cyclic group generated by the reflection κ about the (x_1, x_3) plane. It can be represented by one real variable x and hence the dimension of Fix(Σ) is one. The buckled state (2) is invariant against a rotation (ζ) by $\pi/2$ and a reflection about the (x_1, x_3) plane. Both states are invariant against a time shift, because they are constant.

The two planar oscillations have the same spatial symmetries as before and the additional symmetry $\mathbf{Z}_2^\zeta$ which means a rotation by π in space and a phase shift by π. We may also use the notation $\mathbf{Z}_2^\zeta = \mathbf{Z}_2(\pi, \pi)$. In $\mathbf{Z}_2(\pi, \pi)$ the first entry refers to the spatial and the second to the temporal transformation. Hence, the original solution, if an oscillation about the trivial position occurs, is again obtained. Now Fix(Σ) is given by a complex variable w and hence its dimension is two. The symmetry $\tilde{\mathbf{Z}}_4$ means a rotation by $\pi/2$ and a timeshift by $-\pi/2$, which characterises a (discrete) rotating solution. This completes all the symmetry properties of the first level in Figure 10. On the next level we see how loss of symmetry occurs further. In addition it is seen how different solutions contribute to this loss.

As a more complicated example we explain the symmetry $\mathbf{Z}_2(\kappa\pi, \pi)$ of solution (7). Here the tube is planar buckled in x_2 direction and superposed on this configuration is an oscillation orthogonal to the buckling plane of the tube. A schematic picture is given in Figure 11. Position 1 schematically fixes a momentary position of the tube. The first operation is a rotation by π resulting in position 2. Next we must apply a reflection κ about the x_1, x_3 plane. This results in position 3. Finally a time shift by π results in the original state.

From the isotropy lattice we can also identify heteroclinic cycles as they are described in [17]. For example the cycle $\mathbf{Z}_2(\kappa)\dot{+}\mathbf{S}^1 \to \mathbf{Z}_2(\kappa) \to \mathbf{Z}_2(\kappa)\dot{+}\mathbf{Z}_2^\zeta \to \mathbf{Z}_2(\kappa\pi, \pi) \to \mathbf{Z}_2(\kappa\pi)\times\mathbf{S}^1$ which is also shown in Figure 12. The physical interpretation is the following: $\mathbf{Z}_2(\kappa) \times \mathbf{S}^1$ is a statically buckled planar solution in the x_1, x_3 plane. On the branch $\mathbf{Z}_2(\kappa)$ the tube starts to oscillate in the x_1, x_3 plane with increasing amplitude and at the same time the amplitude of the statically buckled configuration decreases. This leads to the state $\mathbf{Z}_2(\kappa) \dot{+} \mathbf{Z}_2^\zeta$ which is a planar oscillation in the x_2, x_3 plane about the origin. Along the branch $\mathbf{Z}_2(\kappa\pi, \pi)$ this oscillation moves away from the origin into the x_2 direction about a statically buckled state in the x_2, x_3 plane. The more the amplitude of the statically buckled state increases the more the oscillation amplitude decreases. Finally only the planar statically buckled state $\mathbf{Z}_2(\kappa\pi) \times \mathbf{S}^1$

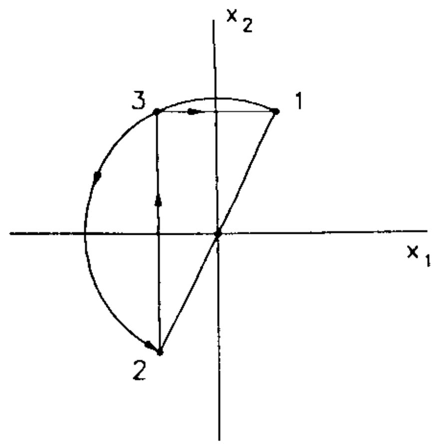

Fig. 11. Symmetry operations for solution (7) of Table 1 with $\mathbf{Z}(\kappa\pi, \pi)$ symmetry: a rotation about π taking $1 \to 2$ is followed by a reflection about the (x_1, x_3) plane taking $2 \to 3$ and finally a time shift by π takes $3 \to 1$.

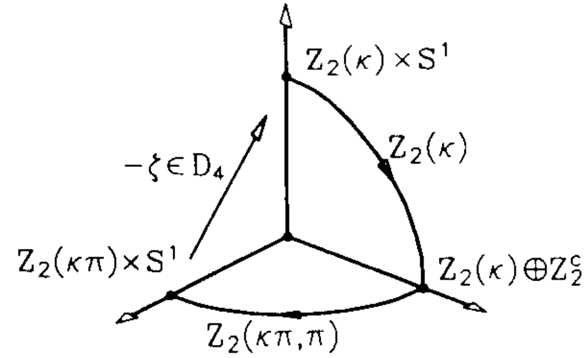

Fig. 12. A possible heteroclinic cycle taken from Figure 10. Starting from the planar buckled state $\mathbf{Z}_2(\kappa) \dot{+} \mathbf{S}^1$ in the (x_1, x_3) plane the tube moves, as it is explained in the text, to the planar buckled state $\mathbf{Z}_2(\kappa\pi) \dot{+} \mathbf{S}^1$ in the (x_2, x_3) plane, which of course is the same as the one in the (x_1, x_3) plane under the symmetry of the system.

in the x_2, x_3 plane remains, which, however, is rotated by $\pi/2$ compared to the original state. Due to the symmetry properties of the system we have an identical state.

Finally we present in Figure 13 a bifurcation diagram in the (μ, λ) parameter plane. In addition also the physical parameters ϱ and c are drawn. To obtain an understanding of the behavior of the tube for increasing the flow rate ϱ we have also drawn a 'loading path' (broken line in Figure 13) for a system where the stiffness c of the support is slightly larger than the critical value c_c. In the following description for a physical explanation of the behavior of the tube the numbers relate to the explanation of Table 1 given above. We see that in the present case the trivial state (0) is followed by the planar buckled state (1) which increasing the flow rate loses its stability to the oscillation (7) orthogonal to the buckling plane. Increasing the

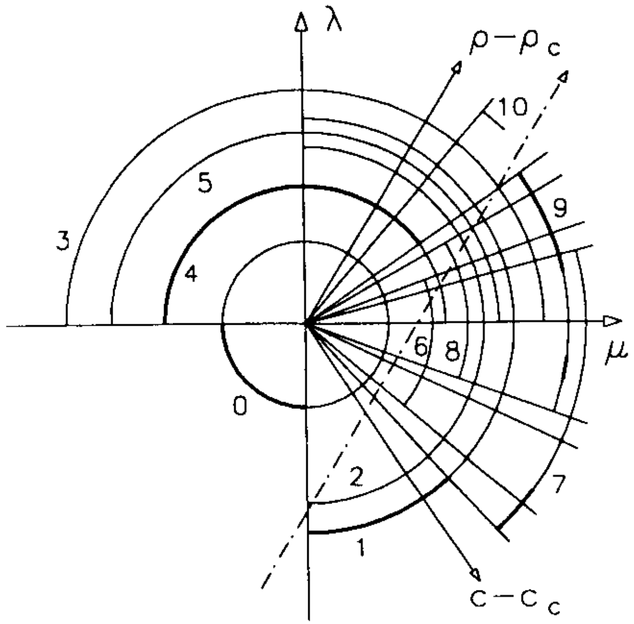

Fig. 13. Bifurcation diagram giving a stratification of the (μ, λ) respectively (ϱ, c) parameter plane in domains of existence of different solutions. The numbers refer to Table 1. Stable solutions are indicated by bold arcs. The broken line parallel to the ϱ-axis represents a physical 'loading path'.

flow rate ϱ solution (7) loses its stability. Then there is a domain of flow rates ϱ where no stable stationary symmetric solutions for the third order bifurcation equations were found. Finally the states (9) and (4) are reached, which are oscillations in diagonal direction.

Appendix A: An Example for the Calculation of the Stability of a Steady State Oscillation in a Symmetric System

The calculation of the stability of the solutions of (34) would in general require the solution of a 4×4 linear eigenvalue problem. However, making use of the symmetry properties of the solutions we show that the dimension of this eigenvalue problem can be reduced by two which finally requires only to calculate a trace and a determinant as indicated before.

We perform the calculation of the trace and the determinant for the planar oscillations SW_{45}. We note that with the notations introduced in Table 1 the symmetry of this solution is $\mathbf{Z}_2(\zeta\kappa)$. Making use of (17 and 18) we may express this by

$$D_{\pi/2} D_S(z_1, z_2) = D_{\pi/2}(z_2, z_1) = (iz_2, -iz_1). \tag{47}$$

Looking for the eigenvector of the corresponding operator we have to solve

$$\begin{pmatrix} 0 & i \\ -i & 0 \end{pmatrix} \begin{pmatrix} z_1 \\ z_2 \end{pmatrix} = \lambda \begin{pmatrix} z_1 \\ z_2 \end{pmatrix}. \tag{48}$$

From (48) follow the eigenvalues $\lambda_{1,2} = \pm 1$ and the corresponding eigenvectors are

$$w_1 = \begin{pmatrix} 1 \\ i \end{pmatrix} w, \quad w_2 = \begin{pmatrix} 1 \\ -i \end{pmatrix} w. \tag{49}$$

Since the eigenspaces are invariant under the symmetry transformations it is sufficient to calculate the linearization of the nonlinear right hand sides of (34) at these vectors. In addition we only need to consider one equation because from the second one the same terms are obtained.

We obtain formally from the nonlinear function $g(z_1, \bar z_1, z_2, \bar z_2)$ in (28) the linearization

$$dg \cdot \mathbf{w} = g_{z_1} w_1 + g_{z_2} w_2 + g_{\bar z_1} \bar w_1 + g_{\bar z_2} \bar w_2 \tag{50}$$

and evaluated at $w_2 = (w, -iw)^T$ we have

$$dg|_{w_2} = (g_{z_1} - ig_{z_2}) w + (g_{\bar z_1} + ig_{\bar z_2}) \bar w = Uw + V\bar w. \tag{51}$$

Inserting from (34)

$$\begin{aligned} g_{z_1} &= \mu + i\omega - i\nu + 2A_1 z_1 \bar z_1 + A_2 z_2 \bar z_2 \\ g_{z_2} &= A_2 z_1 \bar z_2 + 2A_3 \bar z_1 z_2 \\ g_{\bar z_1} &= A_1 z_1^2 + A_3 z_2^2 \\ g_{\bar z_2} &= A_2 z_1 z_2 \end{aligned} \tag{52}$$

into (51) we obtain

$$\begin{aligned} dg &= (A_1 - A_2 + 3A_3) a^2 w + (A_1 - A_2 - A_3) a^2 \bar w \\ &= Uw + Vw \\ &= (U_1 + iU_2)(u + iv) + (V_1 + iV_2)(u - iv). \end{aligned} \tag{53}$$

In real variables (u, v) the linearized system has the form

$$\begin{pmatrix} u \\ v \end{pmatrix}' = \begin{pmatrix} U_1 + V_1 & -U_2 + V_2 \\ U_2 + V_2 & U_1 - V_1 \end{pmatrix} \begin{pmatrix} u \\ v \end{pmatrix} = A \begin{pmatrix} u \\ v \end{pmatrix}. \tag{54}$$

The eigenvalues are

$$\mu_{1,2} = \mathrm{tr}\, A/2 \pm \sqrt{(\mathrm{tr}\, A)^2/4 - \det A}. \tag{55}$$

Inserting (54) into (55) we obtain

$$\begin{aligned} \mathrm{tr}\, A &= 2U_1 = 2\,\mathrm{Re}\, U \\ \det A &= |U|^2 - |V|^2. \end{aligned} \tag{56}$$

Acknowledgement

This research project has been supported by the Austrian Science Foundation (FWF), under the project P07003.

References

1. Bajaj, A. K. and Sethna, P. R., 'Bifurcations in three-dimensional motions of articulated tubes', Part 1 and 2, *Journal of Applied Mechanics* **49**, 1982, 606–611 and 612–618.

2. Bajaj, A. K. and Sethna, P. R., 'Flow induced bifurcations to three-dimensional oscillatory motions in continuous tubes', *SIAM Journal of Applied Mathematics* **44**, 1984, 270–286.
3. Bajaj, A. K. and Sethna, P. R., 'Effect of symmetry-breaking perturbations on flow-induced oscillations in tubes', *Journal of Fluids and Structures* **5**, 1991, 651–679.
4. Buzano, E., Geymonat, G., and Poston, T., 'Post-buckling behavior of a non-linearly hyperelastic thin rod with cross-section invariant under the dihedral group D_n', *Archive of Rational Mechanics and Analysis* **89**, 1985, 307–388.
5. Carr, J., *Applications of Centre Manifold Theory*, Applied Mathematical Sciences, Vol. 35, Springer-Verlag, New York–Heidelberg–Berlin, 1981.
6. Golubitsky, M., Stewart, I., and Schaeffer, D., *Singularities and Groups in Bifurcation Theory II*, Applied Mathematical Sciences, Vol. 69, Springer-Verlag, New York–Heidelberg–Berlin, 1988.
7. Melbourne, I., Chossat, P., and Golubitsky, M., 'Heteroclinic cycles involving periodic solutions in mode interactions with $O(2)$ symmetry', *Proc. Roy. Soc. Edinburgh* **113A**, 1989, 315–345.
8. Sethna, P. R. and Shaw, S. W., 'On codimension-three bifurcations in the motion of articulated tubes conveying a fluid', *Physica* **24D**, 1987, 305–327.
9. Simo, J. C., 'A finite strain beam formulation. The three-dimensional dynamic problem. Part I', *Computer Methods in Applied Mechanics and Engineering* **49**, 1985, 55–70.
10. Steindl, A., 'Flatter- und Divergenverzweigung eines flüssigkeitsdurchströmten Schlauchs', *ZAMM* **69**, 1989, T362–T365.
11. Steindl, A., 'Mehrfache Hopfverzweigung eines flüssigkeitsdurchströmten, elastisch gelagerten Schlauchs unter $O(2)$-Symmetrie', *ZAMM* **70**, 1990, T128–T130.
12. Steindl, A., *Hopf/Steady-State Mode Interaction for a Fluid Conveying Elastic Tube with* $\mathbf{D}_4$*-Symmetric Support*, International Series of Numerical Mathematics, Vol. 104, Birkhäuser Verlag, 1992, pp. 305–315.
13. Steindl, A., 'Bifurcations of a fluid conveying tube with $\mathbf{D}_n$-symmetric support', *Bifurcation and Chaos*, to appear.
14. Steindl, A., 'Hopfverzweigung eines flüssigkeitsdurchströmten Schlauchs mit $\mathbf{D}_4$-Symmetrie', *ZAMM* **74**, 1994, T366–T368.
15. Steindl, A. and Troger, H., 'Flow induced bifurcations to three-dimensional motions of tubes with an elastic support', in *Proceedings of Trends in Application of Mathematics to Mechanics*, Besseling, J. F. and Eckhaus, W. (eds.), Springer-Verlag, Berlin–Heidelberg–New York, 1988, pp. 128–138.
16. Steindl, A. and Troger, H., 'Nonlinear three-dimensional oscillations of an elastically constrained fluid conveying viscoelastic tube with $O(2)$-symmetry', AMD-Vol. 152, *ASME Winter Annual Meeting Anaheim, CA*, 1992, pp. 47–62.
17. Swift, J. W., 'Hopf bifurcation with the symmetry of the square', *Nonlinearity* **1**, 1988, 333–377.
18. Troger, H. and Steindl, A., *Nonlinear Stability and Bifurcation Theory, An Introduction for Engineers and Applied Scientists*, Springer-Verlag, Wien–New York, 1991.